DAM BREACH ANALYSIS OF BISANDIMA DAM, SIDAMA REGINAL STATE, ETHIOPIA

MSc. THESIS

TAFESE FONA DEBESA

HAWASSA UNIVERSITY, INSTITUTE OF TECHNOLOGY, HAWASSA, ETHIOPIA

MAY, 2023

DAM BREACH ANALYSIS OF BISANDIMA DAM, SIDAMA REGINAL STATE, ETHIOPIA

TAFESE FONA DEBESA

A THESIS SUBMITTED TO

HAWASSA UNIVERSITY

SCHOOL OF BIO-SYSTEMS AND WATER RESOURCE ENGINEERING,

DEPARTMENT OF HYDRAULIC ENGINEERING

INSTITUTE OF TECHNOLOGY, SCHOOL OF

GRADUATE STUDIES,

HAWASSA UNIVERSITY,

HAWASSA, ETHIOPIA

IN PARTIAL FULFILLMENT OF THE

REQUIREMENTS FOR THE

DEGREE OF

MASTER OF SCIENCE IN HYDRAULIC ENGINEERING

MAY, 2023

School of Graduate Studies

Hawassa University

Advisors Approval Sheet

This is to certify that the thesis entitled **"Dam Breach Analysis Case of Bisandima Dam"** submitted in partial fulfillment of the requirements for the **degree of Master's** with specialization in **Hydraulic Engineering**, the Graduate Program of the School of **Bio-systems and Water Resource Engineering,** and has been carried out by **Tafese Fona Debesa** Id. No **GpHydrw/0018/12**. Under our supervision. Therefore, we recommend that the student has fulfilled the requirements and hence hereby can submit the thesis to the department.

Shemelies Asseffa (PhD)	_____	_____
Name of major advisor	Signature	Date
Mr. Gonse Amalo	_____	_____
Name of co-advisor	Signature	Date

EXAMINERS' APPROVAL SHEET

SCHOOL OF GRADUATE STUDIES

HAWASSA UNIVERSITY EXAMINERS' APPROVAL SHEET

We, the undersigned, members of the board Examiners of the final open defense by Tafese Fona Debesa have read and evaluated his thesis entitled "Dam Breach Analysis a Case of Bisandima Dam", and examined the candidate. This is therefore, to certify that the thesis has been accepted in the partial fulfillment of the requirements of the degree of Master of Science in Hydraulic Engineering.

_____	_____	_____
Name of chairperson	Signature	Date
_____	_____	_____
Name of Internal Examiner	Signature	Date
_____	_____	_____
Name of External Examiner	Signature	Date
_____	_____	_____
SGS Approval	Signature	Date

Final approval and acceptance of the thesis are contingent upon the submission of the final copy of the thesis to the School of Graduate Studies (SGS) through the Department/School PGP of the candidate's department

Stamp of SGS Date: _____

DECLARATION

I, the undersigned person, declare that this thesis is my original work and that all sources of materials used for the thesis has been duly acknowledged.

Name: **Tafese Fona Debesa**

Signature _____

Place Hawassa University

Date of submission _____

ACKNOWLEDGEMENT

My sincere gratitude to Dr. Shimelis Assefa and Mr. Gonse Amalo, my thesis advisors, for their suggestions, criticism, support, and wisdom. I would like to express my genuine gratitude to all the Hawassa University, School of **Bio-systems, and Water Resource Engineering** staff who gave me the postgraduate courses.

I would like to thank the Dam Hydropower and Energy Process Department, Surveying Geospatial and civil informatics of the Ethiopian Construction Design and Supervision Works Corporation, and Water and Energy Design and Supervision Works Sector that provided me data and information needed for this work.

I also acknowledge the Study and Design Department of the Sidama National Regional States, Irrigation Development Agency that provided me data and information needed for this work.

I want to thank my beloved family and friends, who were encouraging and supporting me to finish this research. I am genuinely gratefulness thank my friend **Mr. Girma Gadissa** who invested his time, knowledge, and energy throughout the whole research work.

Above all, my sincere thanks go to the Almighty God for all my successful works. This day, God what you have done for me is really beyond what I can imagine and I have dreamt. Indeed, thanks for everything you have been doing for me.

Table of Contents

LIST OF FIGURES

LIST OF TABLES

LIST OF ABBREVIATIONS AND ACRONYMS

BEED	Breach Erosion of Earth Dam
DAMBK	Dam Break-Forecasting Model
DEM	Digital Elevation Model
ECDSWC	Ethiopian Construction Design and Supervision Works Corporation
FEMA	Federal Emergency Management Agency
FLDVWAV	Flood wave dynamic modeling
GIS	Geographic Information System
GPS	Global Positioning System
HEC	Hydraulic Engineering Centre
HEC-GeoRAS	Hydraulic Engineering Center Geographical River Analysis System
HEC-HMS	Hydrologic Engineering Center's Hydrologic Modeling System
HEC-RAS	Hydraulic Engineering Center for River Analysis System
HSG	Hydrologic Soil Group
m a.s.l	Meter above Sea Level
MCM	Million Cubic Meters
MOWIE	Minister of Water, Irrigation and Energy
NMA	National Meteorological Agency
NWS	National Weather Service
PMF	Probable Maximum Flood
PMP	Probable Maximum Precipitation
RAS	River Analysis System
SCS	Soil Conservation Service
SMPDK	Simple Dam Break Model
2D	Two dimensional
USACE	United States Army Corps of Engineers
USBR	United States Bureau of Reclamation
WMO	World Meteorological Organization

ABSTRACT

Due to the construction of Bisandima dams, the downstream ecosystem is highly changed in that a huge area is covered with irrigation farms, new settlements, and residence areas of inhabitants living on the farms, and fishery communities were formed due to this dam. All these investments and newly settled inhabitants are highly exposed to flooding and they are at risk from the possible failure of this dam. The objective of this study was to model the Bisandima dam breach phenomena and to develop flood inundation maps. In this study dam breach, flood routing was carried out by using unsteady flow routing in HEC-RAS 2D model using geometric data to determine flood-susceptible areas downstream of the dam for the study area. The key inputs required in the dam breach flood routing processes include Precipitation data to determine PMF, digital Elevation model, and land use data were used as input for the HEC-RAS model. Some parametric methods were also used to predict dam breach parameters for use in the model. The breach discharge resulted from the HEC-RAS model for all methods such as Thun & Gillete (1990), Froehlich (2008), Froehlich (1995), MacDonald and Langridge –Monopolis (1984), Xu & Zhang (2009) were 2079.01, 1040.21, 1332.49, 531.91, 592.22 m^3/s and 1796.52, 620.37, 572.02, 530.53, 498.46 m^3/s for overtopping failure and piping failure respectively and also breach outflow at the downstream cross-section were 969.32, 625.48, 699.46, 538.96, 592.38 m^3/s for overtopping failure respectively. The hazard mapping due to the combined effect of flood depth and velocity showed that an area of 28ha, 9.5ha, 11ha, 3ha, and 0.5ha are under low, medium, high, very high, and extreme hazard respectively for overtopping failure and an area of 20ha, 8ha, 10ha, 2.2ha, and 0.8ha are under low, medium, high, very high and extreme hazard respectively for piping failure. As noticed from the flood inundation map almost all critical areas downstream of the dam are in immediate danger. Based on the finding of the study outcomes the following recommendations are drawn: flood early warring, watershed treatment, provide dike at both sides of the downstream.

***Keywords**: HEC-RAS, Dam breach model, Inundation Map, breach parameters, Bisandima dam*

1. INTRODUCTION

1.1. Background

Dams are hydraulic structures used to store, control, and divert water impounding it behind the upstream side of the dam in a reservoir for different purposes, like hydropower generation, water supply, irrigation, navigation, transportation, etc. Although dams have many advantages, the risk that may happen due to failure still exists. Dams can have a risk to downstream communities and properties if not designed, operated, and maintained properly (Lejissa, 2015a). In Ethiopia, the function of dam breach analysis is not known clearly. More than 85% of the dam do not have flood inundation maps due to dam breaches (Nugusa, 2018). It is a critical issue to analyze the downstream damages caused by the dam breach and to set an early warning for people living downstream of the dam, and downstream infrastructures that can be affected if the dam breach occurs. The term dam breach analysis is usually related to the process of studying a dam failure phenomenon and analyzing the resulting consequences downstream of the dam. Dam breach analysis generally deals with the simulation of probable failure for existing dams and analyzing the resulting consequences (Pandya, 2013). Dam breach modeling is typically done within a larger study context that develops inflow hydrographs from various frequency storms, evaluates project spillway adequacy, estimates breach parameters, and performs routing and mapping of the resultant flood, (Gee, 2010).

Different organizations and researchers have contributed their findings in the analysis of dam breaches and its consequence. They have derived regression equations based on data from historical dam failure events that are used in predicting the breach geometry. These include (MacDonald and Langridge-Monopolis, 1984), USBR (1988), and (Froehlich, 1995), (Froehlich, 2008). Developments of analytical models using the principle of hydraulics and sediment transport are also useful in simulating the breach process and downstream flooding (Leoul, 2015).

According to (Brunner, 2014), In dam breach analysis there are three practical dam breach parameter prediction methods: (1) comparison analysis method: comparing a dam under study with recorded failed dams of similar size and type, (2) empirical equations: use of different equations developed based on historical records of failed dams, and (3) physically based models:

use of computer-based models that model the physical breaching process using sediment transport equations, soil mechanics, and principles of hydraulics.

Bisandima embankment dam is an irrigation project; the irrigation infrastructure is found on the left side of the downstream of the dam and the Gidabo irrigation dam is also downstream of the dam. Since the Bisandima embankment dam study and design document did not include the dam breach analysis and therefore, this study was planned to fill this gap so that it is possible to reduce the impact of the possible breaching of this dam.

1.2. Statement of the problem

Impounding water behind a dam creates a risk to downstream areas because of the potential for uncontrolled release of the reservoir pool caused by dam failure which could result in a peak outflow that greatly exceeds any possible natural flood event. Due to the construction of dams, the downstream ecosystem is highly changed in that huge area is covered with irrigation farms, new settlements, and residence areas of inhabitants living on the farms and fishery community were formed due to this dam. All these investments and newly settled inhabitants are highly exposed to flooding and they are at risk from the possible failure of this dam. Therefore, the dam breach analysis and downstream flood inundation mapping for the worst conditions are important for the safety of the dam and to prevent life loss and property damage. Therefore, the study of dam breach analysis is vital to predicting the breach outflow discharge during dam failure. This is important to evaluate economic, social, and environmental impacts downstream and to prepare an emergency response plan.

1.3. The Objective of the Study

1.3.1. General Objective

The objective of this study is to estimate the maximum breach outflow hydrograph and route the downstream to prepare a flood inundation map and select the flood-prone area using HEC-RAS.

1.3.2. Specific Objectives

The specific objectives of the study include:

1. To estimate dam breach parameters such as breach bottom width, breach formation time, and breach side slope.
2. To estimate the peak outflow hydrograph for different modes of dam failure
3. Rout the outflow hydrograph from the breached dam to downstream using HEC-RAS and map the inundation area in the Arc GIS environment.
4. Map the inundation area using ArcGIS.

1.4. Research Questions

1) What are the possible causes of the Bisandima dam failure?
2) What are the most important hydraulic breach parameters defining the cross-section of that failures?
3) What will be the magnitude of breach outflow hydrograph for this study area?
4) What will be the size and extent of the flooded area?

1.5. Scope of the Study

This study covers the dam breach analysis using the new HEC-RAS version 5.0.7 model and prepared the flood inundation map using RAS Mapper which is a GIS tool. The key inputs required in the dam breach analysis and flood routing processes include PPt data to determine PMF, digital Elevation model, and land use data were used as input for the HEC-RAS model.

1.6. Significance of the Study

The result from modeling of a dam and downstream flood inundation mapping is used for emergency action plan. The resulting flood-inundation maps can provide valuable information to a government official, emergency managers, and residents for planning an emergency response if a dam breach occurs. It also helps land use planners to identify flood zones and to put them them into consideration while investing in huge projects in the area. Huge losses in both

human lives and economic properties can result from an embankment dam failure. Therefore, modeling of embankment dam breaching is of tremendous significance for dam failure damage assessment, risk analysis, disaster control, and mitigation (Zhu & Vrijling, 2004). Dams are an important part of this nation's infrastructure, providing flood control, water supply, and irrigation and hydropower benefits. Despite their many beneficial uses and value, dams also present risks to property and life due to their potential to fail and cause catastrophic flooding. This research was assessing the possible dam failure scenarios and downstream flood inundation area and coverage if the Bisandima dam fails in the future.

2. LITERATURE REVIEW

2.1. The uses of the dam

The dam is a man-made barrier, together with appurtenant structures, constructed above the natural surface of the ground for impounding water. Dams are an important part of this nation's infrastructure, providing flood control, water supply, irrigation, hydropower, navigation, and recreation benefits. Despite their many beneficial uses and value, dams also present risks to property and life due to their potential to fail and cause catastrophic flooding (Wahl, 2010).

2.2. History of dam breach analysis

A dam is a barrier across flowing water that obstructs, directs, or slows down the flow, often creating a reservoir, lake, or impoundment. Dams are considered "installations containing dangerous forces" due to the massive impact of possible destruction on the civilian population and environment. As indicated in Table 1, hundreds of dams have been failed and every year many dikes breached due to high flow in the river, sea storm surges, etc. often leading to catastrophic consequences (Zagonjolli, 2007)

Table 1: List of the major dam failures, (Leoul, 2015)

Dam	year	Location	Fatalities	Details
Mohne Dam	1943	Ruhr, Germany	1579	Destroyed bombing during Operation Chastise in world war 2.
Kurenivka Mudslide	1961	Kiev, Ukraine	1,500	Caused by heavy rains
Vajont dam	1963	Monte Toc, Italy	2,000	The dam did not collapse but a 110km/h landslide fill the reservoir, and the water escaped over the top of the dam.
Sempor Dam	1967	Central Java Province, Republic of Indonesia	2,000	Flash floods overtopped the dam during construction.
Banqiao Dam Shimantan Dam	1975	Zhumadian, China	171,000	With extreme rainfall, 11 million people lost their homes. worst dam failure
Machchu-2 Dam	1979	Morbi, India	5,000	Heavy rain and flooding beyond spillway capacity.

2.3. Modes of dam failures

Characteristics of dam failure are difficult to identify a distinct, single cause for a dam failure. Often, several causes are involved in a failure and these causes are interrelated with each other. Most of the cases are caused by either overtopping or quality problems. These two causes led to nearly 80% of all failures. It is seen that 58% of quality problems are associated with piping in

the dam body or foundation. Overall, the most common causes of earth dam failures are overtopping and piping in the dam body or foundation. The principal influence factor on overtopping is the insufficiency of spillway capacity. For piping in the dam body or foundation, the most single adverse factor is crack, which can be caused by differential settlement, material shrinkage, foundation defects, and imperfect interface, (Zhang, 2007). The most common causes of dam failure between January 1975 and January 2011 are summarized in annex, Table 10. Flood or overtopping was the most common cause of dam failure, followed by piping or seepage, (Asfaw, 2016). According to Ashraf et al. (2018), Loss of embankment materials due to either overtopping or seepage erosion or piping is the principal reason for the failure of embankment dams. Materials are detached from the embankment in layers by tractive stresses for non-cohesive embankments. According to Zhao et al. (2015), the erosion development for overtopping initiates at a point where the tractive shear stress goes above a critical resistance that retains the material in place. Breaching occurs by head cutting for cohesive embankments. Usually, a head cut starts close to the downstream toe of the dam and then expands upstream till the crest of the dam is breached. As pointed out by Sharma and Kumar (2013), The erosion mechanisms and rates are different for granular and cohesive embankments. Surface slips occur rapidly because of the seepage presence on the downstream slope for granular embankments, and later granular materials are detached quickly layer by layer. There is no seepage occurring on the slope because of the small permeability for cohesive embankments. As an alternative, erosion often initiates at the embankment toe and progresses upstream, undercutting the slope and then making the removal of huge amounts of materials due to shear failure of the soil on the over-steepened slope. Piping and internal erosions of embankment dams are another usual mode of failure in addition to overtopping. According to ASTM (2002), Piping occurrence is the advanced elimination of soil elements from a bulk of soil by an infiltrating water directing to the growth of channels. According to McCook, (2004), seepage erosion happens when the water running through cracks or defects erodes the soil from the walls of the crack or defect. According to Wang et al. (2016), piping and internal erosion may be separated into four phases: commencement and prolongation of erosion, advancement to form a pipe and full development of a breach. In over-all, the seepage failure starts when the erosion resistant forces are slighter than the erosion driving forces, leading to taking away of soil particles through large voids or discontinuities present in the soil. A free path called “pipe” is made through the dam next to

washing away of huge quantity of embankment materials by leaking flow. Then, the erosion progresses very quickly until the portion of the materials above the pipe becomes unbalanced and breakdowns. After the breakdown, the successive erosion goes forward in the similar way as in the circumstance of overtopping.

2.3.1. Overtopping failure

In general, during an overtopping failure of an earthen dam, a head-cut erosion process will first start on the downstream side of the dam embankment. While water is going over the dam crest, the dam crest acts like a broad-crested weir. The head cut begins to cut into the dam crest, the weir crest length will become shorter, and the appropriate weir coefficient will trend towards a sharp-crested weir value. When the head cut reaches the upstream side of the dam crest, a mass failure of the upstream crest may occur, and the hydraulic control section will act very much like a sharp-crested weir. The head cut will continue to erode upstream through the dam embankment, as well as erode down through the dam and widen at the same time (Brunner, 2014). Failure due to overtopping is one of the commonly known reasons for dam failures, specifically for embankment dams. Dam disasters may occur when overtopping hits embankments. The overtopping of a dam is commonly the consequence of severe flood occurrence and is frequently an antecedent of partial or complete dam failure, Sharma and Kumar (2013). According to historical case analysis, the main cause of such failure is the unfitness of previously used hydrological methods to evaluate extreme floods and the conditions for the choice of the spillway design. Better approximations of extreme flood events with a reduction of overtopping occurrence may be obtained due to current advancements in hydrology and climatic process, Hanson et al. (2005). Hence, consistent hydrological data are critical for dam safety, and standards of minimum risk have to be expected in the estimation of the design flood.

2.3.2. Internal erosion (piping) failure

Piping failure, Water is seeping through the dam at a significant enough rate, such that it is initially eroding material and transporting it out of the dam. As the material is eroded, a large hole is formed, thus able to carry more water and erode more material. The movement of water through the dam during this process is modeled as a pressurized orifice-type flow. During piping

flow processes, erosion and head cutting will begin to occur on the downstream side of the dam as a result of flow exiting the pipe. As the piping hole grows large, materials above the hole will begin to slough off and fall into moving water. The head-cutting and sloughing processes will continue to move back towards the upstream side of the dam while the piping hole continues to grow simultaneously. If the piping hole is large enough, the weight of the material above the hole may be too great to be maintained, and a mass caving of material will occur. This will result in a large rise in outflow through the breach and will accelerate the breaching process. Also at this point, the hydraulics of the flow transitions from orifice-type flow to open-air weir-type flow. The head-cutting and erosion process then continues back through the dam, as well as downward. Additionally, the breach will be widening. Depending on the volume of water behind the dam, the breach may continue to cut down and widen until the natural channel bed is reached. Then the breach will go into a widening phase (Brunner, 2014). Piping may be happened in the embankment, through the foundation, and from the embankment into the foundation as a development of internal erosion produced by seepage. In the event of piping failure, the frequency of piping through the embankment is two times higher than piping through the foundation and twenty times higher than piping from the embankment into the foundation Redda (2016). Additionally, it was perceived that partial of all piping failures through the embankment is linked with the existence of conduits. The different modes of piping allied with conduits are piping into the conduit, along and above the conduit, or out of the conduit, ICOLD (2016). In addition to conduit, internal erosion in the body of the dam may be produced by settlement cracks or even channels formed by animals. Any outflow does not have to be undervalued and has to be widely perceived since fast erosion can rise initial minor defects and can become possibly dangerous, Omofunmi et al. (2017).

2.4. Models Used for dam breach analysis

To do the study of dam breach and flood routing, Numerical models may be used as 1-D, 2-D, or a combination of both, Horritt and Bates (2002). The Accuracy of 1-D models reduces when the width of the channel increases or the flow is converted to non-channelized flow, thus 2-D models are more consistent in investigating the study of a floodplain, Kumar et al. (2017). A two-dimensional model is considered as a high-accuracy model to do flood modeling. Two-dimensional unsteady equations consist of continuity equations and momentum equations, solved

numerically in the flood-flooding model in floodplains. In the determination of dam breach hydrograph and flood routing, parametric models are the most broadly used models. It can either be hydraulic or hydrologic models, Lejissa (2015). A rainfall-runoff model is a mathematical model describing the rainfall-runoff relations of a catchment area, drainage basin, or watershed. A rainfall-runoff model can be really helpful in the case of calculating discharge from a basin, (Askar, 2014). Hydrologic models offer a reduced flood hydrograph at the required position. Nevertheless, they do not bring precise output overflow velocity and water surface elevation, USACE (2008). Due to such limitations of the hydrologic models particularly for flood inundation mapping and dam breach study, it is better to apply dynamic routing and unsteady flow routing techniques Kumar et al. (2017). Dynamic routing technique is called hydraulic routing or transient flow and it solves continuity and momentum equation thus, they are implemented to predict the dam breach flood occurrence and its downstream progression. These models include the solution of two partial differential equations derived by Barre De Saint Venant in 1871, (John D Anderson, 2009). These equations are developed based on: Conservation of mass or Continuity equation and Conservation of momentum. Some of the models used for the study of dam breach and flood mapping are described in the section shown below.

2.4.1. DAMBRK

DAMBRK was developed in 1984 by NWS, United States of America and it was updated by BOSS International, Zhou et al. (2005). DAMBRK predicts the formation of a dam breach wave and its downstream progression. The necessary features of DAMBRK are the capability to illustrate the mode of failure geometrically and temporarily, the ability to compute the breach hydrograph through the breach section, and its capacity to route the breach flow hydrograph through a downstream channel. The DAMBRK model is important in determining potential influenced areas letting users input geometric and temporal data to precisely predict the initial breach wave, Yohannes (2019). The updated BOSS DAMBRK has so many advances including quick calculations and it has a graphic interface.

2.4.2. FLO-2D

This model was developed in 1989 depending on the MUDFLOW model, Cook et al. (2015). It predicts the flood hazard, debris flow, and mudflow over the alluvial rivers and it utilizes a grid scheme to determine floodplain based on elevation and roughness coefficient. FLO-2D is best at predicting flow area and path, Kumar et al. (2017). Discharge is estimated depending on the depth of flow over each sector and summing up all sectors on all four sides of the grid. The density of the grid system and the data available decide the accuracy of the model.

2.4.3. FLDWAV

National Weather Services of the USA developed this model as a substitution for the DAMBRK model, Zhou et al. (2005). FLDWAV has high accuracy and it requires less computational time. This makes dam breach prediction and potentially worried areas more planned. FLDWAV utilizes real forecasting technology to model fast flood events or occurrences of dam break such that it predicts flow through a single stream or network of streams and take into account terrain and material properties at a different time interval and adjust flow pattern.

2.4.4. SMPDBK

This model was designed as an easy version of DAMBRK, FERC (2014). Thus, it is used mainly for classification of dams and the risk of dam breach potential. Different from DAMBRK, this model is fast and simple to use and so many parameters are not required that it gives similar outputs compared to DAMBRK when done on easier cases. The required information about the areas that are inundated downstream is produced by the model. Computer with the high specification is not needed to run the model the model has high efficiency to simulate the dam break scenarios for the preparation of an emergency action plan, (Hadush, 2019).

2.4.5. MIKE 11

MIKE 11 is a new generation of software with fast computation speed compared to former versions of MIKE and other software, DHI (2007). It is easy to use, fully dynamic, and one-dimensional tool for the analysis of dam breaches such that it simulates flood waves, sediment

transportation, and water quality in channels or water bodies. Having combined components such as advection–dispersion, hydrology, water quality model, cohesive and non-cohesive sediment transport, hydrodynamic model, rainfall–runoff model and flood forecasting model makes the model more popular, Etemad et al. (2010).

2.4.6. MIKE 21

This model is a two-dimensional modeling scheme that depends on a flexible mesh method, DHI (2016). It is more appropriate for free surface flows, Uddin et al. (2014). It has a Hydrodynamic Component which is the key computational component. This key component is depending on the numerical solution of the two-dimensional shallow water equations and Naive-Stokes equations. Accordingly, the model contains the equations of continuity, momentum, temperature, salinity, and density. Nevertheless, being a general modeling system for 2D and 3D free surface flows, it may also be applied for studies of inland surface waters, e.g. overland flooding and lakes or reservoirs, Ulke et al. (2017).

2.4.7. HEC-RAS

The HEC-RAS model is a free license that was broadly used by many individuals and organizations for the simulation of dam breach flood. The model above version 5.0.7 has the capacity of simulating 2-D flow, which is better than 1-D flow for the estimation of flood inundation, Ali (2018). It was developed based on the fully 2-D Saint-Venant equations and solved using a finite difference approach. The model is strong and accurate, Yakti et al. (2018).

This model supports overtopping and piping modes of failure. Mode of failure, breach size, and breach time are required to model dam breach failure in HEC-RAS, Balogun, and Ganiyu (2017). HEC-RAS has simple graphical users‟ interface (GUI) to understand and this gives astrongly effective management of files, data entry and editing, hydraulic analyses, tabulation, and graphical shows of input and output data, (USACE, 2010).

Mainly, the model has four components: steady flow simulation; unsteady flow simulation; sediment transport computations; and water quality analysis. HEC-RAS has also so many numbers of options, such as mixed flow regime analysis, letting analysis of both sub- and supercritical flow regimes in a single computer run, culvert, and bridge routines allowing for

multiple openings of different types and sizes, quasi 2-D velocity distributions, and XYZ graphs of the river channel system. There are two basic principles in stream flow profile and they are conservation of mass and conservation of momentum. These two principles are stated mathematically and denoted as continuity and momentum equations. In unsteady flow, changes based on time are explicitly analyzed as a variable, while steady flow analysis models ignore time altogether, USACE (2010).

HEC-RAS can do steady state and unsteady state, 1-D and 2-D dam breach modeling. HEC-RAS figures out velocities of flood, extreme flood wave levels, flood profiles, and likely inundated areas when discharge flow, geometry of channel, and geometry of structures were available, (Husain, 2017). Based on the Saint-Venant equations, there are 3 overall steps for dam breach modeling, these are: (1) evaluation of the way of failure, (2) estimation of the outflow discharge consequential from the dam breach, and (3) routing of flood wave through the downstream valley, Leoul (2015). By exporting the output of HEC-RAS to GIS, dam breach models can be delineated along the area most probable to be inundated, (FEMA, 2014).

2.4.7.1. One-dimensional numerical models

The one-dimensional method to dam breach modeling only considers the flood flow in the direction of the x axis (the downstream direction), (Zhang, 2012). The simulation of the downstream river circumstances in the occasion of a dam failure by one dimensional hydraulic models needs the knowledge of the lateral and longitudinal geometry of the river and its frictional resistance, (Soleymani et al, 2015). This governs the way the maximum flood wave is reduced as it attenuates downstream, the arrival time of the maximum flood discharge between points of interest, the highest water level at points of interest, and the change in the shape of the hydrograph as it moves downstream. The most extensively used method to model 1D flow is Saint- Venant Equations based on conservation equations of mass and momentum, (Moore, 2010).

$$\frac{\partial A}{\partial t} + \frac{\partial Q}{\partial t} = 0 \quad \text{..... (2.1)}$$

$$\frac{\partial Q}{\partial t} + \frac{\partial}{\partial x}(uQ) + gA\left(\frac{\partial h}{\partial x} - So\right) + gASf = 0 \quad \text{..... (2.2)}$$

Where Q is flow discharge, A is the cross-sectional area, u is flow velocity, h is flow depth, S_o is bed slope, and S_f is friction slope.

2.4.7.2. Two-dimensional numerical models

In the two-dimensional method, cross-sections are not used, as with one-dimensional flow modeling. As a substitute, the riverbed is well-defined by a series of mesh such that, the shape can be square or polygonal thus, every single grid has an allied elevation, (Tayefi et al., 2007).

Within the two-dimensional flow model, water spreads on a grid-to-grid evaluation basis. The Manning coefficient is so variable and applied at every grid location, (Dottori and Todini, 2010). The exchange of impulses between cells is possible, and hence, the momentum exchange between the main channel and the flood area is possible. The ccurrence of Complex interaction of channel and floodplain flow fields makes 2D simulation codes more necessary than 1D codes in many modeling conditions, (Gilles and Moore, 2010). The ost widely used for modeling 2D flood flow is the Navier-Stokes equation, regularly called the Saint-Venant equation described below, (Moore, 2010).

$$\frac{\partial h}{\partial t} + \frac{\partial (hU)}{\partial x} + \frac{\partial (hV)}{\partial y} = 0 \quad \text{(2.3)}$$

$$\frac{\partial (hU)}{\partial t} + \frac{\partial (hUU)}{\partial x} + \frac{\partial (VU)}{\partial y} = \frac{\partial (hTxx)}{\partial x} + \frac{\partial (hTxy)}{\partial y} - gh\frac{\partial z}{\partial x} - \frac{\tau bx}{\rho} \quad \text{(2.4)}$$

$$\frac{\partial (hV)}{\partial t} + \frac{\partial (hUV)}{\partial x} + \frac{\partial (VV)}{\partial y} = \frac{\partial (hTxy)}{\partial x} + \frac{\partial (hTyy)}{\partial y} - gh\frac{\tau by}{\rho} \quad \text{(2.5)}$$

Where h is flow depth, U and V are velocities in the x and y directions, Txx, Txy, and Tyy are depth-averaged turbulent stresses, z is the water surface elevation and τbx, τby are bed shear stresses. 2D models reject many of the assumptions needed by 1D modes and, hence, offer a more accurate illustration of complex hydraulic situations that come across in the real world, (FHWA, 2019).

2.5. Dam breach model selection criteria

Choosing the best and proper model is a vital part of any research task. There are several principles for selecting the most appropriate model. According to (Cunderlik and Simonovic, 2010), the selection based primarily on the necessity and requirements of the research under interest. (Cunderlik and Simonovic, 2010) put the following as criteria:

a) Required output of the model
b) Availability of input data
c) Prices and availability of the model
d) The model structures

There are different flood modeling tools that have their own distinct model structure and solution procedures. The most widely used 2D flood modeling tools are; HEC-RAS, FLDWAV, ISIS, FLUCOMP, and MIKE11 (Shiferaw, 2011). (Gilles and Moore, 2010) found that FLDWAV can simulate complex dam breaches, but is not as "easy" as HEC-RAS, which has a higher ability of pre-and post-processing, demonstrations of flood animation, and simple to make modifications of an input.

2.6. Dam breach parameters and their estimations methods

Dam breach analysis is the simulation of a breach hydrograph (flow through the breach in the dam versus time) and the subsequent downstream inundation. In recent years, dam safety draws increasing attention from the public. This is because floods resulting from dam failures can lead to devastating disasters with tremendous loss of life and property, especially in densely populated areas. Analysis of dam failures is of critical importance for disaster prevention and mitigation. Hence, a robust understanding of the characteristics of dam failures (e.g., failure mode, cause, and key influence factors) is needed (Zhang, 2007). Studies have been carried out worldwide to understand the causes of failure for different types of earth dams (zoned earth fill dam, earth fill dam with core wall, and homogeneous earth fill dam). The world data as of 2000 indicate that there are about 50,000 large man-made dams in operation (Nemmert, 2010). Approximately 80% of the world's dams are earth or rock-fill dams. In the past few years, more

than 1609 dam failure cases were seen and compiled these failure cases into a database. Among these cases, 66% are earth dams (Zhang et al., 2010).

2.6.1. Dam breach parameters

For this discussion, the term breach parameters include the parameters needed to physically describe the breach (breach depth, breach width, and side slope angles) as well as parameters that define the time required for breach initiation and development. According to (Brunner, 2014) the geometric parameters can be defined as follows:

1. **Breach depth (h_b)**: This is the vertical extent of the breach, measured from the dam crest down to the invert of the breach. Some publications cite the reservoir head on the breach, measured from the reservoir water surface to the breach invert.
2. **Breach width:** The ultimate breach width and the rate of breach width expansion can dramatically affect the peak flow rate and resulting inundation levels downstream from the dam. Case studies typically report either the average breach width (B_{ave}) or the breach width at the top (B_t), and bottom of the breach opening (W_b).
3. **Breach side slope factor (H: V):** The breach side slope factor along with the breach width and depth fully specifies the shape of the breach opening. Accurately predicting the breach side slope angles is generally of secondary importance to predicting the breach width and depth.

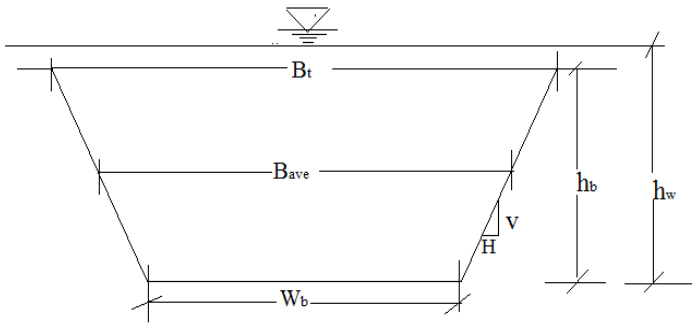

Figure 1: Dam breach parameters, (Brunner, 2014)

4. **Breach initiation time:** The breach initiation time begins with the first flow over or through a dam that will initiate warning, evacuation, or heightened awareness of the potential for dam failure. The breach initiation time ends at the start of the breach formation phase.

5. **Breach formation time:** The duration of time between the first breaching of the upstream face of the dam until the breach is fully formed. For overtopping failures, the beginning of breach formation is after the downstream face of the dam has eroded and the resulting breach has progressed back across the width of the dam crest to reach the upstream face. A dam breach usually occurs in two distinct phases starting with the breach initiation followed by the breach formation.

2.6.2. Dam breach parameter estimation methods

Important factors governing failure studies are the breaching parameters that help to quantify the risk associated with dam-break floods. Many empirical equations have been developed for predicting the breaching parameters associated with peak outflow, and these equations are generally developed by regression analysis from the record of dam failure data. The breach parameters include breach depth, average breach width, breach side slope, breach time, and peak outflow. The two major works in the investigation of a dam breach are the prediction of breach outflow hydrograph for the reservoir and the routing of that hydrograph through the downstream gorge, (Wu et al. 2011). The correct prediction of breach parameters is essential to produce a consistent estimation of maximum breach flow and inundation downstream nearby proximity to the dam, Wahl (1998c). Simulation of breach includes the highest uncertainty of all aspects in modeling of a dam breach, Wahl (1998a). The necessity of diverse parameters differs with the size of the reservoir. In large reservoirs, the maximum outflow happens when it reaches its highest width and depth. Fluctuations of water level in the reservoir are fairly small at the time of the breach formation, Dhiman and Patra (2018). Thus, correct estimation of breach geometry is most vital. During breach formation, significant variation in water level may be observed for small reservoirs. Thus, the maximum breach outflow happens before the breach has fully advanced. Hence, the flow rate for breach formation is the critical parameter, Steininger (2014). To do a simulation of a dam breach, all parameters of the breach are necessarily calculated and given as inputs to the dam breach model, Steininger (2014).

The estimation of dam breach location, dimensions, and development time is crucial in any assessment of a dam's potential risk. This is especially true in a risk assessment where dams will be ranked based on the potential for loss of life and property damage. The breach parameters will

directly affect the estimation of the peak flow coming out of the dam, as well as any possible warning time available to downstream locations. Unfortunately, the breach location, size, and formation time are often the most uncertain pieces of information in a dam failure analysis (Brunner, 2014). The correct prediction of breach parameters is essential to produce a consistent estimation of maximum breach flow and inundation downstream nearby proximity to the dam, Wahl (1998c). The necessity of diverse parameters differs with the size of the reservoir.

2.6.2.1. Comparative analysis

This method compares a given dam of interest with those in a database of well-documented volumes compared with a list of similar-sized dams that have failed. Dam breach parameters and peak discharges reported from the failure case histories of similarly configured dams are then directly applied to the dam being analyzed. If the dam under consideration is very similar in size and construction to a dam that failed, and the failure is well documented, appropriate breach parameters or peak outflows may be determined by comparison (Wahl, 1998a). The analytical approach is the model developed by Walder & O'Connor (1997). They developed a mathematical model for peak discharge from an idealized reservoir and breach as a function of a dimensionless parameter combining material erosion rate and reservoir size, a breach shape parameter (width-to-depth ratio), the breach side slope angle, a reservoir shape factor, and the breach depth-to-dam height ratio. They compared their model results to data from case study dam failures (including landslide dams) and identified typical ranges of the key input parameters. After evaluating the influence of the different input parameters and fixing the values of those parameters that had minimal effect on the result, they proposed a set of simplified equations that could be used to compute appraisal-level estimates of peak outflow. The key parameter in the final simplified model was the dimensionless factor based on erosion rate and reservoir size.

2.6.2.2. Physically based models

A physically-based model (also referred to as a "process" or "causal" model) utilizes generally accepted relationships based on physical principles to establish the framework of a model. The model then attempts to solve those relationships for a given input. This is a relatively simple concept, but it can become very complex when the input is changing with time. In the case of dam breach analysis, both the input and physical constraints are changing with time as the dam

erodes and the reservoir. (Wahl, 1998a) also summarizes these physical-based erosion models. Some of these are Cristofano (1965), BRDAM (1977), DAMBRK (1977), BEED (1985), and NWS BREACH (1988). Although several physically-based models have been reported as being in the development stage for research purposes, the National Weather Service's BREACH program (NWS BREACH or BREACH) is currently the only widely available model. BREACH predicts the development of a breach and the resulting outflow using an erosion model based on principles of hydraulics, sediment transport, and soil mechanics. It was initially developed in 1987 but has had several upgrades in 1988, 1991, and 2005. The model takes into account several components of a dam and reservoir that are not considered in the empirical methods, such as area versus elevation, dam dimensions, soil properties of the dam, and tailwater effects downstream. It is relatively simple to run and is widely used within the United States. Unfortunately, BREACH is no longer supported by the National Weather Service and significant advances in the understanding of the complex mechanics of a dam failure have not been incorporated also, the model has only been calibrated with a very limited number of cases (Brunner, 2014). This approach to dam failure analysis uses a dam breach model that simulates specific erosion processes to define the development of the breach. The first widely applied and most well-known model of this type is the National Weather Service BREACH model, (Fread, 1988). Since the erosion processes are related to the flow through the breach, models of this type by necessity also predict the breach outflow, but they do so without incorporating some of the features of a dam-break flood routing model, such as tailwater effects on the flow through the breach and dynamic effects on the flow within the upstream reservoir (most breach models have used level-pool storage routing through the reservoir). If these effects might be significant, then a hybrid modeling approach is possible. The erosion-based dam breach model is used to simulate the breach development and its results are used to construct a parameterized representation of the breach development process (i.e., to determine ultimate breach width, breach formation time, etc.). These breach parameters are then provided as input to the dam-break flood routing model, which can determine the breach outflow hydrograph itself, accounting for dynamic effects in the reservoir and downstream tailwater effects.

2.6.2.3. Parametric models

This models gives easy and accessible approaches to approximate the features of a dam breach (West et al., 2018). Historically failed dams data were collected together and statistically examined using regression methods (Shaukat et al., 2017). The result is a set of parametric equations telling parameters of the breach as a function of a simple dam or reservoir properties, characteristically one or several of the following; depth, breach width, side slope angle, formation time, and peak outflow (Xu and Zhang, 2009). The core benefit of this method is the ease of use, the speed, and the saving of costs accompanying utilizing some of the more progressive physically based models. The several equations that can be used for estimating breach parameters. The most common parametric regression equations developed based on information from case studies of historic dam failures are Froehlich (1995), Froehlich (2008), MacDonald and Langridge- Monopolis (1984), Von Thun and Gillette (1990), and Xu and Zhang (2009), (Wahl 1998b). There are, yet, so many drawbacks to these methods that can offset their easiness. The initial drawback is the absence of adequate historical data to exactly guess breach parameters. More newly issued work, such as Froehlich (2016) compared 111 and 182 failure cases respectively, some dating as far back as the 19th Century. Various of these are poorly documented and do not offer correct values for maximum outflow and geometry of breach. (Xu & Zhang, 2009) only issued the results of 75 dams, and this is due to the absence or untrustworthy data related to the remaining 107, dam failures. The popular well-known failures through the different approaches have a height of under fifteen meters (Wahl 1998a). Applying such historical evidence as a wide-ranging rule for dam breaches, particularly those that are bigger dams, can bring substantial uncertainties. Another disadvantage, with the exception of Von Thun & Gillette (1990) and Xu & Zhang (2009), is that these approaches do not consider necessary issues such as construction material, failure mode, and properties of materials, the furthermost key is erodibility of soil, which has been confirmed to perform a significant role in the breach development. Several factors are not accessible in the framework of historic failures, which adds to the uncertainties existing in parametric methods. For expression, many of these equations would offer the same estimated breach geometry values for two identically shaped, but completely differently constructed, dams. Some parametric methods with their proposed equation are shown in Table 2.

Table 2: Breach parameter relations based on dam-failure case studies (Brunner, 2014).

Methods	Number of case studies	Relationship proposed
MacDonald and Langrigde-Monopolis (1984)	42	$BFF=h_w*V_w$……..2.6 Earth fill dams: $V_{er}=0.0261BFF^{0.76}$……..2.7 Non earth fill dams: $V_{er} = 0.0348BFF^{0.852}$…….....2.8 $F_t = 0.0179V_{er}^{0.564}$……2.9 $Bf = \frac{V_{er}-h_b^{2*}(C_m+h_b*m*z_2/3)}{h_b(C+m*z_2/2)}$……2.10
Froehlich (1995)	63	$B_{avg} = 0.1803K_o*V_w^{0.32}*h_b^{0.19}$……2.11 $T_f = 0.00254V_w^{0.53}h_b^{-0.9}$……..2.12
Froehlich (2008)	74	$B_{avg} = 0.27K_oV_w^{0.32}h_b^{0.04}$……2.13 $T_f = 0.0176(V_w/g*h_b^2)^{1/2}$……2.14
Von Thun and Gillette (1990)	57	$B_{avg} = C_b+2.5h_w$……2.15 Highly erodible: $T_f = 0.015h_w$……2.16 Erosion resistance: $T_f = 0.020h_w+0.25$……...2.17
Xu and Zhang (2009)	45	$\frac{B_{avg}}{h_b} = 0.787(h_d/h_r)^{0.133}(V_w^{1/3}/h_w)^{0.652}\ e^{B_3}$……2.18 $\frac{B_t}{hb} = 1.062(h_d/h_r)^{0.092}(V_w^{1/3}/h_w)^{0.508}\ e^{B_2}$……2.19 $\frac{T_f}{T_t} = 0.304(h_d/h_r)^{0.707}(V_w^{1/3}/h_w)^{1.228}\ e^{B_5}$……2.20 $Z = \frac{B_t-B_{avg}}{Hb}$……..2.21

Where, BFF = Breach formation factor

B_{ave} = average breach width (m)

V_{er} = volume of material eroded from the dam embankment (cubic meters)

K_0=constant, (if overtopping, ko = 1.3 & piping , ko = 1.0)

V_w = Reservoir volume at the time of failure (m^3)

h_b = Height of final breach (m)

h_d = height of dam (m)

h_t = 15 meters which is considered to be a reference height for distinguishing large dams from small dams

h_w = height of water above breach bottom elevation at the time of the breach (m)

$B_3 = b_3 + b_4 + b_5$ coefficient that is a function of dam properties

b_3 = -0.041, 0.026, and -0.226 for dams with the core walls, concrete-faced dams, and homogeneous/zoned-filled dams respectively

b_4 = 0.149 and -0.389 for overtopping and seepage/piping respectively

b_5 = 0.291, 0.14, and -0.391 for high, medium, and low dam erodibility respectively

B_t = breach top width

$B_2 = b_3 + b_4 + b_5$ coefficient that is a function of dam properties

b_3 = 0.061, 0.088, and -0.089 for dams with the core walls, concrete-faced dams, and homogeneous/zoned-filled dams respectively

b_4 = 0.299 and -0.239 for overtopping and seepage/piping respectively

b_5 = 0.411, 0.062, and -0.289 for high, medium, and low dam erodibility respectively

T_f = breach formation time (hrs.)

T_t = 1 hour (unit duration)

Vw = Reservoir volume at the time of failure (m^3)

h_d = height of dam (m)

h_t = 15 meters which is considered to be a reference height for distinguishing large dams from small dams

h_w = height of water above breach bottom elevation at the time of the breach (m)

$B_5 = b_3 + b_4 + b_5$ coefficient that is a function of dam properties

b_3 = -0.327, -0.674, and -189 for dams with the core walls, concrete-faced dams, and homogeneous/zoned-filled dams respectively

b_4 = -0.579 and -0.611 for overtopping and seepage/piping respectively

b_5 = -1.205, -0.564, and 0.579 for high, medium, and low dam erodibility respectively

Z = breach side slope

2.7. Design of flood Inflow

In the design of major hydraulic structures such as spillways in large dams, the hydrologist and hydraulic engineer would like to keep the failure probability as low as possible, i.e. virtually zero. This is because the failure of such a major structure will cause very heavy damage to life, property, economy, and national morale. In the design and analysis of such structures, the maximum possible precipitation that can reasonably be expected at a given location is used. This stems from the recognition that there is a physical upper limit to the amount of precipitation that can fall over a specified area in a given time. The probable maximum precipitation (PMP) is defined as the greatest or extreme rainfall for a given duration that is physically possible over a station or basin. From the operational point of view, PMP can be defined as that rainfall over a basin that would produce a flood flow with virtually no risk of being exceeded. The development of PMP for a given region is an involved procedure and requires the knowledge of an experienced hydro meteorologist. Basically, two approaches are used (i) Meteorological methods and (ii) the statistical study of rainfall data. Details of meteorological methods that use storm models are available, (Subramanya, 2008).

2.7.1. Probable maximum precipitation

PMP is the theoretical maximum precipitation for a given duration possible in a specific location considering the meteorological conditions at a particular time of year with no consideration of long-term climatic trends, (WMO, 2009). PMP values are referred to as upper physical limits of storms. Due to the physical complexity of the phenomena and limitations in data and the meteorological and hydrological sciences, only approximations of the upper limits of storms can be made. Hence, PMP values are not exact but are estimated values, and various methods have been developed to obtain these values.

The most commonly used types are statistical and inferential methods (Rohidas & Srinivas, 2015). The statistical method is based on statistical analysis. Whereas the inferential method generalizes the 3D spatial structure of a storm to generate a simplified physical storm equation or storm model, and it requires meteorological analysis and focuses on the conditions for maximum precipitation development (WMO, 2009). The U.S. Weather Bureau used two methods to estimate PMP in U.S. Weather Bureau (1961). One of the methods used by the U.S. Weather Bureau (1961) for determining an estimate of PMP is Hershfield's statistical method, developed from a general frequency equation given by (Chow, 1951) and it is found using Equation

$$X_t = \overline{X_n} + K_m S_n \quad \text{(2.22)}$$

Where,

X_t = Rainfall for return period t

$\overline{X_n}$ = Mean of a series on n annual maxima

K_m = Frequency factor

S_n = Standard deviation of a series on n annual maxima

This method requires at least 20 years of precipitation maxima to obtain $\overline{X_n}$ and S_n.

The frequency factor, Km is derived from the chart by Hershfield (1965), which presents Km as a function of rainfall duration and the mean of annual series (WMO, 2009). Hershfield's method is used for estimates in small basins and is advantageous in areas such as the Caribbean where other data, such as dew point, are lacking (WMO, 2009). Statistical analysis was performed on time series data to calculate the 24 h max rainfall. The statistical distributions were subjected to the χ^2 test and Kolmogorov–Smirnov test to evaluate how well they were fitted to the time series, taking into account the concern about the influence of the time series length on distribution performance, (Kastridis et al., 2021).

2.7.2. Probable maximum flood

The probable maximum flood (PMF) is the hypothetical largest flood possible resulting from the prevailing meteorological and hydrological conditions of a specific watershed or drainage area (WMO, 2009). The PMF can be used by engineers for the hydraulic design of high-risk projects to prevent flood-induced failure. It is typically used as a design criterion for spillways of large dams and reservoirs, (Gorouh et al, 2018). The PMF can be found using different methods depending on the data that is available and the size of the area of interest.

Precipitation data for PMF calculation can be found with an estimate of the probable maximum precipitation (PMP), (Gordon, 2019). After PMP is determined, the PMF of a watershed can be found. The SCS curve number method is a simple, widely used, and efficient method that estimates direct runoff from storm rainfall (NEH-630, 2004). The SCS curve number method was developed mainly for agricultural watersheds between 10 and 1000 acres in size, and gives the area's total runoff depth, then peak flow can be calculated using Equation 2.10, using the precipitation of an event and the curve number (CN). Curve number depends on the hydrologic soil group (HSG), cover type, treatment, hydrologic condition, and antecedent moisture conditions, (SCS-USDA, 1986). The unit peak discharge is found by SCS rainfall distribution charts and the time of concentration. The following equations are used to find the time of concentration and peak discharge:

$$q_p = q_u * Q * A \quad \text{(2.23)}$$

$$S = \frac{1000}{CN} - 10 \quad \text{(2.24)}$$

$$I_a = 0.2S \quad \text{(2.25)}$$

$$Q = \frac{(p-0.2S)^2}{P+0.8S} \quad \text{(2.26)}$$

$$T_s = \frac{0.007}{P^{0.5}_{2.24}} [(nL_s)/S^{0.5}]^{0.8} \quad \text{(2.27)}$$

$$T_{sc} = \frac{Lsc}{3600 * KS^{0.5}} \quad \text{(2.28)}$$

$$T_{ch} = \frac{Lch}{3600 * V_{ch}} \quad \text{(2.29)}$$

Where,

q_p= peak discharge (cfs)

q_u= unit peak discharge (csm/in)

Q = total runoff depth (in)

A = area (mi2)

Q = total runoff depth (in)

P = precipitation depth obtained from PMP estimations (in)

S = total retention (in)

Ia= initial abstraction (in)

CN = SCS curve number

Ts = time of concentration for sheet flow (hr)

P2-24 = 2-year, 24-hour event rainfall (in)

n = Manning's roughness coefficient

Ls = length for sheet flow (ft)

S = slope

T_{sc} = time of concentration for shallow concentrated flow (hr)

L_{sc} = length for shallow concentrated flow (ft)

K = coefficient

T_{ch} = time of concentration for channel flow (hr)

L_{ch} = length for channel flow (ft)

V_{ch} = channel velocity (ft/s)

2.8. Manning roughness

It is characterized by friction or resistance to flow formed by the main stream and floodplain area, (Plakane, 2017). Manning's roughness coefficients, showing the main channel and floodplain hydraulic roughness, were also supposed to be varied in HEC-RAS, ignoring the fact that they were extremely irregular and variable, (Papaioannou et al., 2017).

2.9. Flood inundation mapping

An inundation map displays the spatial extent of probable flooding for different scenarios and can be presented either in quantitative or qualitative ways. The inundation or hazard assessment mapping delineates flood hazard areas in the river basin by integrating local knowledge, hydrological, meteorological, and geomorphologic data using different approaches. The inundation or hazard mapping is an essential component of emergency action plans; it supports policy and decision makers to decide how to allocate resources, flood forecasting, and significant land use planning in flood-prone areas (Gebre, 2015).

According to (FEMA), 2013) inundation maps can have adifferent uses that include:

1. **Emergency action plans (EAP):** An Emergency Action Plan is used to identify potential emergency conditions at a dam and specifies preplanned actions to minimize property damage and loss of life. The downstream inundation map is the basis for developing the Emergency Action Plan and is used to show the emergency management authorities and the critical areas for action in case of an emergency.
2. **Emergency response:** Emergency response represents the actions taken in the aftermath of an incident to save and sustain lives, meet basic human needs, and reduce the loss of property and the effect on critical infrastructure and the environment. In the case of dam failures and incidents, this would be the response by the dam owner, and local community emergency management to minimize the consequence of actual dam failure or incident.
3. **Hazard mitigation planning:** Mitigation is the proactive effort to reduce loss of life and property by understanding the effect of disasters. This is achieved by identifying hazard potentials and the risks they pose in a given area. In the case of dam failure, hazard mitigation planning involves identifying the population at risk and identifying the action to reduce their vulnerability. Information required by hazard mitigation planners includes the breach inundation zone boundary, depth of flooding, velocity, and timing.
4. **Dam breach consequence assessment:** Dam breach consequence assessment includes identifying and quantifying the potential consequence of a dam failure or incident. While hazard mitigation planning focuses on the economic and social impacts of a potential disaster and the organizational and government action needed as the result of a dam breach to respond and recover.

2.9.1. Water surface elevation mapping

The steady-flow component of the modeling system uses a standard step method intended for the solution of water surface profiles for steady, gradually varied flow. The momentum equation may be used when the water surface profile is rapidly varied in conditions such as a mixed flow regime. The system can handle a full network of channels, a dendritic system, or a single river reach. The steady-flow component is capable of modeling subcritical, supercritical, and mixed-flow regime water surface profiles.

HEC-RAS can perform inundation mapping of water surface profile results directly using the RAS Mapper or the external HEC-GeoRAS tool. Using the HEC-RAS geometry and computed water surface profiles, RAS Mapper creates an inundation depth and floodplain boundary dataset. Additional geospatial data can be generated for analysis of velocity, shear stress, stream power, ice thickness, and floodway encroachment data. HEC-GeoRAS is a set of GIS tools that prepare the geometric data for import into HEC-RAS and generate the flood inundation data from the HEC-RAS output, (FEMA, 2013).

2.9.2. Flood velocity and water depth mapping

According to (FEMA, 2012), the water depth and velocity constitute the most important factors to understand the water flow and flood procedure, which depends on the failure scenario, distance from the dam, and the morphometric of the inundation area. They directly affect the potential for damage to structures, loss of life, and impact on the environment. As the depth of water inside structures increases, the damage increases. Nevertheless, even shallow water flowing at high velocity can considerably damage a structure, especially when the water carries debris. Excessive water velocity can lead to increased erosion and the loss of environmental assets. The failure scenario, distance from the dam, and topography of the inundation area can affect depth and velocity in various ways. Consider the following examples:

I. If the scenario is the discharge of a limited amount of water due to a malfunction of the dam, the depth and velocity of the water moving through the inundation area may be no more than the depth of water in the watercourse during heavy rain.
II. If the scenario is a sudden collapse of the dam and release of a large amount of water, the depth and velocity of water moving through the inundation area would be greater closer to the dam and somewhat reduced farther from the dam if the topography allows for the water to spread out across flat areas or to be diverted into numerous channels.

Depth and velocity of water depend on several variables, including Failure scenario under consideration, the volume of impoundment and height of the dam, distance from the dam, the topography of inundation area, the existence of levees, and opportunities for the flow of water to be impeded.

A qualitative review of the map of the inundation area can provide insight into the potential depth and velocity of water at various locations. Depth and velocity affect the potential for damage to structures, loss of life, and impacts on the environment.

1. As the depth of water inside structures increases, the damage increases. However, even shallow water moving at high velocity can significantly damage a structure or move it from its foundation.
2. Flowing water can carry debris, which may collide with existing structures or infrastructure and cause significant damage.
3. The faster the water moves the greater the chance of loss of life.

   I). People unable to evacuate may be trapped in a home or business that is being destroyed by high-velocity water or rising floodwaters.

   II). Emergency responders may not be able to access the area.

   III). Vehicles can be washed off roads and bridges - during a typical flood event the leading cause of death is people trapped in their vehicles.
4. Increased velocity will lead to increased erosion, or scour, and loss of environmental assets.

2.10. Flood Hazard Assessment

According to (Kreibich et al., 2009), the intensity of a flood is considered a widely accepted indicator for flood hazard estimation. Intensity refers to the attributes of a hazard that causes damage and is commonly calculated utilizing water depth and flow velocity (Equation 2.30).

Flood intensity = water depth × flow velocity……..... (2.30)

Hazard and risk maps are of particular importance for planning purposes, risk awareness campaigns, and the encouragement of private preventive measures.

The population-at-risk (PAR) includes those people present in the inundation flood zone at the time of failure, including permanent residents and transient individuals such as recreationists or the traveling public. A structure/vehicle/person shall be considered to contribute to the overall PAR when the depth-velocity relationship changes from a “low danger” to “high danger”, due to the breach, for any of the hydrologic conditions modeled, (Boulevard, 2018).

3. MATERIALS AND METHODS

3.1. Description of the study area

3.1.1. Location and Topography

Bisandima Dam irrigation project is located in the Gidabo sub-basin of the Rift Valley Lakes Basin found in the southern part of Sidama National Regional State, 80 km asphalt road from Hawassa City to Chuko town along Hawassa to Dila highway road and 11 km from Chuko town to the dam site in the East direction. The river is a tributary to the Gidabo River, which is one of the main feeders to Lake Abaya. The altitude of the Bisandima river catchment ranges from 1608 to 1920 m a.s.l. and the river floodplain at an average elevation of 1764m a.s.l. The slope generally inclines in a southeast-to-west direction. Flatter and gentler slopes suitable for irrigation are located immediately surrounding Dam and reservoir. Significant steeper slopes and ridges are found middle and tail or remote areas of the watershed. Based on the Digital Elevation Model (DEM) slope of the study area ranges from 0.0% to 40%. The total catchment area of the river draining to the dam outlet is 30.49 km^2.

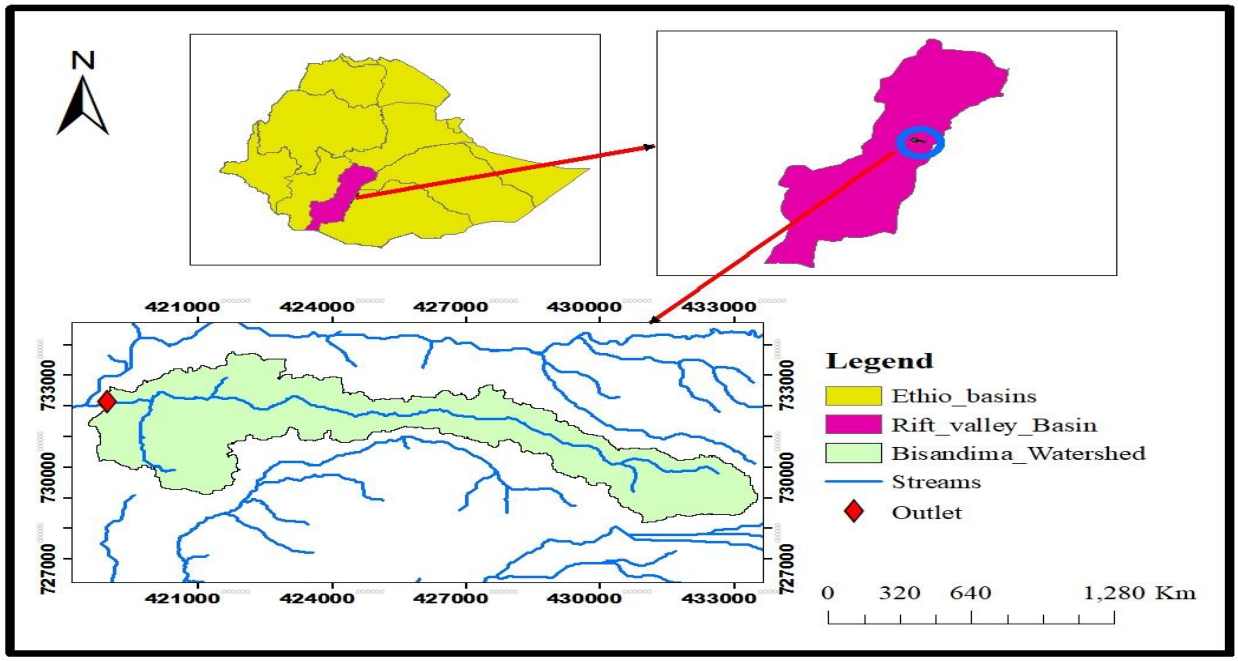

Figure 2: Location map of the study area

3.1.2. Climate

The climate in the Gidabo River Basin ranges from semi-arid in the rift floor to humid in the mountains of the escarpment. In the highlands and escarpment bounding the rift floor precipitation exceeds 1600 mm/year, whilst at the lowest altitude in the rift floor precipitation is often below 800 mm/year. Precipitation is characterized by a bimodal pattern with maximum peaks during April and May ("small rainy" season) and during September and October in the "main rainy" season. Like in most parts of Ethiopia, the diurnal variation of air temperature in the basin is more visible than its seasonal variation. Average monthly temperature varies from 21 °C to 25 °C on the rift floor to less than 11.5 °C to 13.5 °C in the high altitude plateau (highland), (Mechal et al., 2015). The computed long-term monthly rainfall values of representative stations located in the project area have been presented in Figure 3. From the figure, it can be observed that the maximum peak is during April and May and the next peak during September and October are the wettest months, while December to February generally the months with the lowest amount of rainfall recorded. The rainfall pattern in the project area is generally bi-modal type.

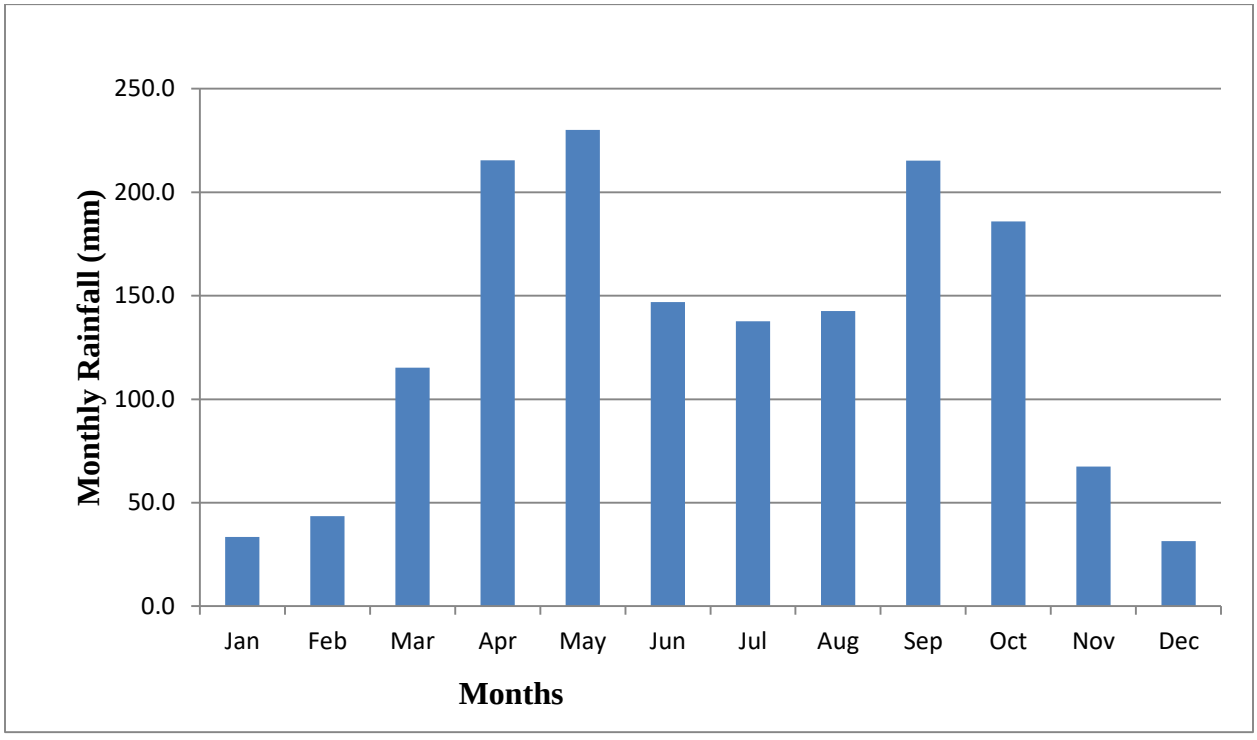

Figure 3: Monthly rainfall distribution of Aleta Wondo stations

3.1.3. Soil

The dominant soil type of the catchment is pellic vertisols cover 1604.84ha (53%) and chromic vertisols cover 1423.16ha (47%) of the area. The soil types of the hydrological soil group "D".

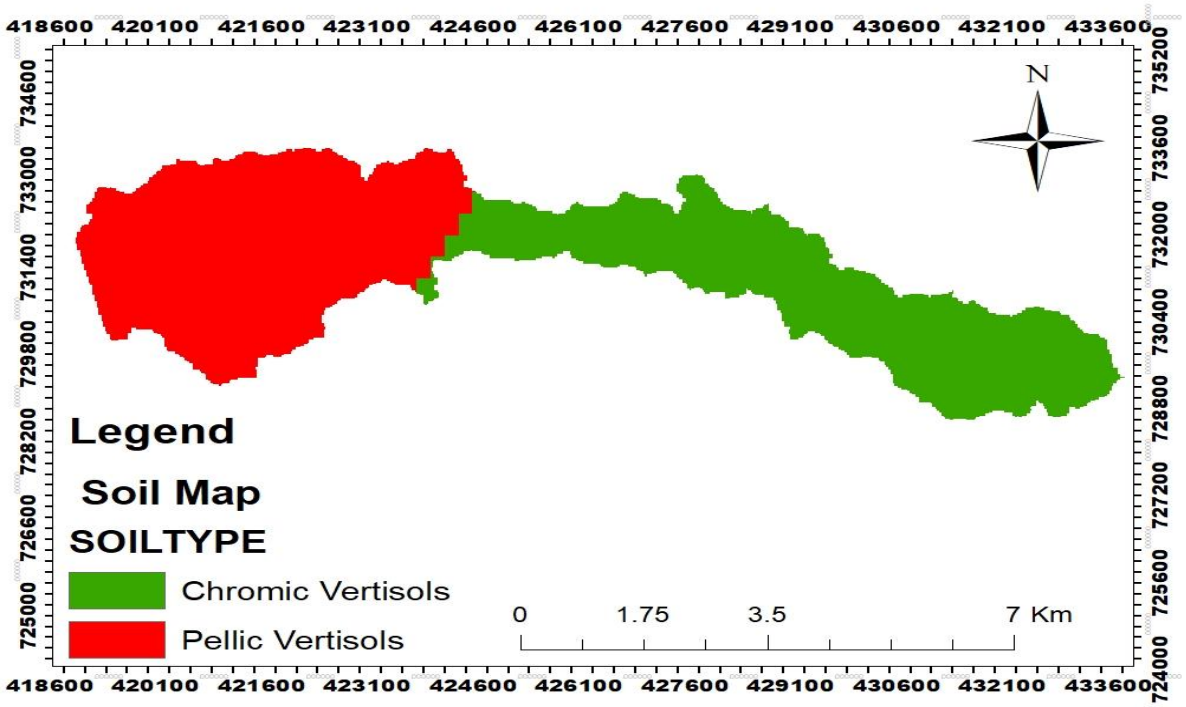

Figure 4: Soil map of the study area (ECDSWC)

3.1.4. Land Use/Land Cover

The rising demand for agricultural land, construction materials, fuel wood, and other natural resources over the past few decades has completely degraded the natural vegetation throughout the whole watershed. The majority of the land usage in the area is traditional rainfed farming as private holdings and traditional grazing on common fields. The overall farming system is heavily reliant on labor for land preparation and is strongly focused on producing grains and perennial crops. Most people keep several animals as moveable assets and for the production of milk byproducts. The primary sources of animal feed are crop residue and substantial grazing in catchment and command areas. In the upper and lower watershed, approximately 80% of the

land area is under intensive cultivation. Agriculture in the Bisandima watershed is dominated by rainfed production of seasonal, annual, and perennial crops such as maize, sugarcane, banana, inset (false banana), pineapple, coffee, and chat respectively. This crop growing covers the watershed as indicated in Figure 5.

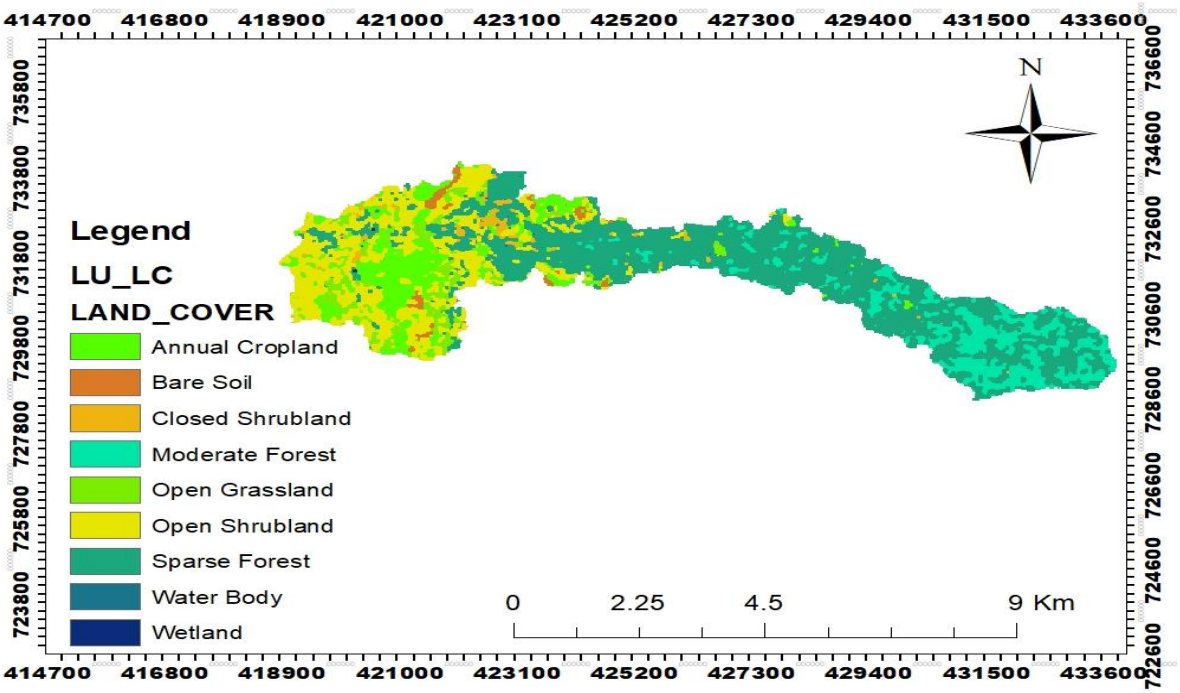

Figure 5: Land use/cover map of Bisandima watershed (ECDSWC)

3.2. Conceptual Framework

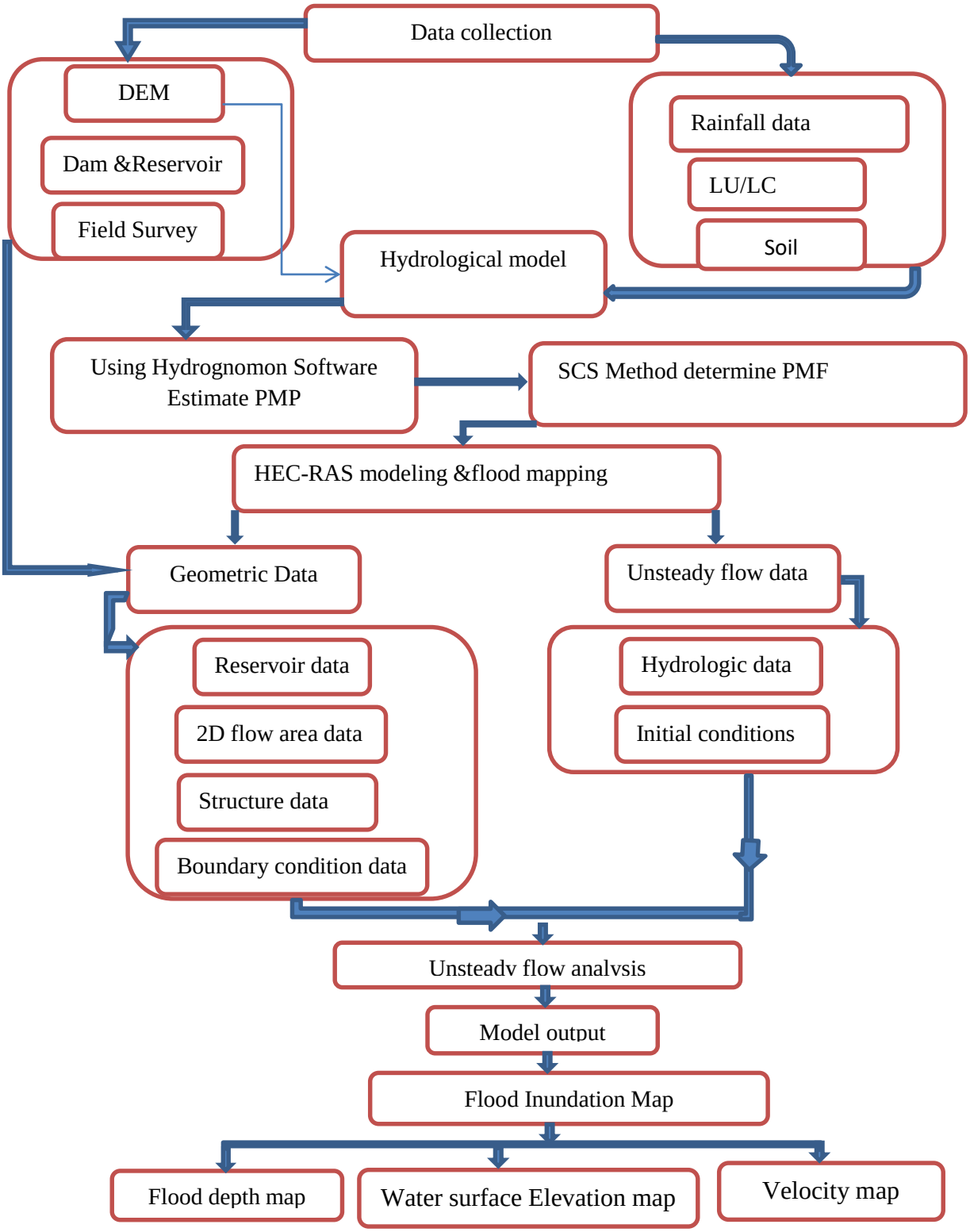

Figure 6: Conceptual framework

3.3. Data collection

To achieve this investigation, different primer and secondary data were gathered from different organizations and field surveys. Some of these data were rainfall data, topographic data, land use/land cover data of the catchment, soil data, reservoir characteristics, and dam characteristics. The rainfall data were collected from National Meteorological Service Agency (NMSA) for metrological stations within and around the catchment. The grid size 30m resolution land use/Land covers of the catchment and also 30m resolution soil data were collected from the GIS department of Ethiopian Construction Design and Supervision Works Corporation.

3.3.1. Primary data

Primer Data such as: - Topographic data is collected from a field detailed survey by using the Total-station of the Bisandima dam axis, reservoir area, and downstream of the dam site.

3.3.2. Secondary data

Different Secondary data was collected from different organizations. All necessary data and collected sources were presented below.

3.3.2.1. Dam and Reservoir data

The main components of the Bisandima dam are a zoned rockfill dam with a central clay core, an average slope of 1V: 2.26H upstream and 1V: 2.29H downstream, a 7m crest width, and a crest elevation of 1638m. The dam is 138 m in length along the crest and 21m in height. At full reservoir (maximum pool) level, the reservoir can accommodate 2.55 MCM. The area submerged at maximum water level is 72ha. The spillway type for the Bisandima Dam is a side ogee weir type designed with a crest level of 1633.7m a.s.l. As indicate Figure 7 storage area elevation relationship of the Bisandima reservoir and its table was attached on annex Table 9. Also the following figure 8 shows the physical characteristics of Bisandima Dam. This data was obtained from Ethiopian Construction Design and Supervision Works Corporation.

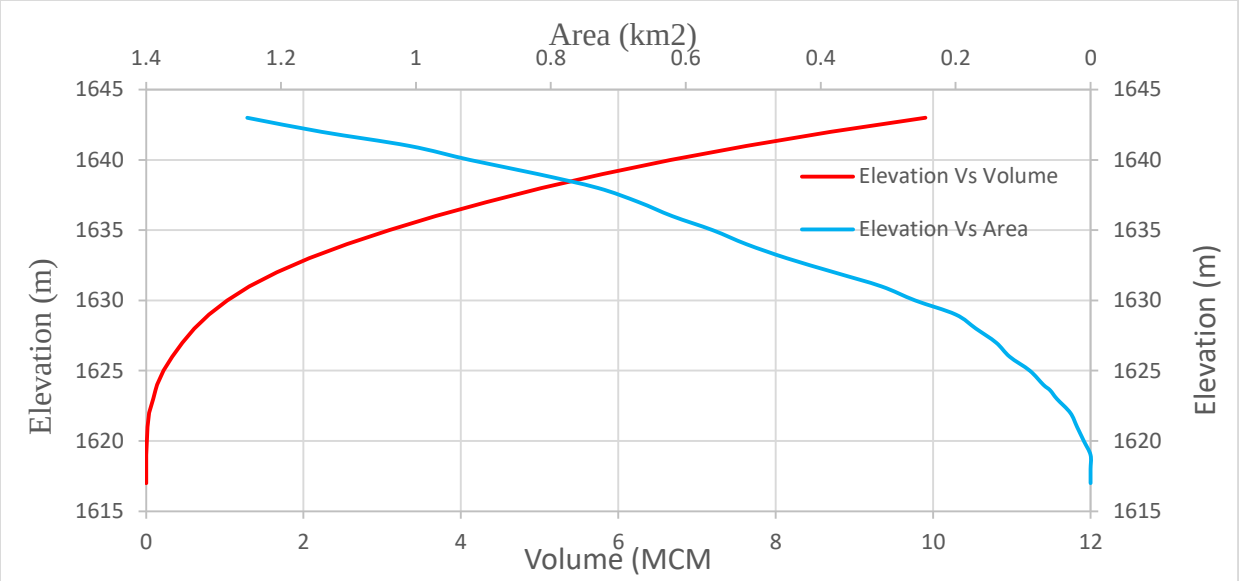

Figure 7: elevation volume area curve of the Bisandima reservoir

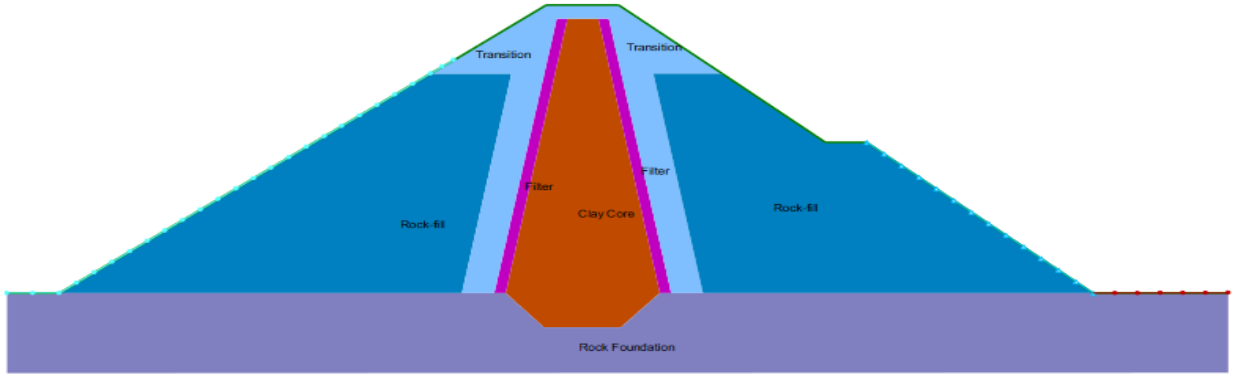

Figure 8: Section view of Bisandima Dam, (from Bisandima Dam final feasibility study and design document)

3.3.2.2. Digital Elevation Model (DEM)

To obtain elevation data for the area under investigation, Digital Elevation Models (DEMs) were used. To generate reliable flood-inundation maps, high-resolution elevation data is needed, according to Saksena (2015). Maps of floods and inundations are more accurate the more precise the elevation data. Therefore 5m grid DEM was created from actual topography data surveyed by using the total station on the field dam axis, around the reservoir area, and downstream 2D area or flood inundation area, as indicated in figure 10, and in annex, table 8. But for the watershed delineation we used 30m DEM which is obtained free download from (USGS).

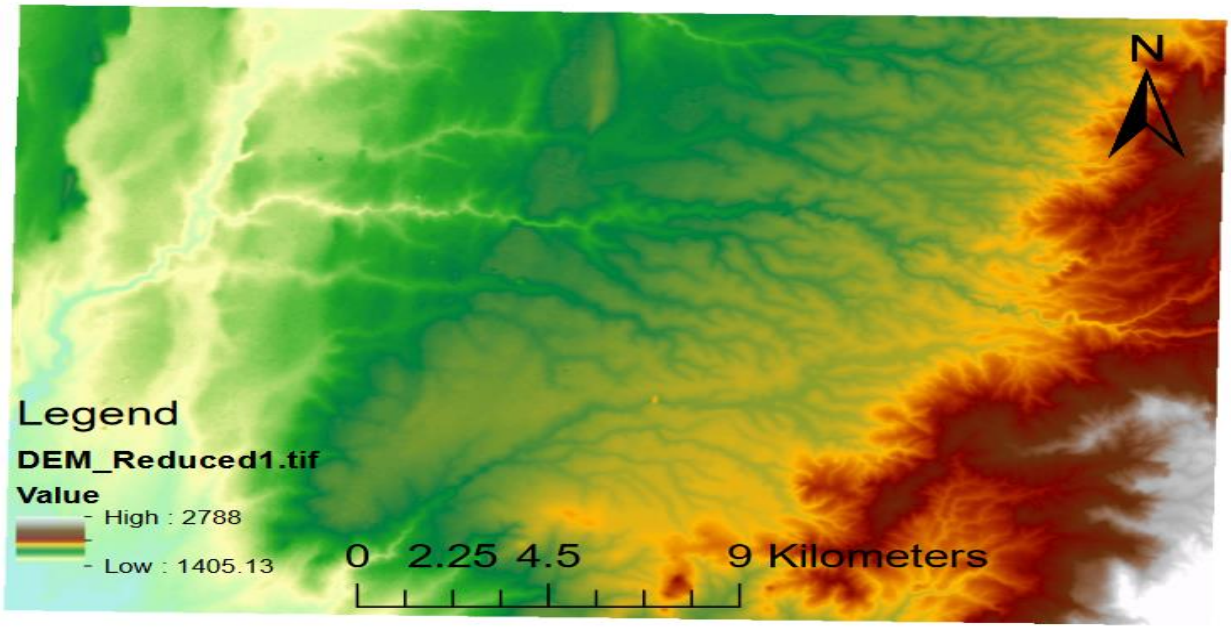

Figure 9: Digital Elevation Model (DEM) 30m resolution

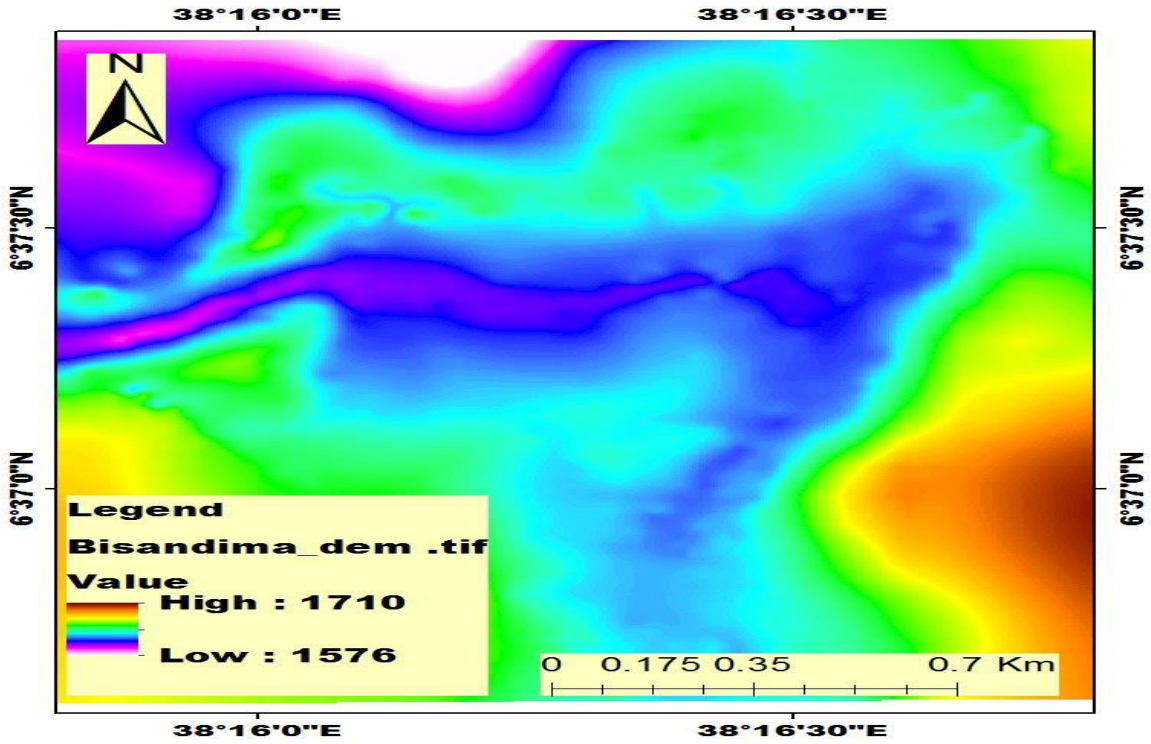

Figure 10: Digital Elevation Model (DEM) 5m resolution

3.3.2.3. Meteorological data

Meteorological data for selected rain gauge stations were collected from the National Meteorological Service Agency. Four stations with more than thirty years of daily rainfall data were collected within and around the catchment. Table 3 presents the longitude, latitude, elevation, and data range of the four selected stations. Aleta Wondo station was found in the watershed and to be representative of the catchment and selected for further analysis. The other three stations around the catchment were used to fill the gaps in the daily rainfall series in the selected station.

Table 3: Location of metrological stations within and around the catchment

No.	Station name	Latitude (m)	Longitude (m)	Elevation (m)	Record period	No. year	Class
1	Aleta Wendo	435280	731007	1878	1986-2020	35	3
2	Haisawita	437059	728016	2249	1991-2020	30	3
3	Aposto/Yekatit 25	429990	746056	1737	1989-2020	31	4
4	Yirgalem	431496	755097	1748	1991-2020	30	3

3.4. Data analysis

3.4.1. Data quality assessments

(I). Filling missing rainfall data

As data series received from NMSA stations contains missing data inside the record, the arithmetic mean method was utilized to fill in the missing data using at least three stations since the average yearly precipitation at each of the nearby stations surrounding the gauge with missing data is within 10% of that of the missing data. According to (Subramanya, 2008), given the annual precipitation values, P_1, P_2, P_3,. . ., P_m at neighboring M stations 1,2,3,..m, respectively, then the missing annual precipitation P_x *was* estimated by equation 3.1.

Px =1/M*[P1+P2+……+Pm]…….. (3.1)

II). Rainfall data consistency assessment

The checking for consistency of rainfall records has been done using the method of double mass curve analysis. This technique is based on the principle that when each recorded data comes from the same parent population, they are consistent. Double mass curve analysis is a graphical method for identifying and adjusting inconsistency in a station record by comparing its time trend with those of adjacent stations. For this purpose, the double mass curve technique was applied using Hydrognomon version 4.1.0 (University of Athens, ITIA research team, 2012). Hydrognomon is capable of performing many of the statistical procedures in hydrology. It is such a powerful tool for double mass curve analysis.

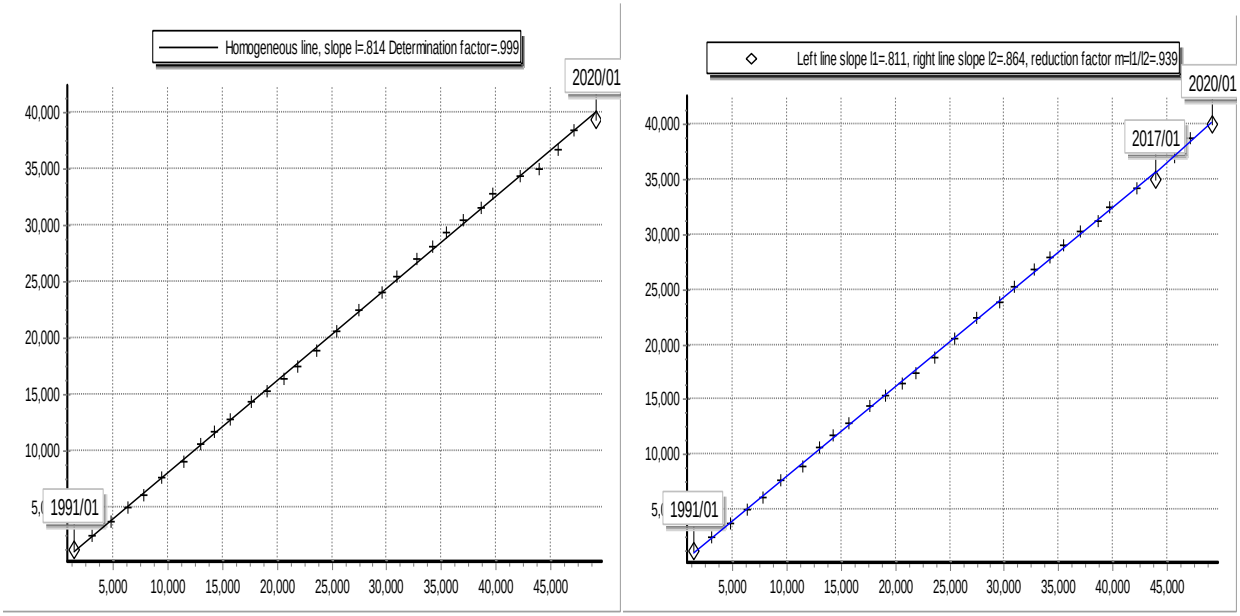

(a). Double mass plot before correction (b). Double mass plot after correction

Figure 11: Double mass plot of Aleta Wondo station versus other stations (a & b).

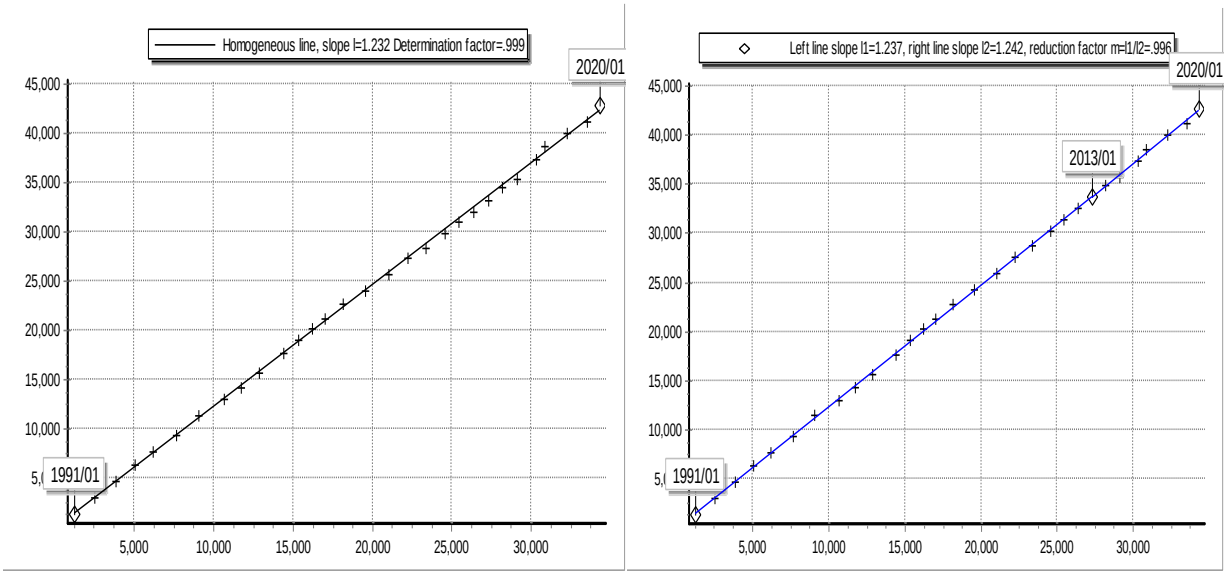

(a). Double mass plot before correction (b). Double mass plot after correction

Figure 12: Double mass plot of Yirgalem station versus other stations (a & b).

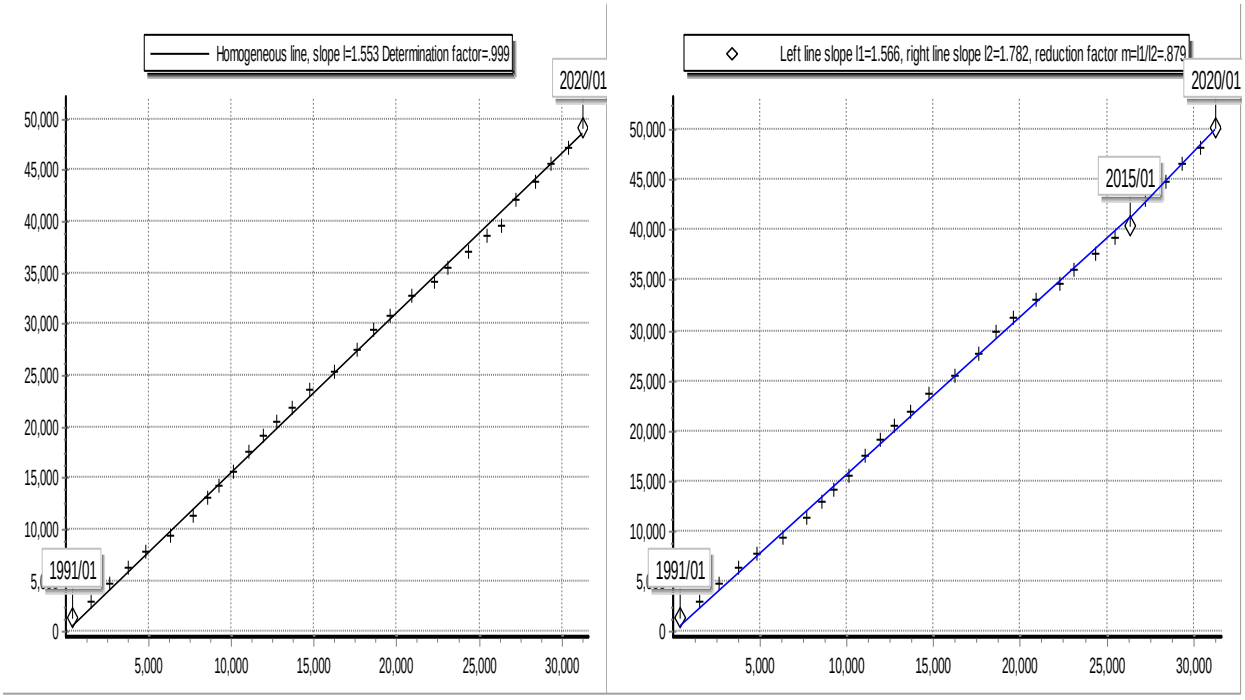

(a). Double mass plot before correction (b). Double mass plot after correction

Figure 13: Double mass plot of Aposto/Yekatit 25 stations versus other stations (a & b).

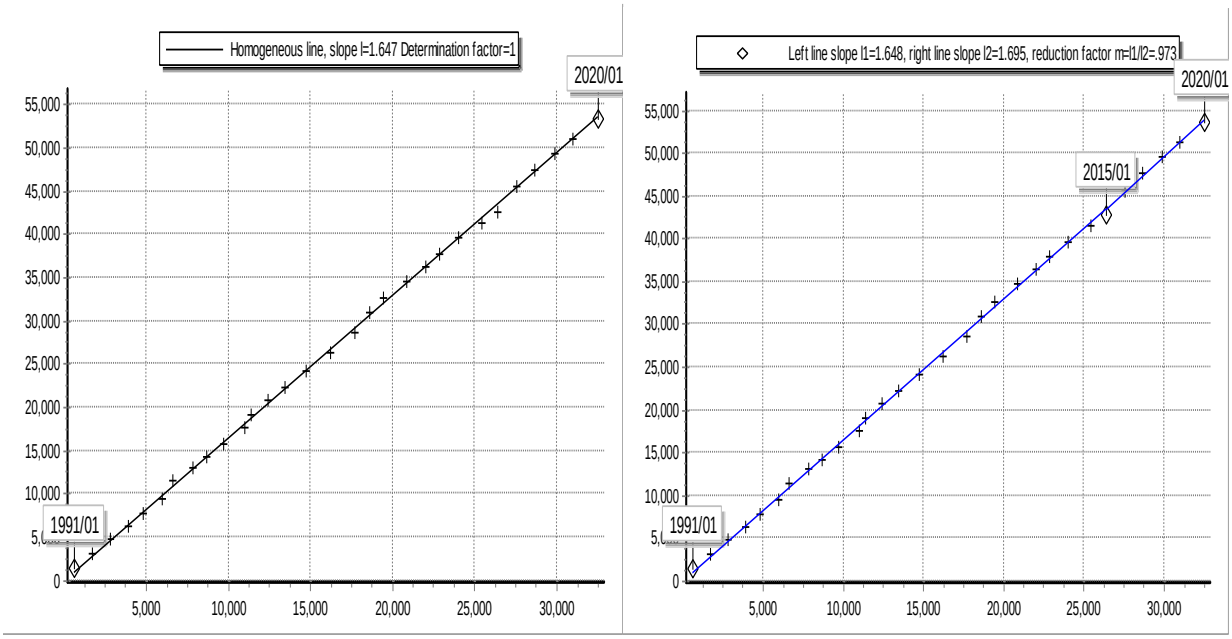

(a). Double mass plot before correction (b). Double mass plot after correction

Figure 14: Double mass plot of Haisa Wita station versus other stations (a & b).

III). Outlier test

Before performing frequency analysis based on the 24 hours maximum rainfall, the outliers need to be checked. Errors in data may occur during recording or reporting. The quality and consistency of data were checked by the outlier test as depicted below. For checking the low or high outlier values the relationship given below was applied. For the coefficient of skewness (Cs) of lower than -0.4, the data should be checked first for the lower outlier test otherwise the checking will be done for the higher outliers. (Engineering Hydrology Books, (Subramanya, 2008).

Lower outlier

$Y_{lo}=Y_{avg} -K_n*S_y$---------- (3.2)

Where,

Y_{lo}: Low outlier,

Y_{ang}: Mean of samples converted to a logarithmic value,

K_n: Coefficient of frequency and

S_y: Standard deviation.

Low outliers should check for the lower value of less than $10^{\wedge Ylo}$

Higher outlier

$Y_{ho}=Y_{avg}+K_n*S_y$---------- (3.3)

Where,

Y_{ho}: high outlier,

High outliers should check for a higher value of greater than $10^{\wedge Yho}$

3.4.2. Estimation of the probable maximum precipitation

According to (WMO, 2009) PMP which helps in calculating PMF is the largest depth of precipitation for a given duration that is physically possible over a particular area and geographical location at a certain time of the year. It may also be used to determine the extent of floodplain areas at risk in extreme flood conditions. If a spillway is not able to safely release the PMF, a breaching of the dam will occur due to overtopping and cause heavy loss of lives and damage to property. Hydrognomon is a software tool for the processing of hydrological data. Here the emphasis is given to the statistical module of Hydrognomon, which provides tools for fitting distribution functions and statistical prediction. Therefore this Hydrognomon tool was used to estimate the PMP of the study area. The frequency analysis was carried out using the annual 24-hour maximum rainfall data of Aleta Wendo station see in annex, table 1 and fitting to the best probability distribution (PDF) as per Kolmogorov-Smirnov and x-square tests acceptance. The frequency analysis was performed using Hydrognomon 4.1.0 software. According to the test, GEV-Max (kappa specified, L-Moments) distribution fits best for the Kolmogorov-Smirnov test, as seen in annex table 2. For the estimation of the maximum rainfall, however, among GEV-Max (Kappa specified, L-Moments) distribution is selected and 24 hrs Maximum rainfalls for Different Return Periods were computed shown in annex table 4.

3.4.3. Probable maximum flood and It's a hydrograph

While utilized as the upstream boundary condition in the HEC-RAS model, the composite hydrograph can be used as input. The standard dimensionless SCS unit hydrograph was used in this work to calculate the inflow hydrograph for the Bisandima dam site. The Soil Conservation Service (SCS) dimensionless unit hydrograph is widely used for hydrologic design. The technique makes use of a dimensionless unit hydrograph along with the drainage area, runoff volume depth, peak time, and SCS peak rate factor. The standard SCS-CN method is based on the following relationship between rainfall, *P* (mm), and runoff, *Q* (mm) (Smithers, 2012).

$$Q = \frac{(P-0.2S)^2}{P+0.8S} \quad \text{..... (3.4)}$$

Where *S* (mm) is the potential maximum retention after runoff begins, which varies with antecedent moisture condition, soil type, and land use/cover, can be estimated as.

$$S = \frac{25400}{CN} - 254 \quad \text{..... (3.5)}$$

Where CN is the runoff curve number

3.4.3.1. GIS-based SCS-curve number determination

In the soil conservation service (SCS) method the curve number determination is the most important task. CN is a dimensionless catchment parameter ranging from 0 to 100. A CN of 100 represents a limiting condition of a perfectly impermeable catchment with zero retention, in which all rainfall becomes runoff. A CN of zero conceptually represents the other extreme, with the catchment abstracting all rainfall and with no runoff regardless of the rainfall amount. The curve number can be determined from empirical information. The SCS has developed standard tables of curve number values as functions of catchment land use/land cover conditions and hydrologic soil group (SCS-USDA, 1986)

The HSG refers to the standard SCS soil classifications ranging from A, which refers to sand and aggregated silts with high infiltration rates, to classification D, which corresponds to soils that swell significantly when wet and have low infiltration rates. The HSG reflects a soil's permeability and surface runoff potential. Table 4 Summarizes the HSG characteristics, (Schulze et al., 1992).

Table 4: Summary of HSG characteristics, (Schulze et al., 1992).

Hydrologic soil group	Surface runoff potential
A	Low
B	Moderately low
C	Moderately high
D	High

For a catchment with sub-areas that have different soil types and land use, a composite curve number CN_c was determined by weighting the curve number values for the different sub-areas in proportion to the land area associated with each, (Desta, 2021).

$$CN_c = \frac{CN_1A_1+CN_2A_2+CN_3A_3+\cdots CN_iA_i}{A_1+A_2+\cdots+A_n} \quad \text{..... (3.6)}$$

Where CN_i is the curve number of the sub-area I, A_i is the area of the sub-area I, and n is the total number of sub-areas.

For this study, a method for SCS-CN determination using GIS-based. Land use/land cover and soil type shape files are first were obtained and compiled in a GIS. Soil and land use shape files are intersected using GIS techniques, to generate new shape files associated with the hydrologic soil group and land use names. This step keeps all the details of the spatial variation of soil and land use. The curve number database was built based on the intersected land soil layer and its relation to the attribute table. Finally, the runoff curve number was determined by using SCS. According to the ERA Manual of Hydrology, (2002) for antecedent moisture conditions (AMC) in Ethiopia Bisandima catchment is under region B as a result average AMC is used.

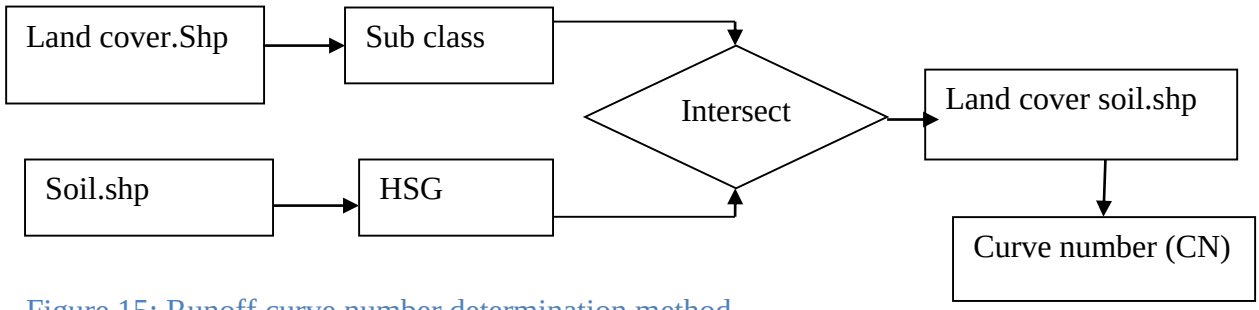

Figure 15: Runoff curve number determination method

The above figure shows the methods used for generating the runoff curve number by intersecting land use shape file and hydrologic soil group.

3.4.3.2. Parameters of the inflow hydrograph

To determine the inflow hydrograph of the catchment the drainage network above the dam site was determined a DEM of 30m x 30m was used in the Arc Hydro tool in the GIS. The GIS processing phase includes the derivation of the important morphological characteristics such as maximum time of flow concentration (TC), the longest flow length (*L*), the centroidal flow length (L_c), and the average slope, (Subramanya, 2008).

3.4.4. Dam breach parameters estimation

One of the capabilities of the HEC-RAS is the possibility to calculate the breach parameters inside the software. For this study, the breach parameters were calculated by using the HEC-RAS breach parameter calculator. The selected methods were Froehlich (1995), Froehlich (2008), Macdonald and Langridge-Monopolis (1984), Von Thun and Gillette (1990), and Xu and Zhang (2009). Because the methods utilized more than 40 case studies or data sets to develop a set of equations to predict dam breach parameters, (Brunner, 2014).

1. **Froehlich (1995):** Froehlich utilized 63 earthen, zoned earthen, earthen with clay core wall (i.e., clay), and rock fill data sets to develop a set of equation to predict average breach with, side slopes, and failure time. The data that Froehlich used for his regression analysis had the following ranges such as the height of dams (3.66m-92.96m), the volume of water at breach time (0.0130-660.0x $10^6 m^3$)

Froehlich's (1995) regression equations for average breach width and failure time are:

$$B_{ave} = 0.1803 K_o V_w^{0.32} h_b^{0.19} \quad \text{(3.7)}$$

$$T_f = 0.00254 V_w^{0.53} h_b^{-0.9} \quad \text{(3.8)}$$

Where:

- B_{ave}=average breach width (m)
- K_o=constant (1.4 for over-topping failure, 1.0 for piping), (Brunner, 2014)
- V_w=reservoir volume at the time of failure (m^3)
- h_b=height of the final breach (m)
- T_f=breach formation time (hr)

Froehlich (1995) states that average side slopes should be 1.4H: 1V overtopping failure and 0.9H: 1V piping failure.

2. **Froehlich (2008)**: Dr. Froehlich utilized 74 earthen, zoned earthen, earthen with a core wall (i.e., clay), and rock fill data sets to develop a set of equations to predict average breach width side slopes and failure time. The data that Froehlich (2008) used for his regression analysis had the following ranges such as the height of dams (3.05m-92.96m), the volume of water at breach time (0.0139-660.0x $10^6 m^3$)

Froehlich's (2008) regression equations for average breach width and failure time are given below.

$$B_{ave} = 0.27 K_o V_w^{0.32} h_b^{0.04} \quad \text{..... (3.9)}$$

$$T_f = 63.2\sqrt{V_w / h_b^2 g} \quad \text{.....(3.10)}$$

Where:

- K_o=constant (1.3 for over-topping failure, 1.0 for piping), (Brunner, 2014)
- g=acceleration due to gravity (g=9.81)

Froehlich (2008) states that average side slopes should be 1.0H: 1V for overtopping failure and 0.7 H: 1V for piping failure.

3. **Macdonald and Langridge-Monopolis (1984):** MacDonal and Langridge-Monopolis utilized 42 data sets (predominantly earth fill dams, earth fill dams with clay core and rock fill dams) to develop a relationship for what they call the "Breach Formation Factor". The Breach Formation Factor is a product of the volume of water coming out of the dam and the height of water above the dam. MacDonald and Langridge-Monopolis then related the breach formation factor to the volume of material eroded from the dam's embankments. The data that MacDonald and Langridge-Monopolis used for their regression analysis had the following ranges such as the height of dams (4.27m-92.96m), the Breach outflow volume (0.0037-660.0x$10^6 m^3$)

The following equations show the volume of material eroded and breach formation time for earth-fill dams.

Earth fill dam:

$$V_{eroded} = 0.0261(V_{out}h_w)^{0.769} \quad \text{(3.11)}$$

$$T_f = 0.0179V_{eroded}^{0.364} \quad \text{(3.12)}$$

Where:

- V_{eroded}= volume of material eroded from the dam embankment (Cubic meter)
- V_{out}=volume of water that passes through the breach (Cubic meter)
- h_W=depth of water above the bottom of the breach (meter)

According to the state of Washington, (1992) the bottom breach width can be calculated as;

$$W_b = \frac{V_{eroded} - (CZ_b + (h_b Z_b Z_3)/3)h_b^2}{h_b(C + \frac{h_b Z_3}{2})} \quad \text{(3.13)}$$

Where:

- W_b =bottom width of the breach (meters)
- h_b =height from the top of the dam to the bottom of the breach(meters)
- Z_3 $=Z_1+Z_2$
- Z_1 = average slope (Z_1:1) of the upstream face of the dam
- Z_2 = average slope (Z_2:1) of the downstream face of the dam
- Z_b =side slopes of the breach (Z_b: 1), 0.5 for the MacDonald method

MacDonald and Langridge-Monopolis (1984) stated that the breach should be trapezoidal with side slopes of 0.5H: 1V.

4. **Von Thun and Gillette (1990):** They used the data of Froehlich (1987) and MacDonald and Langridge-Monopolis (1984) to develop some breach parameters. In their work, they assumed that side slopes of a breach are 1H: 1V except for dams that have cohesive shells or very wide cohesive cores, where slopes of 1:2 or 1:3 (H: V) are more acceptable. The relation proposed by Von Thun and Gillette (1990) is for the average breach width, and it is given by equation (3.14)

$B_{avg} = 2.5h_w + C_b$…….(3.14)

Where:

h_w = the depth of water at the dam at the time of failure (m)

C_b = is constant and dependent on the reservoir storage (see Table 5)

Table 5 Values of C_b according to the reservoir size, (Brunner, 2014)

Size of the reservoir (m^3)	C_b (m)
$<1.23x10^6$	6.1
$1.23x10^6$-$6.17x10^6$	18.3
$6.17x10^6$-$1.23x10^7$	42.7
$>1.23x10^7$	54.9

They plotted the volume of the eroded embankment versus water outflow volume and water depth above the breach invert, with upper bounds of reasonable breach geometry estimates. This method is dependent on the amount of erosion that occurs:

tf (hr) = 0.020hw + 0.25 (erosion resistant)

tf (hr) = 0.015hw (easily erodible)

Where:

tf should be in hours

5. **Xu and Zhang (2009):** Recently developed non-dimensional empirical equations based on 75 case studies for breach depth, breach top width, breach average width, peak outflow rate, and failure time.

$B_{ave}/H_b = 0.787(H_d/H_r)^{0.133}(V_w^{1/3}/H_w)^{0.652} e^{B_3}$ ……(3.15)

where:

H_b = height of the final breach (meters)

H_d = height of the Dam (meters)

H_r = fifteen meters, is considered to be a reference height for distinguishing large dams from small dams, (Brunner, 2014)

H_w = height of the water above the breach bottom elevation at the time of the breach (meters)

$B_3 = b_3+b_4+b_5$ coefficient that is a function of dam properties

b_3 = -0.041, 0.026, and -0.226 for dams with core walls, concrete-faced dams, and homogeneous/zoned-fill dams, respectively

b_4 = 0.149 and -0.389 for overtopping and seepage/piping, respectively.

b_5 = 0.291, -0.14, and -0.391 for high, medium, and low dam erodibility, respectively

$$T_f/T_r = 0.304(H_d/H_r)^{0.707}(V_w^{1/3}/H_w)^{1.228}\, e^{B_5} \quad (3.16)$$

Where:

T_r = 1 hour (unit duration)

$B_5 = b_3+b_4+b_5$ coefficient that is a function of dam properties

b_3 = -0.327, -0.674, and -0.189 for dams with core walls, concrete-faced dams, and homogeneous/zoned-fill dams, respectively

b_4 = -0.579 and -0.611 for overtopping and seepage/piping, respectively

b_5 = -1.205, -0.564, and 0.579 for high, medium, and low dam erodibility, respectively.

Breach side slopes can be computed with the following equation:

$$Z = (B_t - B_w)/h_b \quad (3.17)$$

3.5. Hydraulic model development

Several computer models are already available to simulate flooding, particularly flooding caused by dam breaches. HEC-RAS is one of the most power full software which is intensively used in hydraulic modeling. The newer version of HEC-RAS is capable of modeling 2D flow which is more appropriate to use in flood modeling. In this study, two-dimensional dynamic (unsteady-flow) modeling software, Hydrologic Engineering Centers River Analysis System (HEC–RAS 5.0.7) was used to simulate the hypothetical breach of the dam and its propagation downstream. The flowchart Figure 6, above outlines the standard modeling techniques for dam breaches and flood mapping. The hydraulic model analysis was carried out using HEC-RAS 5.0.7 software which is capable of modeling 2D flows. To provide better Maps, the output of flooding on important sites was processed in ARC GIS. Development of dam breach simulation using 2D-HEC–RAS model requires major data; Terrain/elevation data, hydraulic data/Manning's roughness coefficients, reservoir and dam profile data, breach parameters, and hydrologic Data as a boundary condition. These datasets were used in HEC–RAS (5.0.7) and GIS environment to simulate the hypothetical breach.

3.5.1. HEC-RAS Modeling

Manning's Roughness Coefficient

Manning's n values were used in the model to define roughness for the different land covers in the 2D area. The n-values were assigned by first defining land-use characteristics for common areas. This was done on high resolution rectified image produced by Smart GIS 2017. Each land-use characteristic was given an n-value based on published values for similar conditions (Chow, 1959); (Barnes, 1967). The roughness values associated with each land use within the model, area was then linked through land use terrain association in the geometric data editor on HEC–RAS 5.0.7

The latest version of HEC-RAS 5.0.7 now can perform two-dimensional flow routing. For the dam breach study the user can model the downstream area entirely with 2D elements (cross-sections, storage areas, and 2D flow areas); or the entire downstream area can be modeled as 2 D flow area. The first thing to do in HEC-RAS is to insert the tiff elevation file in the RAS Mapper with the appropriate projection. Once the tiff file is imported, then land use and land cover data are imported to create Manning's roughness coefficient (n). Manning's values were inserted in a table based on the land cover type and ID. Once this step was completed it is possible to go to the geometric editor window. RAS Mapper is also the component of the software where all the output results were displayed with background satellite maps. In the geometric editor window, all necessary data for the reservoir, dam, and flood area were inserted. There are different ways to model the reservoir but in our case, the reservoir was modeled as a storage area. The storage elevation, area, and capacity data of the reservoir were inserted here. The 2D flow areas were directly connected to the storage area by using a hydraulic structure called storage area/2D flow area hydraulic connector ("SA/2D Area connection"). All the data required for the dam break were also inserted in this section. The geometric data including the reservoir, the dam, and the 2D flow area downstream of the dam have been defined over a digital terrain model and are presented in Figure 16.

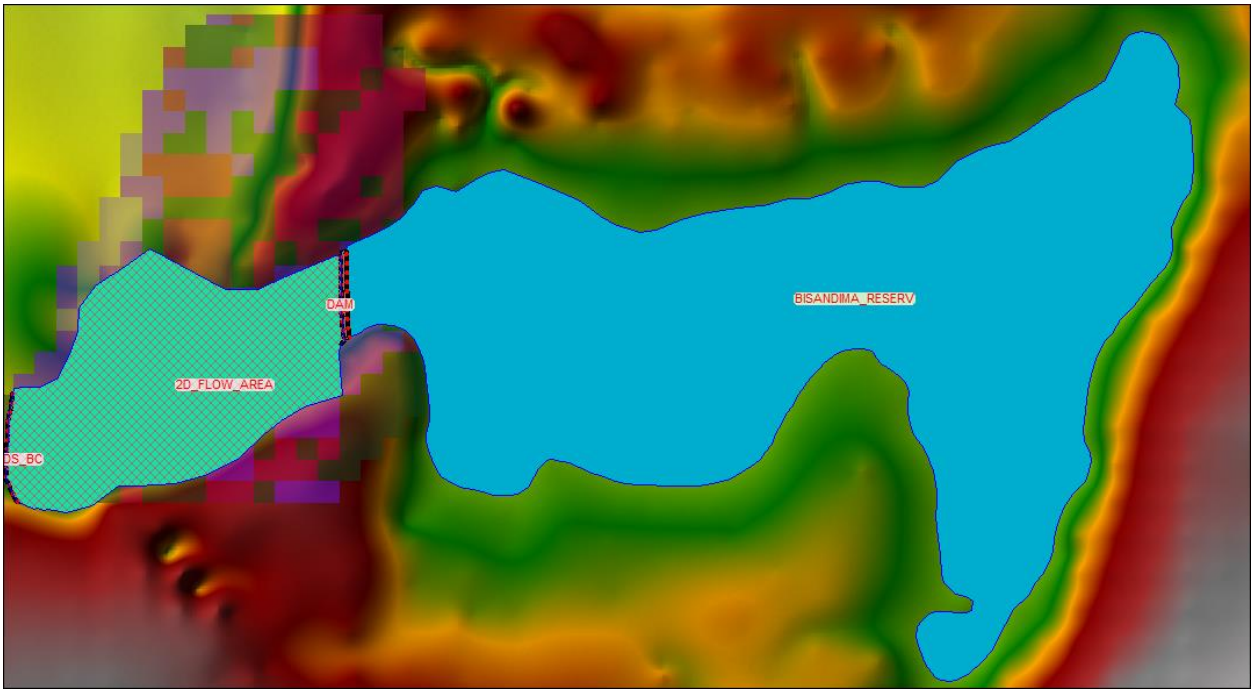

Figure 16: HEC-RAS Geometric data

And finally, the flood area will be marked using the 2D flow area editor tool. Using these tool downstream locations where flooding is expected will be marked. The area within the mark will be gridded into small cells where every cell represents a unique elevation. Once a 2D flow area is created, HEC-RAS will generate cross-sectional data at any given location for hydraulic computation. The Manning n value is also incorporated for every cell. Since HEC-RAS requires boundary conditions for hydraulic computations, both upstream and downstream boundary conditions were inserted using SA/2D Area BC line tool. Once all the required data were inserted in the geometric data editor window then the final input data such as inflow data, boundary condition, and initial conditions were given to the model. For the inflow data, the spillway design discharge was used where the boundary condition, normal depth, or slope at the outlet of the flow was used, (Leoul, 2015). For the initial condition, the reservoir water level was used. After these, the model was run and the outputs were displayed in RAS Mapper and exported to GIS to produce inundation maps and hazard maps.

3.5.2. Unsteady flow analysis

Flood is a typical example of unsteady flow since the stage of the flow changes instantaneously as the flood wave pass by, (Chow, 1960). Once all of the geometric data are entered into HEC-RAS, required unsteady flow data were entered to undertake the unsteady flood simulation.

The unsteady flow data required were boundary condition and initial condition. Unsteady flow data used as a boundary condition in this study were PMF Inflow Hydrograph and Normal depth. The PMF Inflow Hydrograph was used as an upstream boundary condition. Normal depth was used as a downstream boundary condition. In addition to the boundary condition, the initial condition should be established at the beginning of the unsteady flow simulation. The initial condition consists of flow and stage information at each of the cross sections, as well as elevations for any storage areas defined in the system (HEC, 2010). Once all the geometric and unsteady flow data have been entered, unsteady flow calculations were performed.

3.6. Flood Plain Mapping

One of the major advantages of dam breach modeling is to map the flood-affected area due to the breach outflow. After 2D unsteady flow analysis in HEC-RAS where water surface elevation at locations from upstream boundary to downstream boundary is observed on RAS Mapper window. This water surface elevation was used for flood mapping. For this study, the Floodplain mapping was prepared by using ArcGIS. HEC-GeoRAS was a set of ArcGIS tools which is specially designed to serve as a bridge between HEC-RAS and ArcGIS. It prepares geometric files on ArcGIS and also exports and imports geometric files from and to HEC-RAS and ArcGIS. To prepare the map in ArcGIS; GIS information was exported from HEC-RAS and read into the GIS with GeoRAS. The geo-referenced cross sections were imported and water surface elevations attached to the cross sections were used to create a continuous water surface. The water surface is then compared with the terrain model and the floodplain was identified where the water surface is higher than the terrain. HEC-GeoRAS produces inundation maps for flood extent and depth, (Desta, 2021).

4. RESULT AND DISCUSSIONS

Based on the methodology and input requirement of the model selected, all the necessary steps were undertaken and the dam breach analysis was simulated. So in this part, all the necessary results were shown and discussed to meet the objectives of this research.

4.1. Probable maximum precipitation

As mentioned in the methodology part Hydrognomon tools were used to estimate the probable maximum precipitation (PMP) of rainfall stations from the annual maximum daily rainfall of the rainfall stations within the study area. Finally, the depth of probable maximum precipitation calculated was 247.53mm. This areal PMP will be used for the computation of the inflow hydrograph.

4.2. Inflow Hydrograph

From the study, the computed composite inflow hydrograph resulting from triangular hydrographs at the dam site by using the standard dimensionless SCS unit hydrograph method has a peak flow of 307.43 m^3/s as shown in Figure 17. As a result there is a probability of occurrence of overtopping and piping failure. Furthermore, the computed inflow hydrograph was used as an upstream boundary condition for the 2D unsteady flow simulations in HEC-RAS.

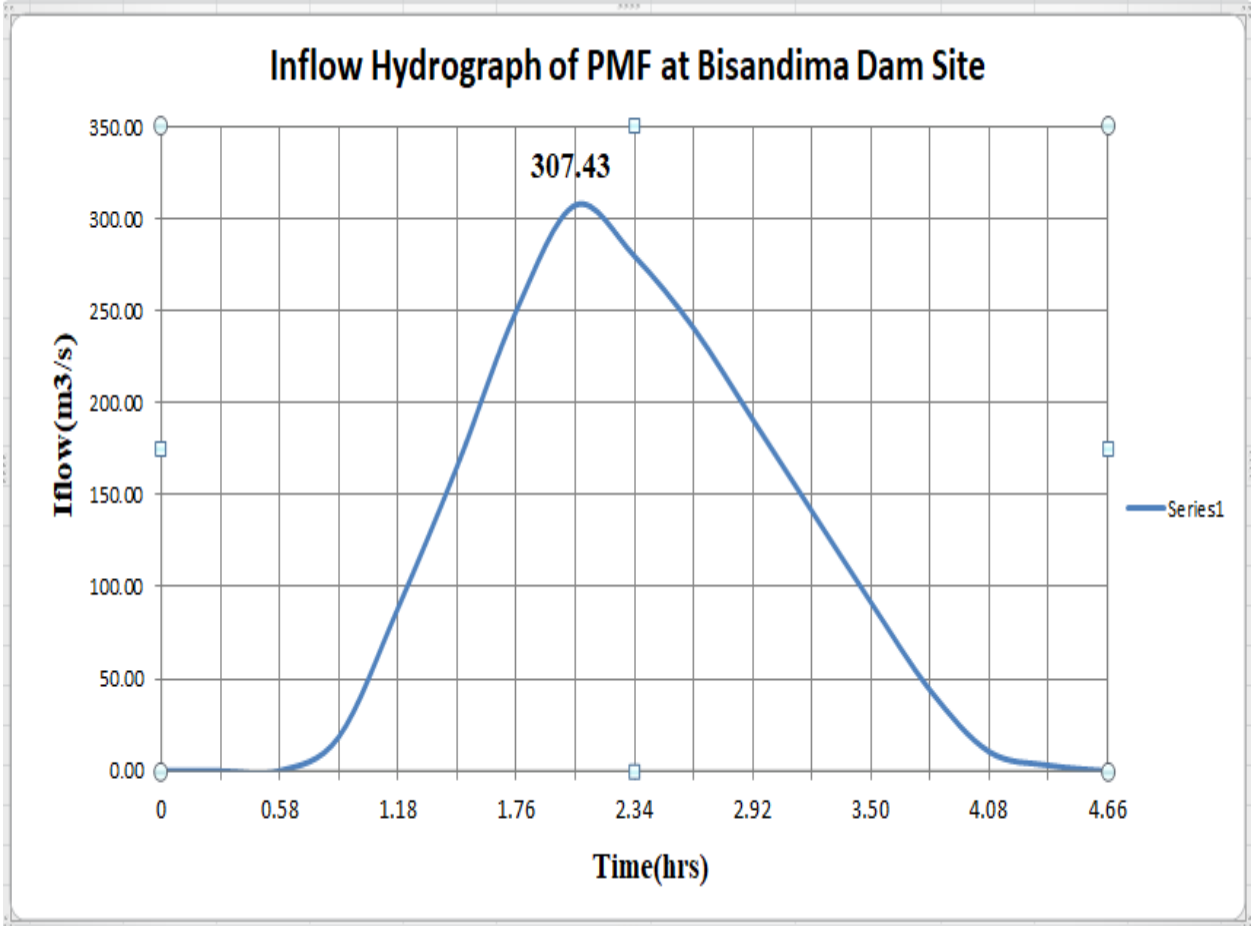

Figure 17: Inflow hydrograph at the dam site

4.3. Dam breach parameters

One of the most crucial tasks that need to be completed before 2D unsteady analysis is simulated on HEC-RAS is estimating the dam break parameters. The methods used to estimate breach parameters were given in Table 6. Breach parameters were estimated for both overtopping and piping and are used as input for HEC-RAS to determine the breach outflow hydrograph from the dam. Table 6 shows the results for the dam breach parameter for overtopping and the piping failure mode for all methods.

Table 6: Summary of estimated breach parameters

Method	Breach bottom width(m)	Breach side slopes (H: V)	Breach Development time (hours)
Overtopping case			
Froehlich (1995)	31	1.4	0.97
Froehlich (2008)	35	1	1.12
MacDonald et al	22	0.5	0.40
Von Thun & Gillette	31	0.5	0.38
Xu & Zhang	31	1.24	1.89
Piping case			
Froehlich (1995)	23	0.9	0.97
Froehlich (2008)	27	0.7	1.12
MacDonald et al	22	0.5	0.40
Von Thun & Gillette	31	0.5	0.38
Xu & Zhang	18	0.72	1.83

As indicated in Table 6, the result obtained from estimated breach bottom width, side slope, and development time. According to, (Desta, 2021), the result from estimated breach parameters such as breach bottom width, side slope, and development time for methods such as Froehlich(1995), Froehlich(2008), and MacDonald and Langridge-Monopolis(1984) was 143m, 1.4 and 2.57hrs; 127m, 1 and 2.35hrs and 322m, 0.5 and 2.14hrs respectively for overtopping. In dam breach analysis, the Case of Kesem Kebena Dam (Leoul, 2015), the result from estimated breach parameters such as breach bottom width, side slope, and development time for methods such as Froehlich (2008) were 215.14m, 1.0 and 1.98hrs and 136.95m, 0.7 and 1.53hrs for overtopping and piping failure respectively and MacDonald and Langridge-Monopolis (1984) were 356.13m, 0.5 and 4.36hrs and 148.7m, 0.5 and 3.81hrs for overtopping and piping failure respectively. According to the Koga dam breach parameter under the overtopping mode, (Dagne, 2020) the parameters were estimated using the three most currently used regression equations, i.e. Macdonald and Langridge-Monopolis (1984), Von Thun and Gillette (1990) and Froehlich (2008). For the case of overtopping failure, the bottom breach width for the three methods were

206 m, 91 m, and 117m respectively. Their breach development times were 1.6 hrs, 0.61 hrs, and 2.84 hrs. The estimated results of breach bottom width and development time were significant differences compared with the other estimated breach parameter result as shown above. Because, breach parameters, such as breach base width, side slope angles, and failure time, as functions of one or more dam and reservoir properties, such as storage volume, depth of water at failure, depth of breach, the volume of eroded material, etc. The large-reservoir/fast-erosion and small reservoir/slow-erosion cases, (Wahl, 2004).

4.4. Simulation results for the mode of failures

In this study's analysis of unsteady flow, the Bisandima River PMF inflow hydrograph and the normal depth of the area furthest downstream were utilized as boundary conditions, while the initial flow and elevation for the storage area were used as initial conditions. For comparison all the five empirical formulas were used to estimate breach parameters. Unsteady flow analysis of overtopping and piping in HEC-RAS is done for all methods. Using breach parameters from all five methods for unsteady flow analysis in HEC-RAS outflow hydrograph from the breached dam and hydrograph at the dam and downstream critical cross section were obtained after the unsteady flow simulation. Figure 18, Figure 19, and Figure 20 show flow hydrographs at the dam and at a critical point downstream from the dam for all methods for overtopping and piping mode of failure and downstream critical cross-section for overtopping failure case respectively. From the simulation results of this study the mode of failure such as overtopping and piping the methods tested for breach parameter estimation, method by Von Thun & Gillete (1990) and MacDonald and Langridge-Monopolis (1984) were found to be similar while methods such as Froehlich (1995), Froehlich (2008) and Xu & Zhang (2009) the breach formation time is similar but the two breach parameters: breach bottom width and breach side slope has a difference as shown in Table 6.

The simulation results of this study the modes of failure such as overtopping and piping the methods for peak outflow estimation, methods such as Von Thun & Gillete (1990), MacDonald and Langridge-Monopolis (1984), Froehlich (1995), Froehlich (2008) and Xu & Zhang (2009) as shown below. The simulation results obtained from the methods were different compared with the other previous study, for example 2D unsteady flow simulation the peak breach outflow from

Gidabo dam on HEC-RAS was found 15848.85m^3/s and 15194.9 m^3/s for Froehlich (1995) and Froehlich (2008) methods respectively, for overtopping mode of failure, (Desta, 2021). The computed peak outflow from the HEC-RAS model for both Froehlich (2008) (Qp = 123,685.8m3/s) and MacDonald and Langridge Monopolis (1984) (Qp = 72,670.8m3/s) for overtopping failure, (Leoul, 2015). Under overtopping failure, the peak outflow from the dam is about 4132.51m3/s (1 hour average peak the method used to estimate was Froehlich (2008), (Dagne, 2020). To relate the peak breach outflow to dam height, breach height, or depth of water above breach bottom), storage or outflow volume, or a product of height and volume. The breach outflow increases with the increase in this parameter which are in direct relation to each other.

4.4.1. Simulation results for the overtopping mode of failure

Overtopping failure occurs when the flood due to the PMF inflow passes over the embankment. Figure 18, shows the breach hydrograph estimates of each method. The breach from Von Thun & Gillete's (1990) estimation was the maximum, which was 2079.01m^3/s, while the maximum breach flow estimates based on Froehlich (2008), Froehlich (1995), MacDonald and Langridge – Monopolis (1984), Xu & Zhang (2009) were 1040.21, 1332.49, 531.91, 592.22 m^3/s respectively. Therefore, the capacity of the spillway was found to be inadequate to pass the PMF safely.

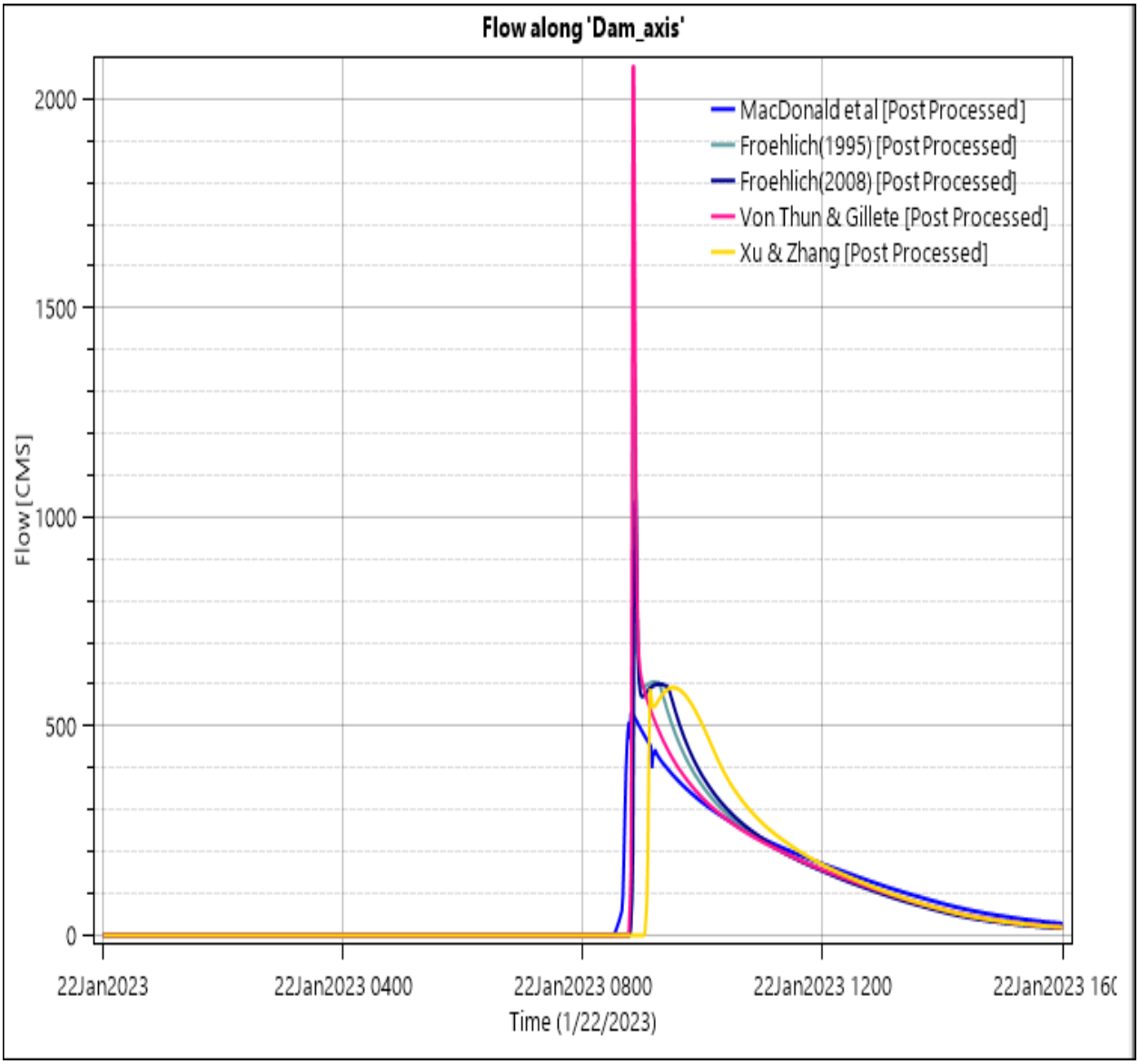

Figure 18: Dam breach outflow hydrographs for comparison for overtopping failure

4.4.2. Simulation results for a piping mode of failure

Piping is one of the most important causes of dam failure. Concentrated leak erosion, which occurs in cracks or a system of interconnecting voids, accounts for a large percentage of dam failures. As indicated in Figure 19, the breach outflow hydrograph estimation of each method. The unsteady flow analysis using HEC-RAS indicated that the maximum breach outflow was obtained from Von Thun & Gillete (1990) as 1796.52m^3/s, while the other method such as

Froehlich (2008), Froehlich (1995), MacDonald and Langridge –Monopolis (1984), Xu & Zhang (2009) were 620.37, 572.02, 530.53, 498.46 m^3/s respectively.

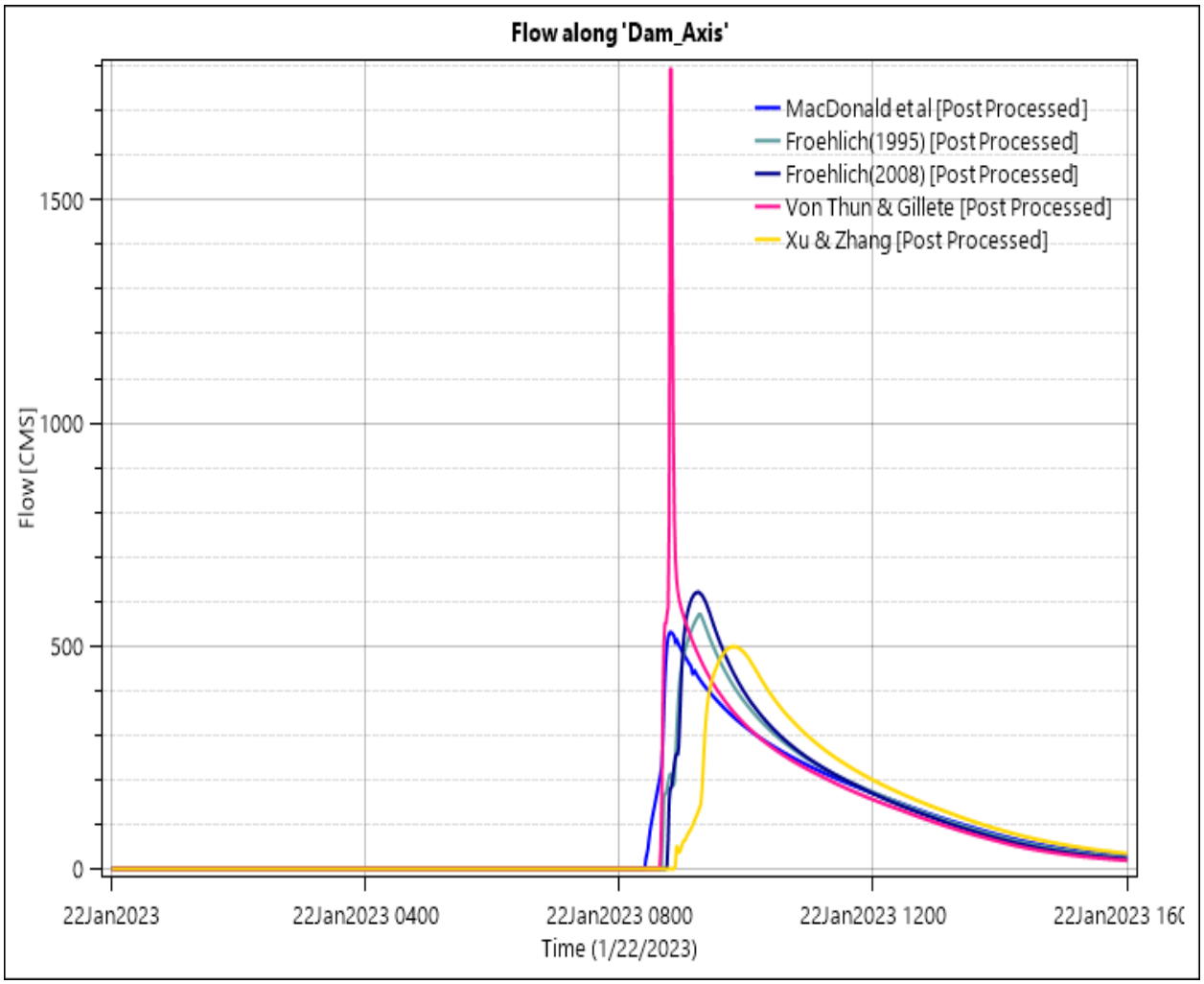

Figure 19: Dam breach outflow hydrographs for comparison of piping failure

4.4.3. Routing results of the downstream breach outflow

The maximum breach outflow was obtained for Von Thun & Gillete (1990) for both overtopping and piping mode of failure and the maximum breach outflow was obtained for overtopping failure mode compared to piping failure mode. Therefore downstream peak outflow flood routing is done in the case of overtopping. Each breach hydrograph was routed downstream. As indicated in Figure 20, the results from all the methods for the overtopping

failure are shown and this flow hydrograph is for the cross-section adjacent to the settlement zone. Also as indicated in Figure 20, the attenuated flow in m^3/s for the methods such as Froehlich (2008), Froehlich (1995), MacDonald and Langridge –Monopolis (1984), Xu & Zhang (2009) and Von Thun & Gillete (1990), were 625.48, 699.46, 538.96, 592.38 and 969.31 respectively.

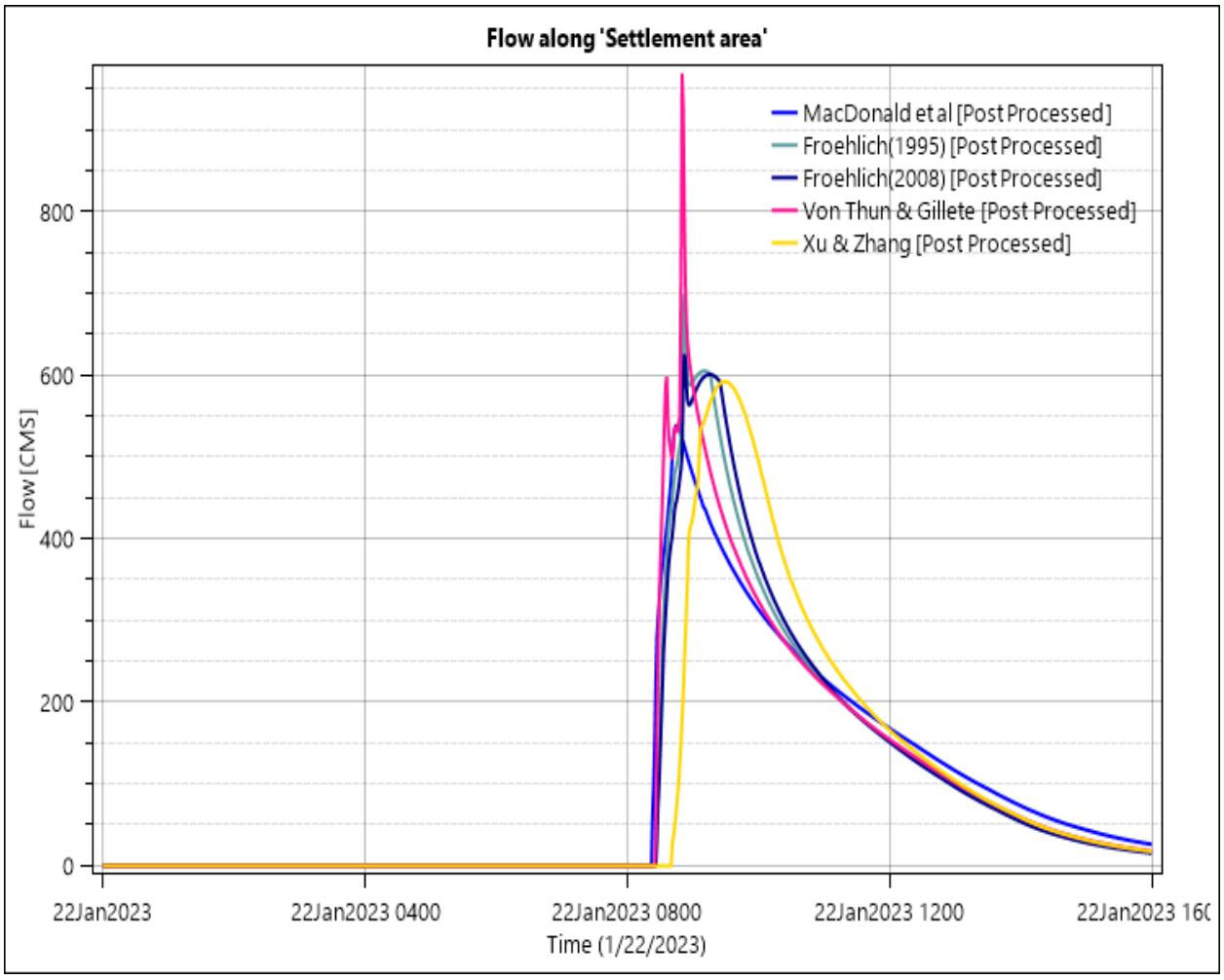

Figure 20 Attenuated breach hydrograph near the settlement areas for overtopping failure

4.5. Flood mapping

4.5.1. Flood inundation boundary polygon

The total areal coverage of the flood was found 52 hectares as read from the attribute table of ARC-GIS for the inundation polygon. Figure 21 and 22 present a flood inundation boundary map of the area for overtopping and piping failure.

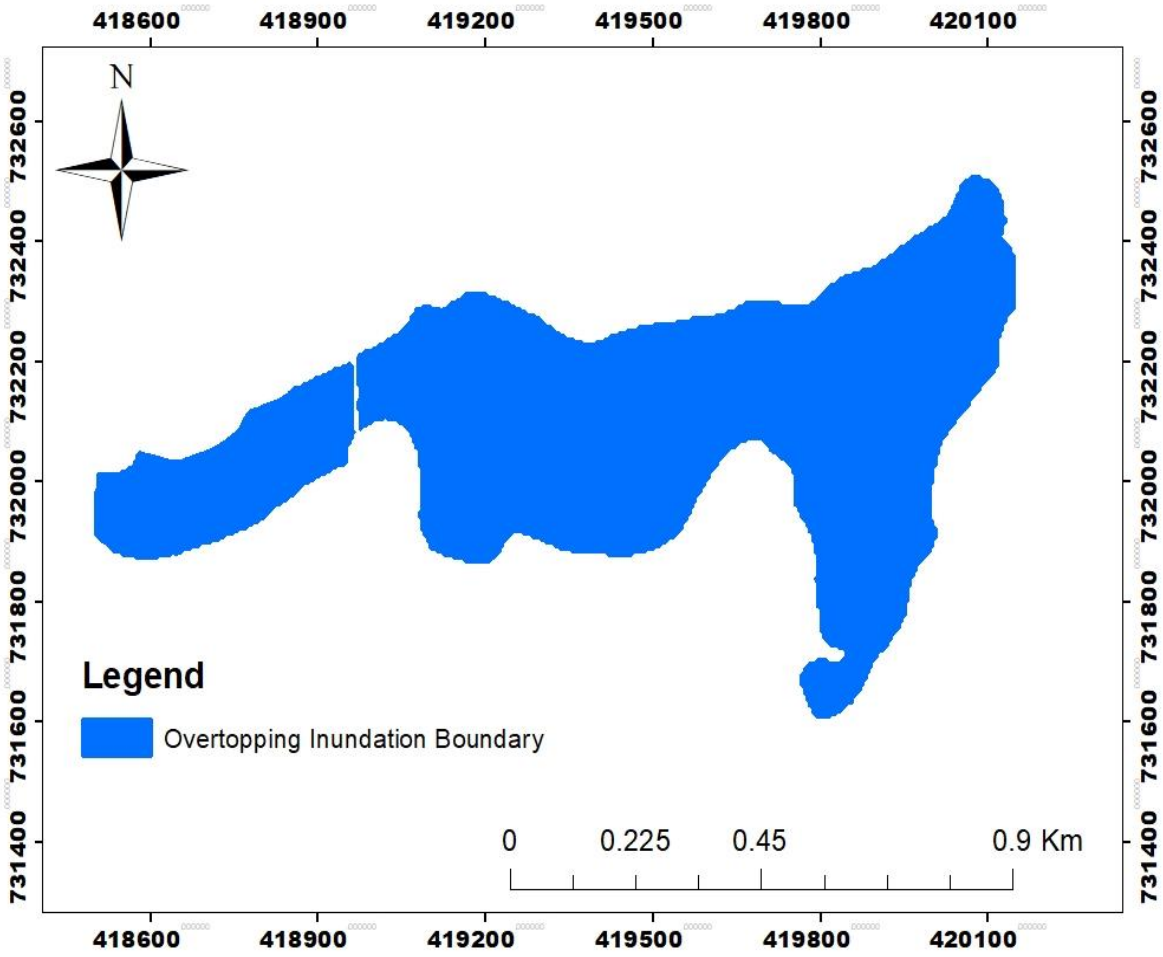

Figure 21: Flood inundation boundary map for overtopping failure

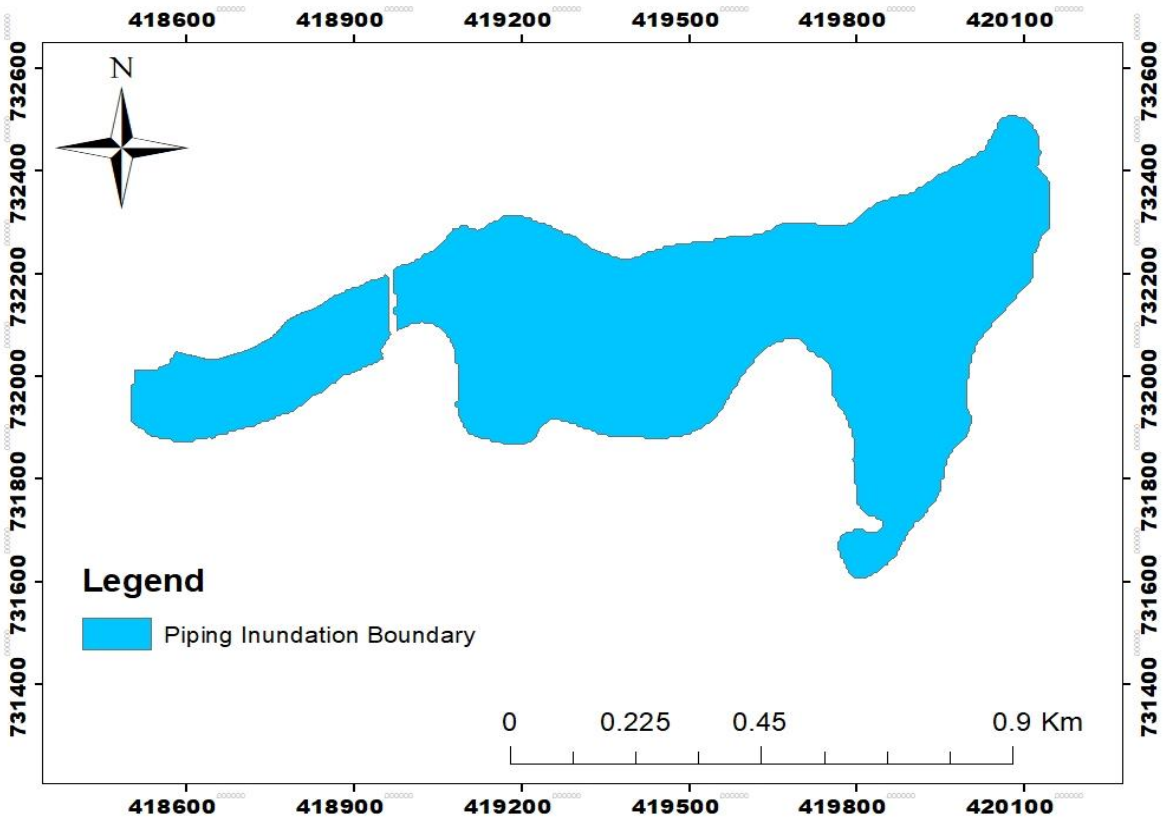

Figure 22: Flood inundation boundary map for piping failure

4.5.2. Water surface elevation

In unsteady flow analysis computed water surface profile can be exported from RAS Mapper to ARC-GIS, and overlaid on a contour map of the flood-inundated area. Figure 23 &24 shows the water surface elevation of the floodplain area for overtopping and piping. From this figure, the maximum and minimum water surface elevation downstream of the dam for both overtopping and piping failure cases were found to be 1629.77 and 1636.73m a.s.l respectively.

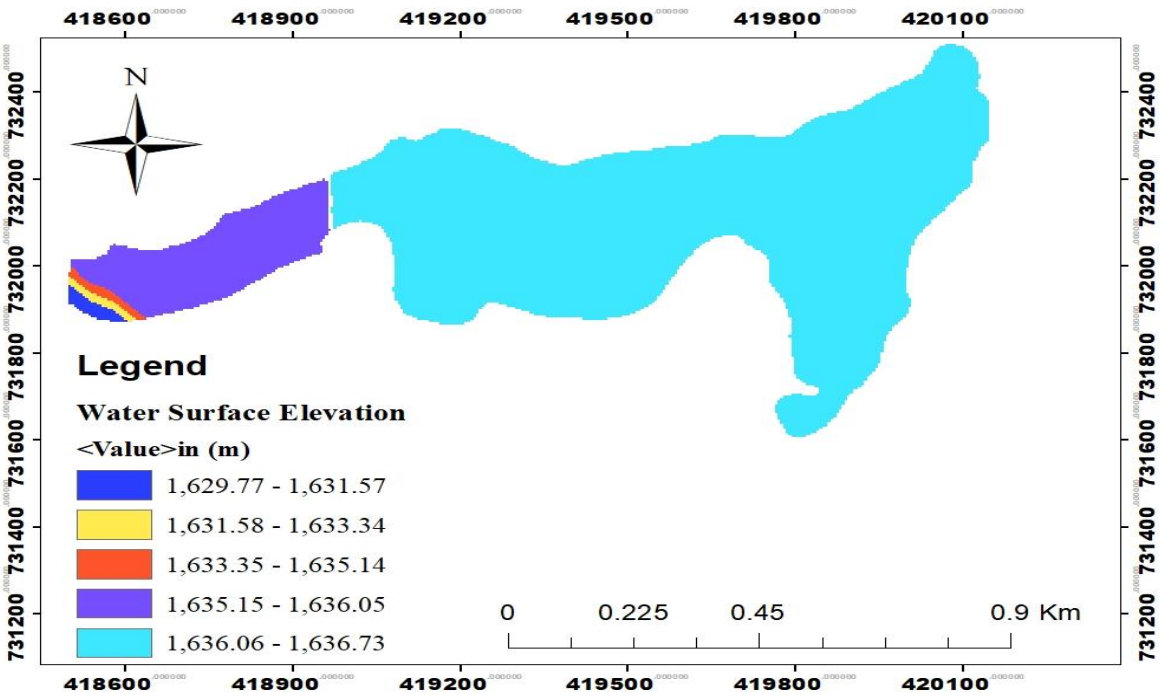

Figure 23: Water surface elevation map for overtopping

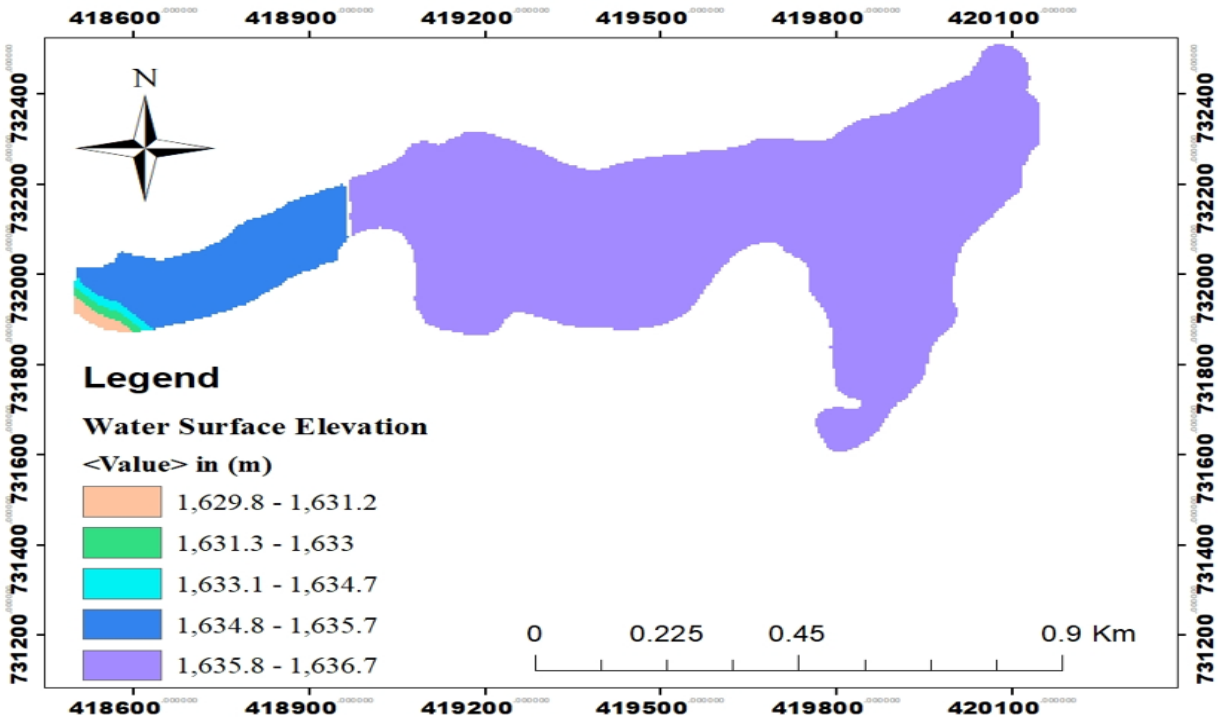

Figure 24: Water surface elevation map for piping

4.5.3. Flood depth mapping

Unique combinations of flooding events, dam release type (piping, failure, or overtopping), and the hydrologic condition of the reservoir at the time of the release is used to differentiate the WSEL for dams and flood mapping area, (Dagne, 2020). Flood depth maps show the water level at the given flood frequency. Flood depth maps are used to create maps of flood susceptibility and risk, which also aid in estimating the potential effects of flooding on social, cultural, economic, and environment. Emergency responders are primarily interested in the extent and depth of inundation rather than the elevation of flooding. The result shows a maximum flood depth of more than 19m occurred in the area for the overtopping case and more than 13.5m for the piping case, as indicated in figure 25 & 26. In general, high water depth occurred along the main channel and spreads gradually to the floodplains.

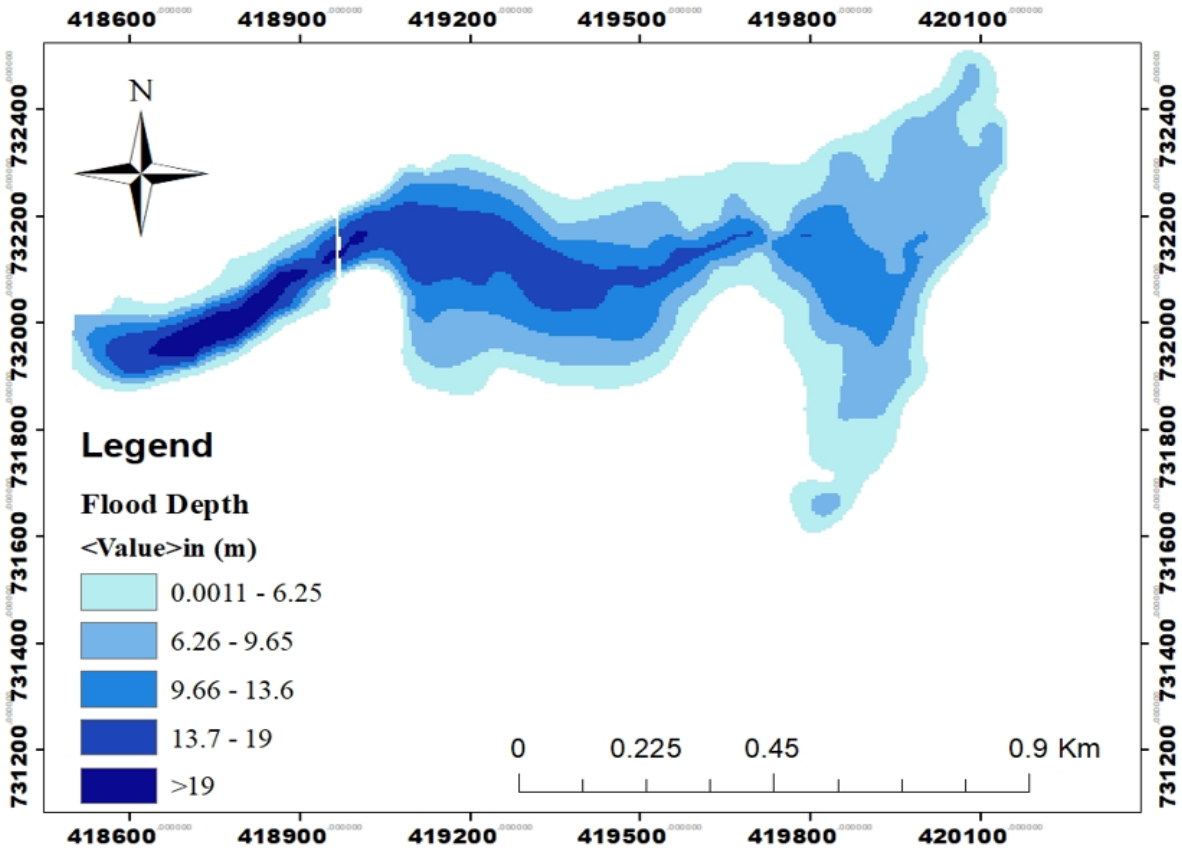

Figure 25: Flood depth map for overtopping

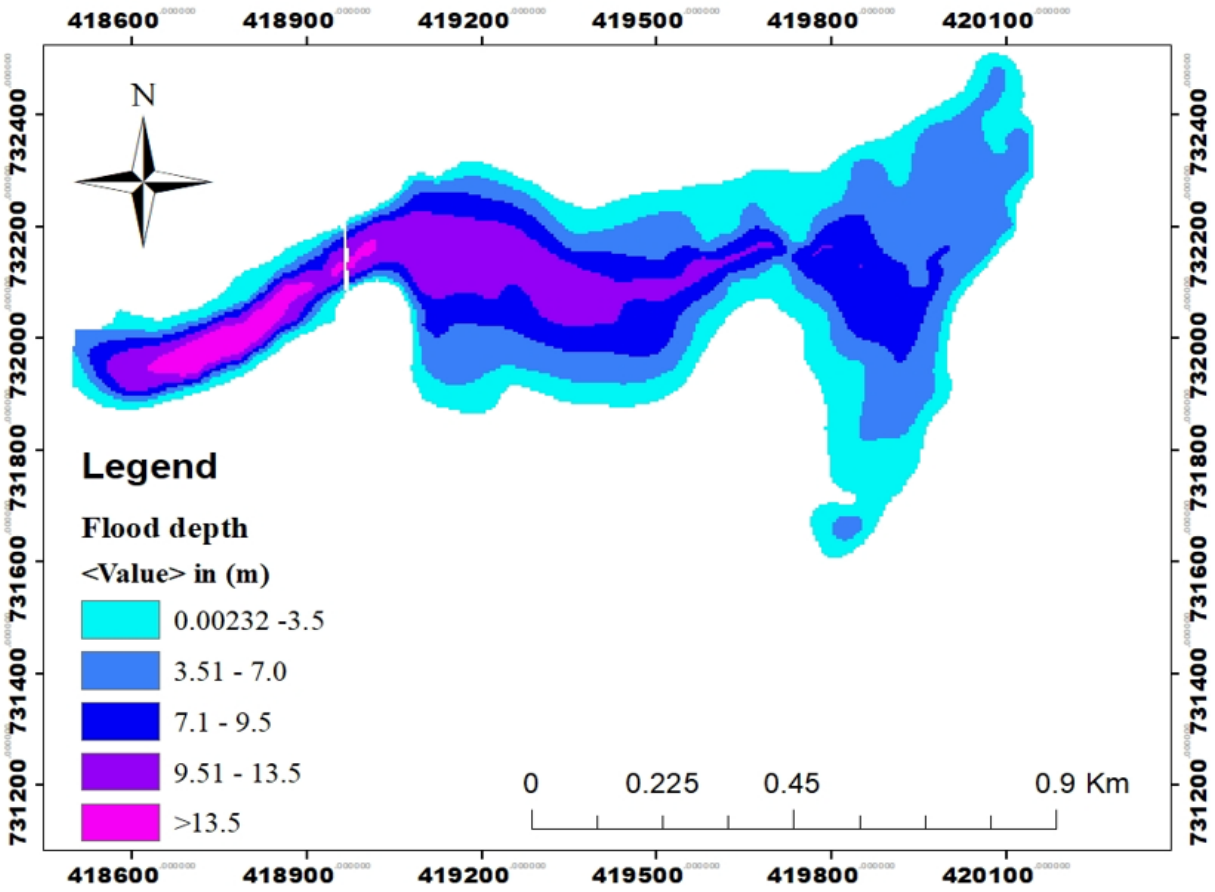

Figure 26: Flood depth map for piping

4.5.4. Flood velocity mapping

According to (Dagne, 2020) Velocity data provides additional information about the flood hazard and can offer a wide range of other floodplain management and risk communication benefits that may be difficult to convey with flood depths alone. Velocity maps are crucial for engineering and emergency activities. Emergency workers use the latter to determine how fast the water flows in areas where rescue operations take place. It is also necessary to determine the water's velocity when building flood protection structures. Figure 27 &28 shows a velocity (m/s) map of the floodplain area. The maximum flood velocities for overtopping and piping failure were more than 7m/s and 5m/s respectively. This map combines with a flood depth map to make hazard mapping. The maximum velocity found across the river channel and the minimum velocity found out of the river channel.

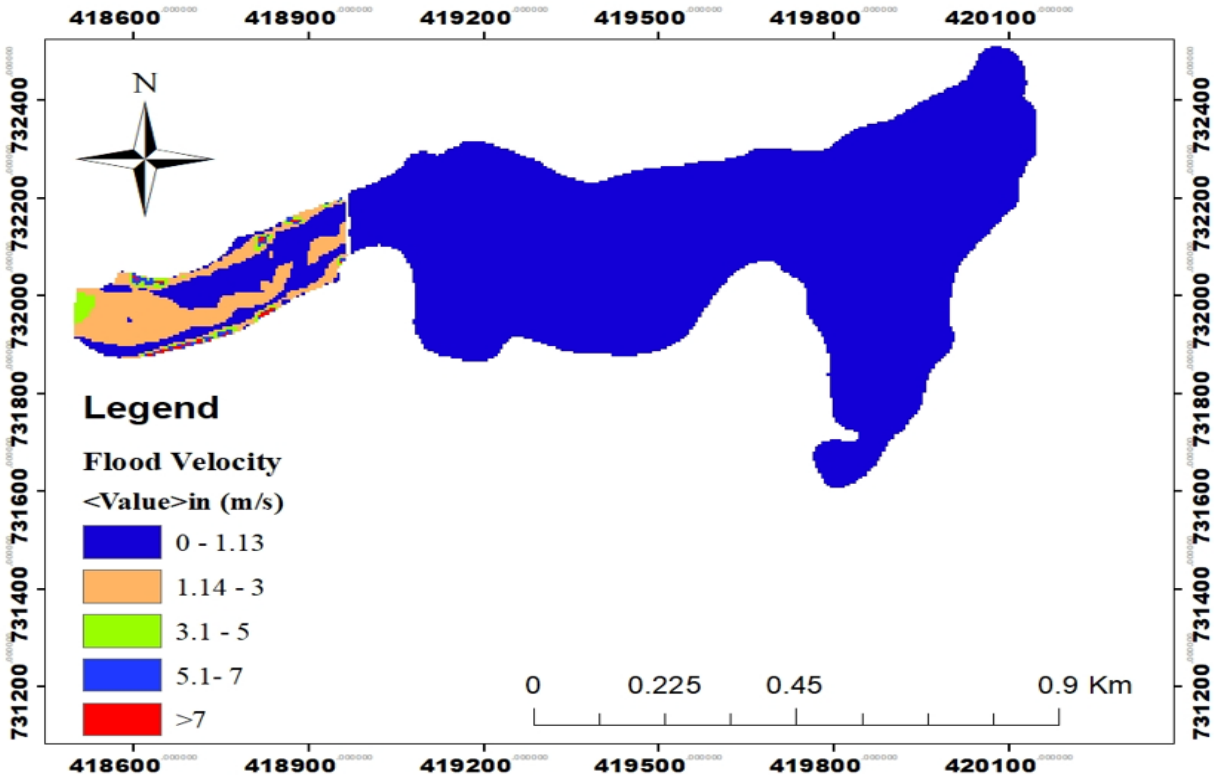

Figure 27 Flood velocity profile for overtopping

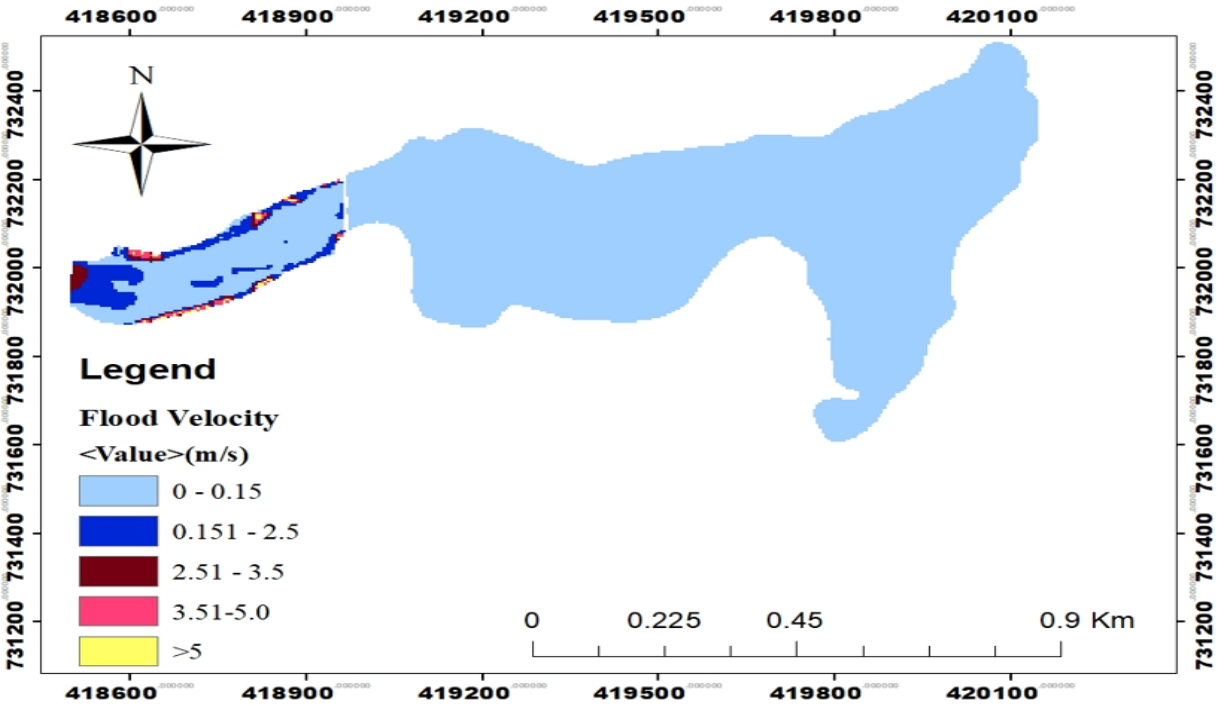

Figure 28 Flood velocity profile for piping

4.4. Flood Hazard Classification and Mapping

A flood hazard is the occurrence of the expected source of danger because of flooding. It alters with flood severity and place of occurrence within the floodplain for a similar flood event. This variation with both flood behavior and the interaction of the flood with the topography. The most important factors affecting human stability in flood waters are firstly depth and secondly velocity. Depth dictates what type of failure is to occur, either sliding (friction) or tumbling (moment) failure, (FEMA, 2012). As the depth of water increases, the damage increases. Nevertheless, even small-depth water moving at high velocity may knowingly damage a structure or damage its foundation. Faster the velocity of flood water, the higher the chance of loss of life. Persons incapable to evacuate may become trapped in a home or business center that is being destroyed by high-velocity water or rising floodwaters. High depths increase buoyancy and reduce friction underfoot. Low depth-high velocity flows may cause instability but the chances of drowning are less than in the more dangerous deep-water situations. At velocities over 2 m/s, the stability of foundations and poles can get affected by scouring. As grass and earth surfaces begin to erode, scour holes may develop. At depths over 2 m, lightly framed buildings may be damaged by water pressure, floatation, and debris impact, even at low velocities. Therefore, there is a need for a combined set of hazard vulnerability curves, which can be used as a general classification of flood hazard on a floodplain.

Different studies and guidelines have different flood hazard classification limits and justifications. The depth-velocity hazard classification diagram considered in this study is based on FEMA (2018) guidelines. The flood severity grid prepared by FEMA (2018) as indicated in Figure 29 to obtain upper limits of the depth *velocity product for each category of hazard level.

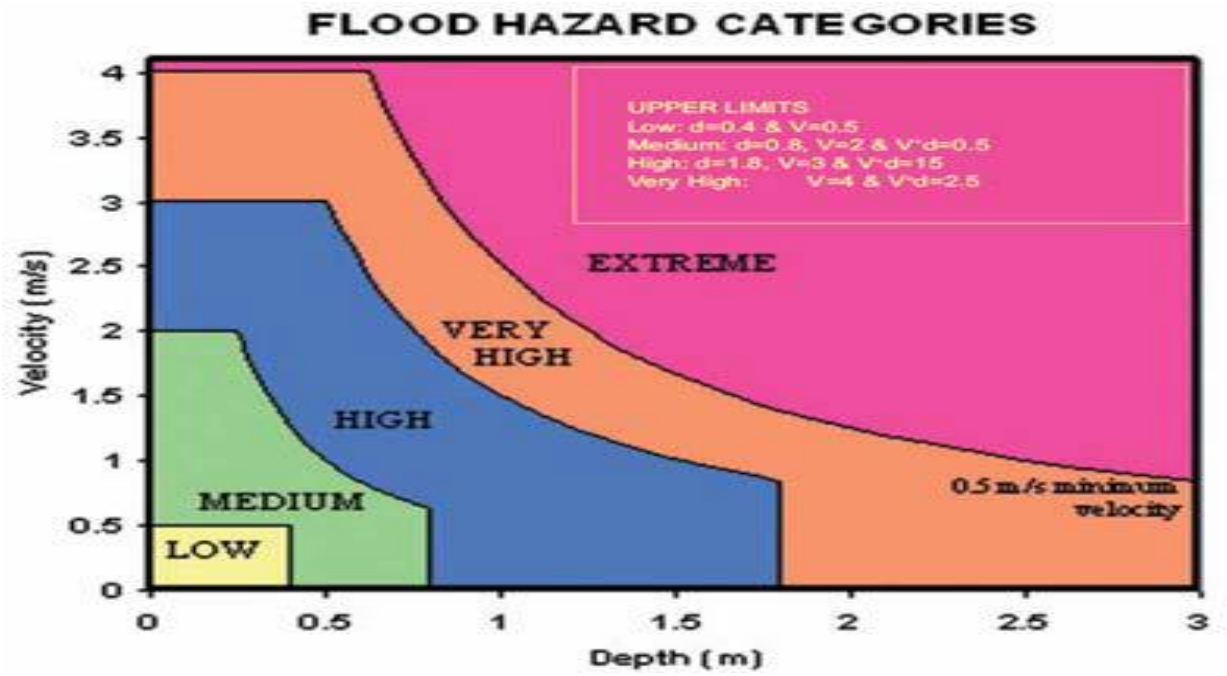

Figure 29: Flood hazard category, (FEMA, 2018)

The combined effect of depth and velocity has been considered while classifying the hazard at a grid point. This hazard criterion are assigned hazard index on 0-5scale, 0 being the blow hazard category and 5 being the extreme hazard category. The hazard classification scheme is indicated in Table 7.

Table 7: Flood depth and velocity severity grid symbolization categories, FEMA (2018)

Flood index	Flood severity category	Depth *velocity range (m^2 /sec)	Description
1	Low hazard	$\leq$ 0.2	Generally safe for vehicles, people, and buildings.
2	Medium hazard	0.2 - 0.5	Unsafe for small vehicles.
3	High hazard	0.5 - 1.5	Unsafe for vehicles, children, and the elderly.
4	Very high hazard	1.5 - 2.5	Unsafe for vehicles and peoples
5	Extreme hazard	> 2.5	Unsafe for all vehicles, people, and buildings

Using the maps of (Depth * Velocity) for the two cases and using the hazard classification scheme mentioned in Table 7, the hazard map for overtopping and piping failure has been prepared and is shown in Figures 30 and 31, respectively. These maps are the backbone for the preparation of emergency action plan in the short term and floodplain regulatory management in the long term.

As indicated in Figure 30, about 1% of the total flooded area is under an extreme hazard of flooding which means unsafe for all people, vehicles, and structures vulnerable to flooding and whereas 5.8%, 21.2%, 18.3%, and 53.8% of the total area are under very high, high, medium and low hazard respectively for overtopping failure on Figure 30 and 2%, 5.4%, 24.4%, 19.5% and 48.8% of the total area are under extreme, very high, high, medium and low hazard respectively for piping failure on Figure 31. The extreme and very high hazard areas are relatively covers small areas with high slope gradients and the high, medium, and low hazard areas are relatively covering high areas with relatively low slope gradients.

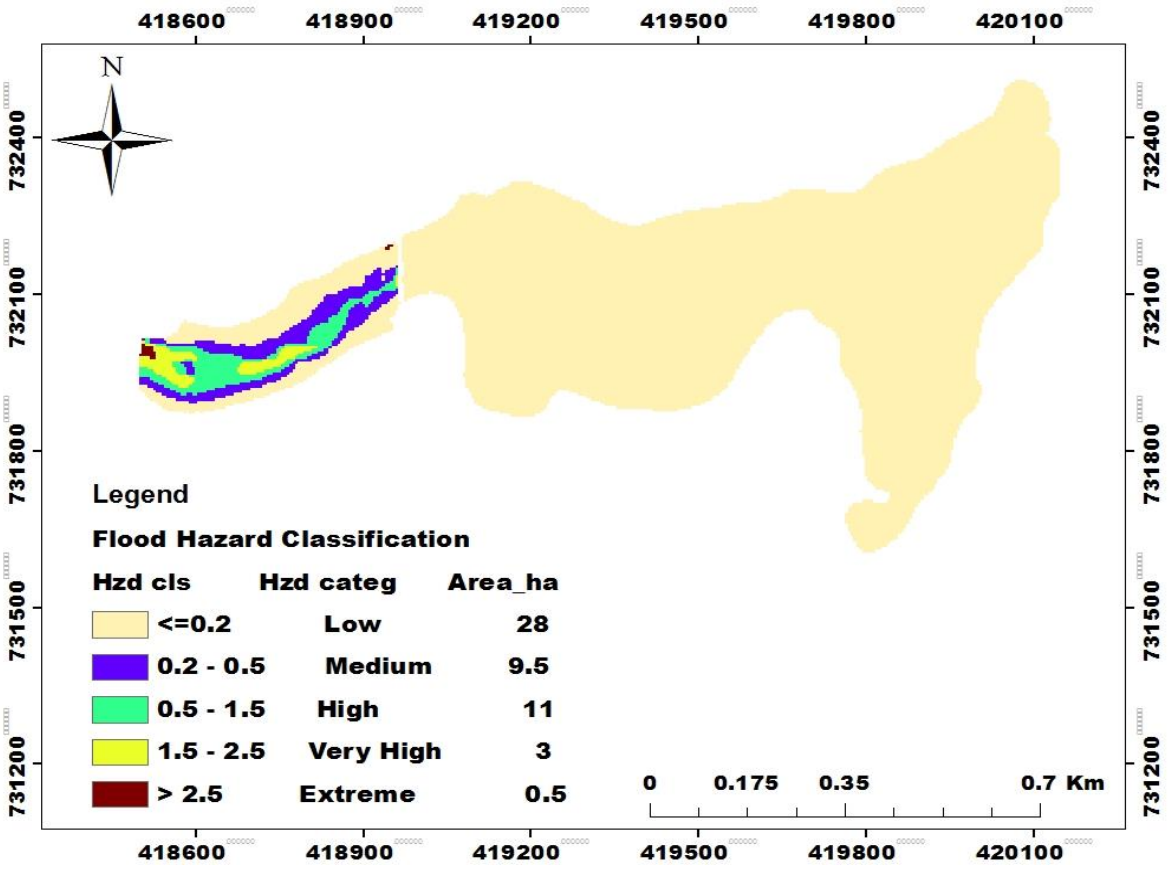

Figure 30: Flood hazard mapping for overtopping failure

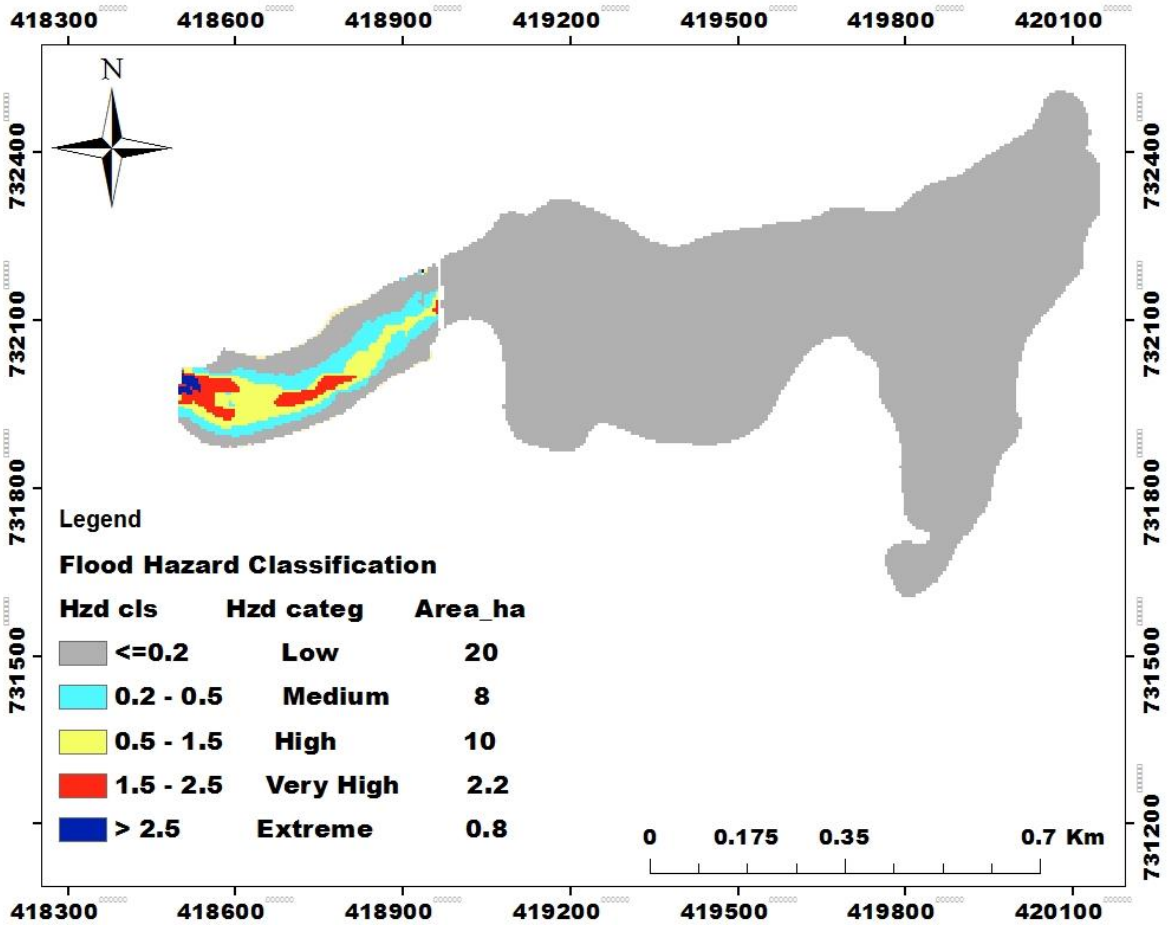

Figure 31: Flood hazard mapping for piping failure

The most important damages to human life and property are expected to occur at the first 500m below the failed dam which includes some rural villages, irrigation infrastructure, and local farms.

5. CONCLUSION AND RECOMMENDATION

5.1. Conclusion

Generally, the aim of this study was dam breach analysis and to develop flood inundation maps of Bisandima Dam to provide valuable information to Area officials, emergency managers, and residents for planning an emergency response and to identify flood zones. The primer tasks involved in the dam breach analysis are computing dam breach parameters, prediction of the reservoir outflow hydrograph, and the routing of that hydrograph through the downstream valley to determine the flood inundation area. In this study, the hydrodynamic models HEC-RAS have been used for calculating flood waves resulting from a dam failure scenario. The Bisandima Dam breach has been simulated for overtopping and piping failure scenario; with a breach Bottom Width of 31m and breach formation time of 0.38hrs. The simulated results on HEC-RAS reached peak outflows were 2079.01m^3/s and 1796.52m^3/s, for overtopping and piping failure respectively. The flooding induced by an overtopping failure is anticipated to have the greatest impact on the two scenarios. The maximum outflow at the lower end, 0.5 km below the dam, was reduced to 969.31m^3/s. The flood inundation map was prepared by RAS Mapper on ARC-GIS to visualize coverage of the flood-affected area due to the breach. The areal extent of the flood due to the breach downstream of the dam was found 52.01 hectares with flood depths greater than 19m and 13.5m for overtopping and piping failure cases respectively and maximum water surface elevation of 1636.73m a.s.l. As noticed from the flood inundation map almost all critical areas downstream of the dam are in immediate danger. The left side main canal and pump station on the main canal which is irrigated elevated command area will be under flood. Local farmers on the right side of the main river channel will also be affected. The main canal and small parts of irrigation land will also be affected by the flooding.

5.2. Recommendations

The research area's flooding hydrograph, velocity, and flood depth map, along with their level of hazard, serve as indicators of the impact of dam breaches.

To prevent the dam from failing and vulnerability of the population settled on the right side of the river, irrigation infrastructure (main canal and pump on the main canal), every stakeholder should participate. Based on the finding of the study outcomes the following recommendations are drawn.

- To prevent the dam from failure may facilitate a forestation of the upstream catchment to reduce runoff and sediment, increase freeboard, and Provide erosion protection on the downstream slope by placing riprap or other appropriate materials.
- A flood early warning system can be developed after a disastrous dam breaching flood has been identified.
- The flood-affected areas should be free of permanent development structures.
- Protection dike can be provided at both the right and left banks of the downstream with their top level considerably higher than the propagating flood level, especially on the stretches along the residence area.

6. REFERENCES

Ali, A. bin M. (2018). Flood Inundation Modeling and Hazard Mapping Under Uncertainty in the Sungai Johor Basin, Malaysia. *Flood Inundation Modeling and Hazard Mapping Under Uncertainty in the Sungai Johor Basin, Malaysia*. https://doi.org/10.1201/9780429469015

Asfaw, Y. S. (2016). *Dam Breach Analysis & Inundation Map for Melka Wakena Dam*.

Ashraf, M., Soliman, A. H., El-Ghorab, E., & Zawahry, A. El. (2018). Assessment of embankment dams breaching using large scale physical modeling and statistical methods. *Water Science*, *32*(2), 362–379. https://doi.org/10.1016/j.wsj.2018.05.002

Askar, M. K. (2014). *Rainfall-runoff model using the SCS-CN method and geographic information systems : a case study of Gomal River watershed*. *178*, 159–170.

ASTM. (2002). *Standard terminology relating to soil,rock, and contained fluids*. *January*.

Balogun, O. S., & Ganiyu, H. O. (2017). *Study and Analysis of Asa River Hypothetical Dam Break using HEC-RAS*. *36*(1), 315–321.

Boulevard, W. (2018). *Guidance for Completing a Dam Breach Analysis for Small Ponds and Dams in Maryland*. *May*.

Brunner, G. (2014). Using HEC-RAS for Dam Break Studies. *US Army Corps of Engineers Hydrologic Engineering Center*, *August*, 74. https://www.scopus.com/inward/record.uri?eid=2-s2.0-84876361807&partnerID=40&md5=dfcbf4adad65f78943b9945d7689f84d

Chow. (1951). *general formula for hydrologic frequency analysis.*

Chow. (1959). *Open Channel Hydraulics, Caldwell, New Jersey, USA:*

Chow, 1960. (1960). *Open Channel Hydraulics, Chow*.

Cunderlik, J., & Simonovic, S. P. (2010). Hydrologic models for inverse climate change impact modeling. *18th Canadian Hydro-Technical Conference*, *June*, 1–9.

Dagne, B. (2020). *Dam breach analysis and flood inundation mapping the case of Koga dam*.

Desta, H. B. and Belayneh, M. Z. (2021). *Dam breach analysis: a case of Gidabo dam, Southern Ethiopia*.

DHI. (2007). *"Mike 11 a Modelling System for Rivers and Channels." : 278–325*. 278–325.

DHI. (2016). *MIKE 21 & MIKE 3 Flow Model FM Hydrodynamic Module: Short Description*. 14.

Dottori, F., & Todini, E. (2010). *A 2D flood inundation model based on cellular automata approach*.

Etemad-Shahidi, A., Shahkolahi, A., & Liu, W.-C. (2010). Modeling of Hydrodynamics and Cohesive Sediment Processes in an Estuarine System: Study Case in Danshui River. *Environmental Modeling and Assessment*, *15*, 261–271. https://doi.org/10.1007/s10666-009-9203-9

Federal Emergency Management Agency (FEMA). (2013). *Federal Guidelines for Dam Safety - Emergency Action Planning for Dams*. *FEMA 64*(July), 73.

FEMA. (2012). *Assessing the consequences of dam failure*.

FEMA. (2013). *The Federal Guidelines for Inundation Mapping of Flood Risks Associated with Dam Incidents and Failures*.

FEMA. (2014). Federal emergency managment agency. *Administrator*, *January*.

FEMA. (2018). *Guidance for Flood Risk Analysis and Mapping Flood Depth and Analysis Grids*. *February*.

FERC. (2014). *Dam Breach Analysis*.

FHWA. (2019). *Tech Overview of Practices for Adopting 2D Hydraulic Modeling*.

Fread. (1988). *Breach: An Erosion Model for Earth Dam Failures*.

Froehlich. (2008). *Embankment Dam Breach Parameters and Their Uncertainties*.

Froehlich, D. C. (1995). *EmbankmentdambreachparametersrevisitedFroehlich.pdf*.

Froehlich, D. C. (2016). Empirical model of embankment dam breaching. *River Flow - Proceedings of the International Conference on Fluvial Hydraulics, RIver Flow 2016, June 2016*, 1821–1829. https://doi.org/10.1201/9781315644479-285

Gebre SL, G. Y. (2015). Flood Hazard Assessment and Mapping of Flood Inundation Area of the Awash River Basin in Ethiopia using GIS and HEC-GeoRAS/HEC-RAS Model. *Journal of Civil & Environmental Engineering*, *05*(04). https://doi.org/10.4172/2165-784x.1000179

Gee, D. M. (2010). Use of embankment erosion models to estimate HEC-RAS dam breach parameters. *Association of State Dam Safety Officials Annual Conference 2009, Dam Safety 2009*, *2*, 912–923.

Gordon, K. (2019). *Probable Maximum Flood Estimation Using a Statistical Approach and a Storm Model Approach for a Watershed in Southern St. Vincent*.

Gorouh et al. (2018). *Probable Maximum Precipitation Estimation in a Humid Climate*.

Hadush, F. (2019). Dam Breach Analysis and Emergency Action Plan Case Study of Mhtsab Azmati Dam. *Addis Ababa University Institute of Technology, Ethiopia." : 107.*, 107.

Hanson, G. J., Cook, K. R., & Hunt, S. L. (2005). *Physical modeling of overtopping erosion and breach formation of cohesive embankments*. *48*(5), 1783–1794.

Horritt, M. S., & Bates, P. D. (2002). Evaluation of 1D and 2D Numerical Models for Predicting River Flood Inundation. *Journal of Hydrology*, *268*, 87–99. https://doi.org/10.1016/S0022-1694(02)00121-X

Husain, A. (2017). *Flood Modelling by using HEC-RAS*. *50*(1), 1–7.

ICOLD. (2016). *Internal erosion of existing dams , levees and dikes , and their foundations bulletin 164 volume 2 : case histories , investigations , testing , remediation and surveillance Draft of 5 February 2016 For circulation to ICOLD National Committees for Comment*. *2*(February).

John D Anderson. (2009). Computational Fluid Dynamics: Chapter 2: Governing Equations of Fluid Dynamics. *Computational Fluid Dynamics*, 15–51. https://doi.org/10.1007/978-3-540-85056-4

Kastridis, A. ., Theodosiou, G. ., & Fotiadis, G. (2021). Investigation of flood management and mitigation measures in ungauged natura protected watersheds. *Hydrology*, *8*(4). https://doi.org/10.3390/hydrology8040170

Kreibich, H., Piroth, K., Seifert, I., Maiwald, H., Kunert, U., Schwarz, J., Merz, B., & Thieken, A. H. (2009). Is flow velocity a significant parameter in flood damage modelling? *Natural Hazards and Earth System Science*, *9*(5), 1679–1692. https://doi.org/10.5194/nhess-9-1679-2009

Kumar, S., Jaswal, A., Pandey, A., & Sharma, N. (2017). Literature Review of Dam Break Studies and Inundation Mapping Using Hydraulic Models and GIS. *International Research Journal of Engineering and Technology*, *4*(4), 2395–56.

Lejissa, H. (2015a). Dam Breach Modelling and Downstream Risk Analysis (For Arjo-Dedessa). *Thesis*.

Lejissa, H. (2015b). *Dam Breach Modelling and Downstream Risk Analysis (For Arjo-Dedessa Dam) Dam Breach Modelling and Downstream Risk Analysis Using (For Arjo-Dedessa Dam).*

Leoul, A. Z. (2015). *Dam Breach Analysis Using HEC-RAS and HEC- GeoRAS : The Case of Kesem Kebena Dam (Doctoral dissertation)*. *December*, 92.

MacDonald and Langridge-Monopolis. (1984). *Breaching Charateristics of Dam Failures*.

Mechal, A., Wagner, T., & Birk, S. (2015). Recharge variability and sensitivity to climate: The example of Gidabo River Basin, Main Ethiopian Rift. *Journal of Hydrology: Regional Studies*, *4*, 644–660. https://doi.org/10.1016/j.ejrh.2015.09.001

Moore, D. G. and M. (2010). Review of Hydraulic Flood Modeling Software used in Belgium , The Netherlands , and The United Kingdom. In *International Perspectives in Water Resource Management*. http://www.iihr.uiowa.edu/education1/international/UK/projects_files/ipwrsm_paper_gilles_moore_Dan_editted.pdf

Nemmert J., E. F. (2010). *Dam Breack Flood Analysis for Small Dames. Ingenieurbüro Passer & Partner, Andechsstrasse 65, 6020 Innsbruck, Austria.* (p. 3).

Nugusa, J. (2018). Dam Break Analysis and Inundation Mapping, Case Study of Fincha'a Dam in Horro Guduru Wollega Zone, Oromia Region, Ethiopia. *Science Research*, *6*(2), 29. https://doi.org/10.11648/j.sr.20180602.11

Omofunmi, O., Kolo, J., Oladipo, A., Diabana, P., & Ojo, A. (2017). A Review on Effects and Control of Seepage through Earth-fill Dam. *Current Journal of Applied Science and Technology*, *22*(5), 1–11. https://doi.org/10.9734/cjast/2017/28538

Pandya, P. H., & Dixitsinh Jitaji, T. (2013). A Brief Review of Method Available for Dam Break Analysis. *Paripex-Indian Journal of Research*, *April*, 117–118.

Papaioannou, G., Vasiliades, L., Loukas, A., & Aronica, G. (2017). Probabilistic flood inundation mapping at ungauged streams due to roughness coefficient uncertainty in hydraulic modelling. *Advances in Geosciences*, *44*, 23–34. https://doi.org/10.5194/adgeo-44-23-2017

Plakane, R. (2017). *Seasonal Variations of Manning's Coefficient Depending on Vegetation Conditions in Tärnsjö, Sweden*. *405*.

REDDA, H. (2016). *Evaluation of embankment dam failure and rededial measure.* https://doi.org/10.1017/CBO9781107415324.004

Rohidas, S., & Srinivas, V. V. (2015). Probable maximum precipitation estimation for catchments in Mahanadi river basin. *Aquatic Procedia*, *4*(Icwrcoe), 892–899. https://doi.org/10.1016/j.aqpro.2015.02.112

Schulze et al. (1992). *Methods for design flood estimation in South Africa*. *December 2011*. https://doi.org/10.4314/wsa.v38i4.19

SCS-USDA. (1986). *Urban Hydrology for Small Watersheds. Technical Release No. 55 (TR-55).*

Shane Cook,Trevor Timberlake, Davis Murphy, J. S. (2015). *selecting dam breach inundation software* (p. file:///D:/dam breach/Mike11_ShortIntroduction.pdf).

Sharma, R. P., & Kumar, A. (2013). Case Histories of Earthen Dam Failures. *Seventh International Conference on Case Histories in Geotechnical Engineering*, 8.

Shauket, S., Mohammad, T., Ghazali, A., Mohd Sidek, L., & El-Shafie, A. (2017). An evaluation of existent methods for estimation of embankment dam breach parameters. *Natural Hazards*, *87*. https://doi.org/10.1007/s11069-017-2764-z

Shiferaw, M. (2011). *2D Hydrodynamic modeling of rib river*.

Smithers, J. C. (2012). Methods for design flood estimation in South Africa. *Water SA*, *38*(4), 633–646. https://doi.org/10.4314/wsa.v38i4.19

Soleymani, S., Golkar, H., Yazd, H., & Tavousi, M. (2015). Numerical modeling of dam failure phenomenon using software and finite difference method. *Journal of Materials and Environmental Science*, *6*(11), 3143–3158.

Subramanya. (2008). Engineering Hydrology Third Edition. In *Qualitative Market Research: An*

International Journal (Vol. 13, Issue 4). https://doi.org/10.1108/qmr.2010.21613daa.003

Tayefi, V., Lane, S., Hardy, R., & Yu, D. (2007). A Comparison of One- and Two-Dimensional Approaches to Modeling Flood Inundation Over Complex Upland Floodplains. *Hydrological Processes*, *21*. https://doi.org/10.1002/hyp.6523

Uddin, M., Alam, D. M. J., Khan, Z., Hasan, G. M. J., & Rahman, T. (2014). Two Dimensional Hydrodynamic Modelling of Northern Bay of Bengal Coastal Waters. *Computational Water, Energy, and Environmental Engineering*, *03*, 140–151. https://doi.org/10.4236/cweee.2014.34015

Ulke, A., Beden, N., Demir, V., & Menek, N. (2017). Numerical modeling of Samsun Mert River floods. *EWRA Publications*, *57*(October), 27–34.

USACE. (2008). *Hydrologic Modeling System Applications Guide*. *March*.

USACE. (2010). United States Army Corps of Engineers. *Journal of Chemical Information and Modeling*, *53*(9), 1689–1699. https://doi.org/10.1017/CBO9781107415324.004

Wahl, T. L. (1998a). Prediction of Embankment Dam Breach Parameters: Literature Review and Needs Assessment, Dam Safety Research Report. *U.S. Department of the Interior Bureau of Reclamation Dam Safety Office*, *July*, 67.

Wahl, T. L. (1998b). Prediction of Embankment Dam Breach Parameters - A Literature Review and Needs Assesment. *Water Resources Research*, *DSO-98-004*(July), 67. https://doi.org/DSO-98-004

Wahl, T. L. (1998c). *Prediction of Embankment Dam Breach Parameters USBR 1998.pdf*. *July*.

Wahl, T. L. (2004). *Uncertainty of Predictions of Embankment Dam Breach Parameters*. *May*, 389–397.

Wahl, T. L. (2010). Dame breach modeling -an overview of analysis methods. *2nd Joint Federal Interagency Conference, Las Vegas, NV, June 27 - July 1, 2010*.

Wang, Y., Guo, N., Wang, S., & Gu, Y. (2016). *Detection of Internal Erosion and Piping in Embankment Dams*. *Ifeesd*, 114–122. https://doi.org/10.2991/ifeesd-16.2016.21

West, M., Morris, M., & Hassan, M. (2018). *A guide to breach prediction*. *January*, 1–40.

WMO. (2009). *22. Manual for Estimation of Probable Maximum Precipitation, Operational*

Hydrology Report 1, 2nd edition, Publication 332 (Issue 1045).

Yakti, B. P., Adityawan, M. B., Farid, M., Suryadi, Y., & Nugroho, J. (2018). *2D Modeling of Flood Propagation due to the Failure of Way Ela Natural Dam*. *03009*, 1–5.

Yuanhua, X., & Zhang, L. (2009). Breaching Parameters for Earth and Rockfill Dams. *Journal of Geotechnical and Geoenvironmental Engineering - J Geotech Geoenviron Eng*, *135*. https://doi.org/10.1061/(ASCE)GT.1943-5606.0000162

Zagonjolli, M. (2007). Dam break modelling, risk assessment and uncertainty analysis for flood mitigation. *Taylor & Francis Group Plc*, 1–162. http://www.narcis.nl/publication/RecordID/oai:tudelft.nl:uuid:7c5079e7-4b68-4f43-8553-c670c219c18c/Language/en

Zhang, Peng, & Xu. (2010). Assessing risks of breaching of earth dams and natural landslide dams. *Proc. Indian Geotechnical Conference*, 81–92.

Zhang, X. (2007). International Society for Soil Mechanics and. *International Society for Soil Mechanics and Geotechnical Engineering*, *July*, 7. https://www.issmge.org/uploads/publications/89/71/13ANZ_080.pdf

Zhang X., B. W. (2012). Modified Saint-Venant equations for flow simulation in tidal rivers. *Water Science and Engineering*, *5*(1), 34–45. https://doi.org/10.3882/j.issn.1674-2370.2012.01.004

Zhao, G., Visser, P. J., Peeters, P., & Vrijling, J. K. (2015). Hydrodynamic erosion in cohesive embankment breach. *Scour and Erosion - Proceedings of the 7th International Conference on Scour and Erosion, ICSE 2014*, 441–448. https://doi.org/10.1201/b17703-56

Zhou, R. D., Judge, D. G., & Donnelly, C. R. (2005). Comparison of HEC-RAS with FLDWAV and DAMBRK models for dam break analysis. *CDA 2005 Annual Conference*, *October 2005*. https://doi.org/10.13140/2.1.2688.1606

Zhu, Y., & Visser P. J. and Vrijling J. K. (2004). *Review on embankment dam breach modeling* (p. 9).

APPENDIX

Table 1: Annual Maximum Daily Rainfall in mm at Rainfall Stations, (1986-2020)

Aleta Wendo Station					
No.	Year	Max. Daily RF	No.	Year	Max. Daily RF
1	1991	50.6	16	2006	56.6
2	1992	69.7	17	2007	58
3	1993	69.7	18	2008	65
4	1994	48.2	19	2009	70
5	1995	36.2	20	2010	43.2
6	1996	65.2	21	2011	121.2
7	1997	60.1	22	2012	59.5
8	1998	58.3	23	2013	50
9	1999	36.8	24	2014	60
10	2000	33.2	25	2015	50
11	2001	66.3	26	2016	37
12	2002	45.6	27	2017	50.2
13	2003	41	28	2018	58
14	2004	44.5	29	2019	60
15	2005	45.2	30	2020	50.2

Table 2: Probability Fitting a Distribution Kolmogorov _Simonov test

Kolmogorov-Smirnov test for all data	a=1%	a=5%	a=10%	Attained	Dmax
Norma	ACCEPT	ACCEPT	ACCEPT	74.19%	0.1127
Norma (L-Moments)	ACCEPT	ACCEPT	ACCEPT	71.19%	0.11587
LogNormal	ACCEPT	ACCEPT	ACCEPT	93.92%	0.08679
Galton	ACCEPT	ACCEPT	ACCEPT	58.30%	0.12923
Exponential	ACCEPT	ACCEPT	ACCEPT	42.98%	0.1462
Exponential (L-moments)	ACCEPT	ACCEPT	ACCEPT	43.18%	0.14596
Gamma	ACCEPT	ACCEPT	ACCEPT	88.82%	0.09525
Pearson III	ACCEPT	ACCEPT	ACCEPT	42.07%	0.1473
Log Pearson III	ACCEPT	ACCEPT	ACCEPT	76.23%	0.11051
Ev1-Max (Gumbel)	ACCEPT	ACCEPT	ACCEPT	91.75%	0.09072
EV2-Max	ACCEPT	ACCEPT	ACCEPT	42.78%	0.14645
Ev1-Min (Gumbel)	ACCEPT	ACCEPT	ACCEPT	27.16%	0.16789
Ev3-Min (Weibull)	ACCEPT	ACCEPT	ACCEPT	64.53%	0.12277
GEV-Max	ACCEPT	ACCEPT	ACCEPT	64.76%	0.12253
GEV-Min	ACCEPT	ACCEPT	ACCEPT	42.23%	0.14711
Pareto	REJECT	REJECT	REJECT	%	0.55322
GEV-Max (L-Moments)	ACCEPT	ACCEPT	ACCEPT	89.68%	0.09399
GEV-Min (L-Moments)	ACCEPT	ACCEPT	ACCEPT	93.91%	0.08683
EV1-Max (Gumbel, L-Moments)	ACCEPT	ACCEPT	ACCEPT	89.68%	0.09399
EV2-Max (L-Moments)	ACCEPT	ACCEPT	ACCEPT	42.69%	0.14655
EV1-Min (Gumbel, L-Moments)	ACCEPT	ACCEPT	ACCEPT	24.94%	0.1716
EV3-Min (Weibull, L-Moments)	ACCEPT	ACCEPT	ACCEPT	63.43%	0.1239
Pareto (L-Moment)	ACCEPT	ACCEPT	ACCEPT	44.64%	0.14424
GEV-Max (Kappa specified)	ACCEPT	ACCEPT	ACCEPT	53.11%	0.13475
GEV-Min (Kappa specified)	ACCEPT	ACCEPT	ACCEPT	46.58%	0.14199
GEV-Max (Kappa specified, L-Moments)	ACCEPT	ACCEPT	ACCEPT	94.15%	0.06948
GEV-Min (Kappa specified, L-Moments)	ACCEPT	ACCEPT	ACCEPT	48.64%	0.13966

Table 3: Probability Fitting a Distribution test by X-square test

X-Square test for all data	a=1%	a=5%	a=10%	Attained	pearson param
Norma	ACCEPT	ACCEPT	ACCEPT	14.82%	3.81818
Norma (L-Moments)	ACCEPT	ACCEPT	ACCEPT	27.17%	2.60606
LogNormal	ACCEPT	ACCEPT	REJECT	8.09%	5.0303
Galton	ACCEPT	REJECT	REJECT	4.23%	4.12121
Exponential	ACCEPT	ACCEPT	REJECT	8.09%	5.0303
Exponential (L-moments)	ACCEPT	ACCEPT	REJECT	8.09%	5.0303
Gamma	ACCEPT	ACCEPT	ACCEPT	20.07%	3.21212
Pearson III	ACCEPT	REJECT	REJECT	2.49%	5.0303
Log Pearson III	ACCEPT	REJECT	REJECT	1.76%	5.63636
Ev1-Max (Gumbel)	ACCEPT	ACCEPT	ACCEPT	14.82%	3.81818
EV2-Max	ACCEPT	ACCEPT	ACCEPT	27.17%	2.60606
Ev1-Min (Gumbel)	ACCEPT	ACCEPT	REJECT	8.09%	5.0303
Ev3-Min (Weibull)	ACCEPT	ACCEPT	REJECT	6.95%	5.33333
GEV-Max	ACCEPT	ACCEPT	REJECT	5.07%	3.81818
GEV-Min	ACCEPT	REJECT	REJECT	2.49%	5.0303
Pareto	ACCEPT	REJECT	REJECT	2.49%	5.0303
GEV-Max (L-Moments)	ACCEPT	REJECT	REJECT	1.76%	5.63636
GEV-Min (L-Moments)	ACCEPT	ACCEPT	REJECT	5.07%	3.81818
EV1-Max (Gumbel, L-Moments)	ACCEPT	ACCEPT	REJECT	5.97%	5.63636
EV2-Max (L-Moments)	ACCEPT	ACCEPT	ACCEPT	31.62%	2.30303
EV1-Min (Gumbel, L-Moments)	ACCEPT	ACCEPT	ACCEPT	12.74%	4.12121
EV3-Min (Weibull, L-Moments)	ACCEPT	ACCEPT	ACCEPT	27.17%	2.60606
Pareto (L-Moment)	ACCEPT	REJECT	REJECT	4.23%	4.12121
GEV-Max (Kappa specified)	ACCEPT	ACCEPT	ACCEPT	27.17%	2.60606
GEV-Min (Kappa specified)	ACCEPT	REJECT	REJECT	3.79%	6.54545
GEV-Max (Kappa specified, L-Moments)	ACCEPT	ACCEPT	ACCEPT	14.82%	3.81818
GEV-Min (Kappa specified, L-Moments)	ACCEPT	ACCEPT	ACCEPT	27.17%	2.60606

Table 4: Probability of Maximum Precipitation (PMP) for Different Return Periods

Return period T Years	Max 24hrs Rainfall (mm)	Peak Discharge (Qp) in m3/s)
2	52.24	13.11
5	65.31	24.85
10	75.28	35.4
25	89.58	52.42
50	101.59	68.11
100	114.83	86.59
1000	169.88	172.5
10000	247.53	307.43

Table 5: Inflow Hydrograph Parameters

No	Parameter/formula	Symbol	Unit	Value
1	Area of the catchment	A	Km^2	30.49
2	Length of main water course	L	M	19002
3	Slope of main water course	S	M	0.08
4	Time of Concentration ,$Tc=0.000328L^{0.77}S^{-0.385}$	TC	Hr	1.73
5	Rain fall excess duration, D=Tc/6	D	Hr	0.29
6	Time to peak $T_p=0.5D+0.6T_C$	T_p	hr	1.18
7	Time of base of hydrograph $T_b=2.67Tp$	T_b	hr	3.16
8	Lag time of $T_{lag}=0.6TC$	T_{lag}	hr	1.04
9	Peak rate of discharge created by 1mm RF excess on whole of the catchment Qp=0.21*QA/Tp ,Qp=1mm(assumed)	Q_p	$m^3/s/mm$	5.38
10	Runoff curve number (CN), GIS based curve number determination from land use and Hydrologic soil group (Shown on Appendix-G)	CN	_	83.50
11	S is maximum potential difference between rainfall (P) and direct runoff(Q) which is, S=(25400/CN)-254	S	Mm	50.19
12	Relation between direct Runoff(Q) and Rainfall (P), Q=(P-0.2*S) 2/P+0.8S	Q	Mm	Result shown, in annex Table 7

Table 6: GIS Attribute Table for Land Use, HSG and Runoff curve number

Land use	Soil Group (HSG)	Area (A) km^2	CN	CN*A	$CN_{Average}$
Moderate	D	3.92126	79.00	309.7795	83.50
sparse F	D	13.91972	83.00	1155.336	
Open Grass	D	1.934892	89.00	172.2054	
Closed Shurbland	D	0.566236	80.00	45.29888	
open shurbland	D	6.31338	83.00	524.0105	
annual cropland	D	3.161232	88.00	278.1884	
Wetland	D	0.009084	98.00	0.890232	
water body	D	0.027252	98.00	2.670696	
bare soil	D	0.42392	94.00	39.84848	
	Total	30.28	_	2528.229	

Table 7: Inflow flood

Time (Hr)	Q(m^3/s)
00	0.00
0.29	0.00
0.58	0.17
0.87	18.61
1.18	88.58
1.47	165.55
1.76	249.93
2.05	307.43
2.34	279.62
2.63	240.62
2.92	190.93
3.21	141.24
3.50	91.56
3.79	43.85
4.08	10.44
4.37	3.17
4.66	0.00

Table 8: DEM generated topography data at dam, reservoir and downstream of the dam

S.N	Eeasting	Northing	Elevation	Description	S.N	Eeasting	Northing	Elevation	Description
1	418969.1	732303.8	1664.1	BM1	188	419967.7	732328.8	1629.5	
2	418957.1	732294.8	1663.1	BM2	189	419956.7	732227.6	1629.3	
3	418957.0	732294.7	1663.1		190	419941.9	732107.7	1629.2	
4	418957.0	732294.7	1663.1		191	419909.1	732179.3	1630.2	
5	418957.8	732290.3	1660.9	Axis	192	419048.5	732325.0	1640.8	
6	418964.7	732272.4	1653.4	Axis	193	419287.0	732222.5	1627.6	TP-6
7	418968.0	732266.4	1649.8	Axis	194	419203.4	732358.4	1637.2	
8	418970.7	732244.0	1643.3	Axis	195	419012.2	732306.1	1648.8	
9	418968.8	732230.3	1640.0	Axis	196	419229.7	732232.9	1625.6	
10	418968.6	732206.7	1632.9	Axis	197	418994.8	732304.6	1653.9	
11	418970.3	732177.3	1624.1	Axis	198	419165.4	732247.4	1625.5	
12	418970.5	732159.3	1620.6	Axis	199	418973.7	732302.1	1660.9	TUK
13	418970.5	732145.1	1618.7	Axis	200	419121.2	732262.1	1627.2	TUK
14	418970.6	732135.2	1616.4	RR B	201	419089.0	732272.9	1629.1	HOUSE
15	418969.5	732132.6	1615.1	RC	202	419046.0	732279.0	1637.6	
16	418969.1	732127.3	1616.1	RC	203	418938.9	732286.2	1663.8	
17	418969.9	732120.3	1618.9	RC	204	418996.9	732286.6	1649.6	
18	418970.7	732115.4	1622.1	RC	205	418836.4	732109.0	1631.1	
19	418971.7	732091.1	1631.9	RC	206	418855.1	732129.2	1630.8	
20	418978.6	732064.4	1638.1	RC	207	418872.8	732148.2	1631.8	

21	418978.9	732051.9	1642.2	RC	208	418885.7	732168.4	1634.9	
22	419002.8	732025.3	1645.3	RC	209	418897.5	732186.3	1637.5	
23	418996.5	732104.4	1628.7		210	418907.5	732201.3	1639.9	
24	419028.4	732053.6	1644.4		211	418969.1	732303.8	1664.1	BM-1
25	418991.1	732052.7	1641.8		212	418957.1	732294.8	1663.1	BM-2
26	418928.4	732224.6	1644.5		213	418957.1	732294.8	1663.1	
27	418912.3	732176.8	1633.1		214	419799.9	731581.7	1634.0	
28	418937.2	732191.5	1632.9	TP-1	215	419814.4	731527.2	1635.3	
29	418969.0	732303.8	1664.1		216	419827.7	731513.7	1636.2	
30	418901.2	732142.6	1627.2		217	419812.5	731483.0	1636.2	
31	418939.1	732084.2	1626.6		218	419811.7	731592.9	1633.9	
32	418924.2	732123.7	1623.6		219	419581.3	732417.2	1646.5	
33	419006.6	732097.1	1635.8		220	419783.3	731529.4	1634.4	
34	419047.8	732066.9	1642.5		221	419810.2	731609.4	1632.8	
35	419047.7	732066.9	1642.4		222	419702.2	732452.3	1647.2	
36	419023.7	732169.9	1618.4		223	419891.2	731633.9	1638.2	
37	419075.1	732068.4	1630.4		224	419663.7	731564.8	1641.5	
38	418950.7	732031.5	1635.2		225	419710.1	731633.5	1641.5	
39	418943.5	732052.4	1634.4		226	419645.4	731500.0	1639.4	TP-7
40	418879.3	732031.4	1620.7		227	418969.0	732303.7	1664.1	
41	419049.4	732162.6	1620.9		228	419602.1	731594.0	1643.1	
42	419064.3	732139.3	1622.2		229	419834.5	732440.9	1644.1	
43	419079.6	732143.7	1619.3		230	419828.1	731702.3	1633.3	

44	419099.4	732137.9	1619.6		231	419904.5	731706.6	1633.3	
45	419094.5	732097.6	1621.8		232	419947.5	731698.0	1636.8	
46	418878.6	732112.0	1626.2		233	419564.0	731608.7	1642.5	
47	418833.5	732080.3	1623.5		234	419642.2	731719.5	1642.2	
48	418867.1	732054.8	1617.4		235	419539.5	731528.3	1645.0	
49	418915.2	732067.2	1625.6		236	419834.5	731724.7	1633.1	
50	419102.9	732088.7	1621.6	TUK	237	419827.3	731743.4	1632.0	
51	419129.0	732091.1	1621.4	TUK	238	419818.6	731783.5	1631.9	
52	419137.2	732103.0	1621.3	TUK	239	419900.3	731788.7	1631.5	
53	419102.0	732022.0	1626.8		240	419971.2	731776.4	1635.5	
54	419131.6	732038.0	1626.5		241	419810.9	731831.3	1631.3	
55	419179.0	732085.3	1623.2		242	419823.2	731846.4	1631.3	TUKUL
56	419264.8	732033.5	1625.6		243	419541.5	731621.0	1642.8	TUKUL
57	419246.0	732082.4	1624.5		244	419425.1	731623.1	1641.9	
58	419320.8	731993.3	1626.3		245	419400.9	731503.8	1641.9	
59	419408.0	731961.4	1628.0		246	419705.8	731889.8	1639.2	
60	419424.2	732018.3	1623.6		247	419932.3	731900.5	1629.0	
61	419129.0	731961.1	1629.0		248	420002.3	731889.4	1633.1	TP-8
62	419077.9	731941.6	1633.4		249	419645.3	731500.0	1639.4	
63	419178.6	731988.9	1628.4		250	419939.9	731941.6	1628.4	
64	419226.6	731993.7	1628.4		251	419706.6	732292.9	1632.4	TP-8A
65	419149.2	731919.6	1630.3		252	420002.3	731889.4	1633.1	
66	419278.3	731955.7	1629.7		253	419585.4	732257.7	1631.8	

67	419393.7	731848.3	1634.9		254	419844.7	732310.1	1629.9	
68	419518.9	731941.2	1630.2		255	419712.3	732323.0	1634.9	HOUSE
69	419330.7	731892.0	1632.7	TP-2	256	419677.9	731487.0	1635.7	
70	418937.2	732191.5	1632.9		257	419771.0	731501.4	1634.7	
71	419345.1	731721.9	1640.6		258	419734.3	731471.3	1634.1	
72	419419.4	731756.6	1640.7		259	419664.2	731440.0	1635.5	
73	419333.9	731796.9	1638.4		260	419794.6	732313.5	1633.5	
74	419258.3	731690.3	1642.5		261	419799.1	732365.4	1637.3	
75	419341.8	731617.2	1646.2		262	419871.3	732390.4	1636.5	
76	419256.0	731593.0	1648.2		263	420115.1	732360.0	1625.6	
77	419190.2	731941.7	1629.6		264	419989.7	732383.9	1629.6	
78	419330.5	732057.7	1621.3		265	419693.2	731300.6	1637.1	
79	419352.8	732052.1	1621.7		266	419743.2	731258.0	1641.0	
80	419174.7	731868.4	1632.8		267	419576.6	731280.7	1637.8	
81	419112.4	731844.1	1635.1		268	419895.2	732329.4	1631.5	
82	419048.4	731828.8	1636.2		269	419733.7	731348.2	1636.6	TP-9
83	419251.9	731914.0	1633.1		270	420002.3	731889.4	1633.1	
84	419183.5	731831.1	1634.7		271	419763.3	731379.2	1636.6	
85	419373.5	732037.6	1622.3		272	419795.5	731400.2	1637.7	
86	419192.4	731775.1	1637.0		273	419793.9	731485.4	1636.2	TUKUL
87	419408.4	731574.9	1643.6		274	418969.1	732303.8	1664.1	
88	419497.3	731550.4	1643.9		275	418956.9	732294.6	1663.1	
89	419624.9	731353.7	1636.7		276	418957.1	732294.9	1663.1	

90	419731.1	731422.2	1635.5		277	419681.9	731200.4	1636.8	
91	419583.1	731466.2	1641.1		278	419622.7	731170.6	1636.7	
92	419740.6	731589.9	1636.8		279	419573.1	731149.3	1638.0	
93	419737.4	731743.6	1636.8		280	419540.4	731219.5	1637.4	
94	419568.8	731752.1	1642.5		281	419557.5	731137.3	1638.4	TUKUL
95	419624.8	731646.5	1642.6		282	419541.1	731409.2	1638.2	TP-10
96	419508.9	731819.0	1636.8		283	419733.7	731348.2	1636.6	
97	419606.6	731885.1	1637.4		284	419556.5	731104.6	1638.7	TP-11
98	419788.8	732040.0	1631.1		285	419541.1	731409.1	1638.2	
99	419967.9	731825.9	1633.6		286	419686.8	731187.0	1637.1	
100	419861.7	731966.6	1630.0		287	419715.8	731160.3	1638.6	
101	419138.3	731755.4	1639.3		288	419789.6	731102.4	1641.4	
102	419067.5	731738.3	1640.5		289	419527.7	731005.9	1640.8	HOUSE
103	419273.4	731817.2	1637.3		290	419488.2	731058.3	1640.2	
104	419213.1	731722.3	1639.5		291	419443.3	731139.7	1646.0	
105	419147.2	731698.8	1640.3		292	419592.5	730941.2	1638.7	
106	419276.8	731753.2	1639.2		293	419731.6	731121.0	1639.6	
107	419486.6	731995.9	1625.0		294	419709.5	731090.3	1639.0	
108	419541.6	731971.4	1629.9		295	419687.4	731075.0	1638.5	
109	419586.2	731953.1	1634.2		296	419424.6	730979.7	1648.7	
110	419612.5	731798.9	1641.0		297	419375.0	731058.5	1647.8	
111	419513.4	731693.4	1644.4		298	419500.0	730893.9	1646.8	
112	419408.2	731613.8	1645.4	TP-3	299	419400.3	730963.3	1653.0	TUKUL

113	419330.7	731892.0	1632.7		300	419400.8	730899.7	1653.9	
114	419884.0	731896.9	1629.9		301	419422.5	730850.0	1652.3	
115	419760.0	731952.2	1632.9		302	419450.3	730865.3	1650.7	
116	419630.8	732103.4	1630.4		303	419471.0	730890.7	1645.2	
117	419708.2	732123.2	1632.4		304	419495.3	730885.3	1644.1	
118	419673.4	731998.3	1635.1		305	419563.6	730865.6	1641.9	
119	419461.8	732058.0	1624.3		306	419581.8	730796.9	1640.4	
120	419570.6	732044.0	1629.8		307	419606.6	730723.6	1641.3	HOUSE
121	419542.3	732215.3	1630.1		308	419584.7	730951.3	1637.2	
122	419629.9	732199.3	1632.0		309	419515.4	730754.4	1646.9	
123	419587.6	732161.8	1630.1		310	419629.8	730639.9	1642.3	
124	419569.5	732329.9	1638.5		311	419547.2	730682.6	1648.6	
125	419193.0	732312.6	1632.5		312	419648.5	730615.0	1641.0	
126	419677.6	731895.4	1638.8		313	419680.5	730867.8	1639.6	
127	419123.7	731687.5	1643.0		314	419756.4	730833.1	1636.8	
128	419689.2	732084.7	1632.2		315	419631.7	730585.5	1641.4	
129	419689.3	732066.9	1633.1		316	419575.4	730611.1	1646.1	
130	419725.2	732059.1	1632.2		317	419691.6	730892.4	1639.2	TP-12
131	419130.1	731639.2	1645.9		318	419556.5	731104.6	1638.7	
132	419053.6	731625.2	1648.3		319	419682.0	730528.0	1638.6	
133	419142.1	731574.7	1649.9		320	419716.9	730955.5	1639.5	
134	419159.8	731512.9	1652.7		321	419583.4	730531.4	1642.3	
135	419269.3	731547.6	1651.2		322	419745.0	730977.6	1640.7	

136	419060.5	731495.3	1655.8		323	419811.3	730948.6	1644.1	
137	418991.6	732258.7	1643.2		324	419562.3	730506.2	1642.8	
138	419004.9	732254.2	1641.3	TUK	325	419621.2	730691.1	1641.1	TP-13
139	419045.8	732232.1	1629.7	TUK	326	419691.6	730892.4	1639.2	
140	419082.9	732235.2	1624.4		327	419502.6	730535.9	1647.9	
141	419114.1	732225.7	1623.3	TP-4	328	419755.5	730937.3	1639.5	
142	419408.2	731613.8	1645.4		329	419588.8	730481.6	1642.6	
143	419303.2	732284.9	1634.3		330	419740.6	730899.9	1638.2	
144	419479.2	732351.3	1640.6		331	419824.8	730869.9	1643.3	
145	419388.6	732280.1	1635.5		332	419606.0	730427.7	1641.1	
146	419465.9	732258.5	1633.1		333	419721.3	730870.1	1641.3	
147	419449.3	732203.2	1630.4		334	419699.3	730841.6	1640.9	
148	419452.2	732167.2	1628.4		335	419587.3	730378.4	1643.3	
149	419704.1	732394.4	1641.7		336	419500.9	730414.9	1649.6	
150	419657.7	732277.7	1632.2		337	419692.0	730797.4	1640.6	
151	419144.4	732175.6	1620.5		338	419565.6	730325.7	1644.3	
152	419198.4	732160.6	1620.4		339	419622.9	730306.1	1643.5	
153	419246.0	732168.1	1620.9		340	419497.6	730287.8	1646.1	
154	419297.5	732145.2	1621.6		341	419700.1	730726.0	1640.3	
155	419344.3	732126.1	1622.2		342	419834.5	730687.9	1644.8	
156	419407.4	732128.8	1624.5		343	419696.8	730685.4	1640.1	
157	419589.6	732408.7	1645.6		344	419776.6	730660.6	1645.3	
158	419442.2	732105.7	1623.7		345	419654.2	730625.6	1641.0	

159	419540.3	732400.8	1645.3		346	419691.5	731896.4	1639.9	HOUSE
160	419490.7	732126.5	1625.7		347	419627.6	730201.1	1644.2	
161	419423.2	732378.8	1643.1		348	419661.9	730518.5	1641.0	
162	419511.2	732131.3	1626.6		349	419832.8	730477.7	1637.1	
163	419353.9	732365.7	1640.7		350	419618.7	730551.3	1641.5	TP-14
164	419291.6	732357.4	1640.5		351	419621.2	730691.1	1641.1	
165	419280.9	732402.3	1643.8		352	419661.9	730337.4	1642.7	
166	419336.5	732177.7	1627.9		353	419781.6	730310.7	1645.9	
167	419357.6	732172.1	1629.6		354	419680.4	730458.7	1640.1	
168	418884.0	732068.2	1619.4		355	419762.0	730438.0	1639.3	
169	419369.6	732195.1	1630.9		356	419840.9	730424.5	1638.3	
170	419203.4	732358.4	1637.2	TP-5	357	419656.5	731782.1	1641.6	HOUSE
171	419114.1	732225.7	1623.3		358	419569.3	731763.0	1641.7	HOUSE
172	419181.7	732416.2	1641.4		359	419542.1	731625.4	1642.9	TUKUL
173	419333.9	732201.1	1630.3		360	419545.2	731298.7	1638.9	TUKUL
174	419346.1	732265.9	1634.7		361	419408.1	731625.0	1641.9	HOUSE
175	419124.0	732335.7	1635.8		362	419525.9	731250.4	1639.0	TUKUL
176	419103.0	732388.2	1640.7		363	419525.4	731206.1	1639.3	HOUSE
177	419119.5	732294.7	1634.0		364	419552.4	731368.2	1639.4	HOUSE
178	419084.3	732328.1	1636.6		365	419562.9	731460.4	1641.9	
179	419281.1	732216.0	1626.5		366	419631.9	731669.1	1641.0	TUKUL
180	418841.9	732038.9	1613.8		367	419499.9	731278.8	1639.9	
181	419706.9	732214.6	1632.4		368	419710.2	731676.1	1636.7	HOUSE

182	419745.2	732173.6	1632.8		369	419405.8	731259.0	1642.8	
183	419924.4	732399.1	1634.7		370	419394.9	731366.9	1643.1	
184	419787.5	732435.1	1644.2		371	419421.1	731199.6	1645.4	TP-15
185	419812.6	732241.2	1630.6		372	419618.7	730551.3	1641.5	
186	419912.7	732281.9	1630.8		373	419435.5	731265.8	1641.0	
187	420017.2	732302.9	1628.0		374	419429.6	731436.8	1640.2	

Table 9: Elevation, area and capacity relationship of Bisandima reservoir

S.No.	Elevation m a.s.l.	Volume MCM	Area km2
1	1643	9.9	1.25
2	1642	8.7	1.14
3	1641	7.63	1.01
4	1640	6.66	0.92
5	1639	5.8	0.82
6	1638	5.02	0.73
7	1637	4.32	0.67
8	1636	3.68	0.62
9	1635	3.09	0.56
10	1634	2.55	0.51
11	1633	2.07	0.45
12	1632	1.66	0.38
13	1631	1.31	0.31
14	1630	1.03	0.26
15	1629	0.8	0.2
16	1628	0.61	0.17
17	1627	0.46	0.14
18	1626	0.33	0.12
19	1625	0.22	0.09
20	1624	0.14	0.07
21	1623.61	0.12	0.06
22	1623	0.09	0.05
23	1622	0.04	0.03
24	1621	0.02	0.02
25	1620	0.01	0.01
26	1619	0	0
27	1618	0	0
28	1617	0	0

Table 10: Cause of Dam Failure 1975-2011**, Yonatan Sisay (2016)**

Cause of Failure	Number of Dam Failures	Percentage of Dam Failure
Flood or Overtopping	465	70.9%
Piping or Seepage	94	14.3%
Structural	12	1.8%
Human Related	4	0.6%
Animal Activities	7	1.1%
Spillway	11	1.7%
Erosion/Slide/Instability	13	2.0%
Unknown	32	4.9%
Other	18	2.7%
Total number of dam failures	**656**	

Table 11: Recommended Roughness Coefficient**, (Chow, 1959)**

Type of Channel and Description	Minimum	Normal	Maximum
A. *Natural Streams*			
1. **Main Channels**			
a. Clean, straight, full, no rifts or deep pools	0.025	0.030	0.033
b. Same as above, but more stones and weeds	0.030	0.035	0.040
c. Clean, winding, some pools and shoals	0.033	0.040	0.045
d. Same as above, but some weeds and stones	0.035	0.045	0.050
e. Same as above, lower stages, more ineffective slopes and sections	0.040	0.048	0.055
f. Same as "d" but more stones	0.045	0.050	0.060
g. Sluggish reaches, weedy. deep pools	0.050	0.070	0.080
h. Very weedy reaches, deep pools, or floodways with heavy stands of timber and brush	0.070	0.100	0.150
2. **Flood Plains**			
a. Pasture no brush			
1. Short grass	0.025	0.030	0.035
2. High grass	0.030	0.035	0.050
b. Cultivated areas			
1. No crop	0.020	0.030	0.040
2. Mature row crops	0.025	0.035	0.045
3. Mature field crops	0.030	0.040	0.050
c. Brush			
1. Scattered brush, heavy weeds	0.035	0.050	0.070
2. Light brush and trees, in winter	0.035	0.050	0.060
3. Light brush and trees, in summer	0.040	0.060	0.080
4. Medium to dense brush, in winter	0.045	0.070	0.110
5. Medium to dense brush, in summer	0.070	0.100	0.160
d. Trees			
1. Cleared land with tree stumps, no sprouts	0.030	0.040	0.050
2. Same as above, but heavy sprouts	0.050	0.060	0.080
3. Heavy stand of timber, few down trees, little undergrowth, flow below branches	0.080	0.100	0.120
4. Same as above, but with flow into branches	0.100	0.120	0.160
5. Dense willows, summer, straight	0.110	0.150	0.200
3. **Mountain Streams, no vegetation in channel, banks usually steep, with trees and brush on banks submerged**			
a. Bottom: gravels, cobbles, and few boulders	0.030	0.040	0.050
b. Bottom: cobbles with large boulders	0.040	0.050	0.070